分 类 号__________ 学号 D201277241

学校代码 10487 密级__________

華中科技大學

博士学位论文

太阳能光热梯级发电系统建模及其特性研究

学位申请人：张成

学 科 专 业：热能工程

指 导 教 师：高伟 教授

Inmaculada Arauzo 教授

张燕平 副教授

答 辩 日 期：2017 年 9 月 1 日

A Thesis Submitted in Partial Fulfillment of the
Requirements for the Ph.D

Cascade solar thermal power system modeling and research of the key features

Student : Cheng Zhang

Major : Thermal Engineering

Supervisor : Prof. Wei Gao
Prof. Inmaculada Arauzo
Associate Prof. Yanping Zhang

Huazhong University of Science & Technology

Wuhan 430074, P. R. China

September 1, 2017

独创性声明

本人声明所呈交的学位论文是我个人在导师的指导下进行的研究工作及取得的研究成果。尽我所知,除文中已标明引用的内容外,本论文不包含任何其他人或集体已经发表或撰写过的研究成果。对本文的研究做出贡献的个人和集体,均已在文中以明确方式标明。本人完全意识到本声明的法律结果由本人承担。

学位论文作者签名:

日期:　　年　　月　　日

学位论文版权使用授权书

本学位论文作者完全了解学校有关保留、使用学位论文的规定,即:学校有权保留并向国家有关部门或机构送交论文的复印件和电子版,允许论文被查阅和借阅。本人授权华中科技大学可以将本学位论文的全部或部分内容编入有关数据库进行检索,可以采用影印、缩印或扫描等复制手段保存和汇编本学位论文。

本论文属于 保密 □,在 ____ 年解密后适用本授权书。
不保密 □。

(请在以上方框内打"√")

学位论文作者签名:　　　　指导教师签名:

日期:　　年　　月　　日　　日期:　　年　　月　　日

摘 要

随着化石能源消耗和环境污染问题的凸显,太阳能作为一种新能源,具有分布广泛、总量巨大、取之不竭、无污染的特点,越来越受到世界各国的重视,被广泛认为是未来最有潜力替代传统化石能源的清洁能源。在发电领域,太阳能光热发电是除了太阳能光伏发电之外的另一种发电形式。与光伏发电相比,光热发电因具有发电平稳,电网兼容性友好,易于与现有化石燃料电厂组合等优点而受到越来越多的关注。然而,太阳能光热发电大规模应用受限于现有各类技术的成本、效率等问题。

基于此,本文以国家国际合作项目专项"太阳能梯级集热发电系统关键技术合作研究"为背景,目标是研究太阳能光热发电装置,利用各种传统型式的太阳能光热发电系统的优缺点以及热力特性,提出并组建、优化太阳能梯级集热发电系统,为探索出大规模低成本高效率利用太阳能的光热发电技术提供新的方案。主要研究内容包括:

提出了多种采用梯级集热和梯级发电的太阳能光热梯级发电系统。在梯级系统中,采用了多种型式的集热器,实现能量的梯级收集,采用多种形式的热功循环,实现能量的梯级利用。经过系统评估、参数选取、初步计算、方案比较,确定了两种具有代表性的梯级系统方案。一种方案同时选用水工质朗肯循环和斯特林循环,利用给水来冷却斯特林机冷腔,回收利用斯特林机放出的热量;另一种方案选用多级有机工质朗肯循环,利用上一级的凝结热来加热下一级的循环工质,实现能量的梯级利用。

以 EES、MATLAB 等工具,建立了梯级系统中各部件的机理模型,进而组建了梯级系统。采用面向对象的方法,充分利用了继承、多态等特性,保证了各部件之间既具有独立性又具有关联性。其中,斯特林机的建模过程中,考虑了多种不可逆过程及多类损失,建立了较为完善的斯特林机机理模型,并进行了模型验证分析。结果表明,所建立的斯特林机模型的精度要高于传统的经典斯特林机模型。

研究了太阳能光热梯级发电系统中斯特林机组不同排布方式对系统效率的影响。斯特林机组可以采用串联、并联或串并混联的连接型式,连接型式会影响斯特林机的加热流体和冷却流体的温度和流量,进而影响斯特林机的功率和效率,影响整个梯级发电系统的光热发电效率。通过分析斯特林机组的各种不同的排布方式,发现串联连接是最佳的连接型式,斯特林机组具有最佳健壮性和最大的发电效率,梯级发电系统也具有最大的光热发电效率。

提出了分阶段加热的方法,有效降低了蒸汽发生系统中的㶲损。在传统蒸汽发生系统中,加热流体(通常为导热油)和被加热流体(通常为水)流经预热器、蒸发器和过

热器中的流量不变。而在整个换热过程中,加热流体无相变,被加热流体有相变,两者存在较大的换热温差,换热过程有较大的㶲损。本文提出分阶段加热的方法,通过改变加热流体的流量,减小换热温差,降低换热过程的㶲损。

提出了太阳能光热梯级发电系统与传统型式太阳能光热发电系统的对比方法。本文针对新型梯级发电系统提出了其与传统型式太阳能光热发电独立系统的对比方法。梯级系统在一定的参数条件下,相比其对应的独立系统,具有更高的总体光电转换效率。在太阳直射强度为 700 W/m^2,碟式集热器出口空气温度为 800°C 的条件下,方案 1 所选用的太阳能光热梯级集热发电系统比对应的独立系统效率提升 5.2%,方案 2 所选用的太阳能光热梯级集热发电系统比对应的独立系统效率提升 15.3%。

关键词： 槽式集热器,碟式集热器,朗肯循环,斯特林循环,斯特林机组,梯级发电

Abstract

With the increasing awareness of the problem of fossil energy consumption and environmental pollution, solar energy as a renewable energy, which has the advantages of widely distribution, huge amount, inexhaustible and no pollution, has received much attention by many countries and been regarded as the best potential candidate of fossil energy. Concentrating solar thermal power generation is another form of solar power generation technology except solar photovoltaic power generation. Compared to solar photovoltaic, solar thermal power is gaining more attention for its advantages as smooth power generation, good grid compatibility, easy to integrate with existing fossil power plant. However, solar thermal power is not yet widely applied due to the problems of current technologies.

For this reason, this research is based on the national cooperation project ”Collaborative research on key technologies to produce electricity by cascade utilization solar thermal energy” as the background. The objective of this project is to research the equipment of solar thermal power generation system, to propose, develop and optimize a solar thermal cascade system depending on the advantages and disadvantages of the solar thermal power generation technologies, and to explore a new feasible technology for large-scale solar thermal power generation. The main contents and conclusions of this thesis are as follows:

Multiple topological structures with cascade collection and cascade utilization of the cascade systems were proposed. In these systems, different types of collectors were used for cascade collection and different types of thermodynamic cycles were used for cascade utilization. After system evaluation, parameter selection, preliminary calculation and scheme comparison, two representative typical schemes were determined. In one scheme, both Rankine cycle (water as the working fluid) and Stirling cycle are used for power generation. Cooling water of the Rankine cycle is used to cool the hot end of the Stirling engines to recover the released heat. In the other scheme, multiple organic Rankine cycles are used for power generation. Condensation heat of upper cycle is absorbed by lower cycle for energy cascade utilization.

Mechanism models were established for the components of solar thermal power generation system by using EES and MATLAB. The modeling process uses an object-oriented approach, taking full advantage of inheritance, polymorphism and other characteristics, to ensure that each component has both independence and relevance. Among them, the Stirling machine modeling process, considering various irreversibilities and losses, established a more accurate Stirling mechanism model with verification analysis. The results show that the accuracy of the established Stirling model is higher than that of the classical classical Stirling engine models.

The effect of different arrangements of Stirling engines on the efficiency of the cascade system was studied. Stirling engines can be connected in series, in parallel or in hybrid. The connection type affects the temperature and flow of the heating and cooling fluids of each engine, which in turn affects the power and efficiency of the Stirling machines, and the solar-to-electric efficiency of the cascade system. Through the analysis of different arrangements of Stirling engines, it was found that series connection is the best connection type for the best robustness and maximum efficiency of the Stirling engines, and the largest solar-to-electric efficiency of the cascade system.

A method of multi-stage heating was proposed, which can effectively reduce the exergy loss of steam generating system. In conventional steam generation systems, the flows of heating fluid (typically oil) and heated fluid (typically water) through the preheater, evaporator and superheater do not change. In the entire heat exchange process, there is no phase change in the heating fluid, while there is a phase change in the heated fluid. There exist large heat transfer temperature differences between the two fluids in the heat exchangers, which makes large entropy production during the heat exchange process. In this paper, a method of heating in stages is proposed, in which the flow rates of the heating fluid in different heat exchangers are controlled to reduce the heat transfer temperature difference and the exergy losses.

A comparison method of cascade system and traditional solar thermal power generation systems is proposed. In this paper, corresponding independent systems of the cascade system was proposed for comparison. It is found that the cascade system has a higher overall solar-to-electric conversion efficiency under certain parameters compared to its corresponding independent systems. Under the condition of direct solar radiation intensity of 700 W/m^2 and dish type collector outlet air temperature of 800°C, the solar thermal cascade power generation system of Scheme 1 is better than the corresponding The efficiency of stand-alone system is increased by 5.2%. The solar thermal cascade power generation system selected in Scheme 2 is 15.3% more efficient than the corresponding independent system.

Key words: parabolic trough collector, parabolic dish collector, Rankine cycle, Stirling cycle, Stirling engine array, cascade powering

Contents

Nomenclature

$\dot{m}$ Mass flow rate, kg·s^{-1}

$\overline{d_{cav}}$ Effective diameter of the cavity, m

A Heat transfer area, m^2

$A_{dr,1}$ Heat transfer area of dish receiver between tube and air, m^2

$A_{se,1}$ Heat transfer area of Stirling engine at air side, m^2

$A_{se,2}$ Heat transfer area of Stirling engine at water side, m^2

c_p Specific heat at constant pressure, J·kg^{-1}·K^{-1}

c_r Heat transfer correction factor of coiled tube of volumetric receiver

c_v Specific heat at constant volume, J·kg^{-1}·K^{-1}

d Diameter, m

d_i Inner diameter of trough receiver, m

dep Depth, m

e Regenerator effectiveness

J Annular gap cylinder displacer, m

K Dead volume factor

k Specific heat ratio (c_p/c_v), thermal conductivity, W·m^{-1}·K^{-1}

m Mass of working fluid in Stirling engine, kg

n Number of collectors

n_1 Number of columns of the Stirling engine array

n_2 Number of rows of the Stirling engine array

n_g Amount of working gas in each Stirling engine, mol

n_{se} Number of Stirling engines in the Stirling engine array

Nu Nusselt number

P Power of Stirling engine, W

p Pressure, Pa

p_e Extraction pressure of the steam turbine, Pa

Pr Prandtl number

Q Absorbed heat, J

q'' Heat flux, W·m^{-2}

R Gas constant, J·kg^{-1}·K^{-1}

Re Reynolds number

s_{se} Speed of Stirling engine, Hz

T_H Working fluid temperature in the hot space, K

T_L Working fluid temperature in the cold space, K

T_R Effective working fluid temperature in regenerator, K

T_w Wall temperature, K

U Overall heat transfer coefficient, W·m^{-2}·K^{-1}

V_C Compression volume, m^3

V_D Total dead volume, m^3

V_E Expansion volume, m^3

V_{DC} Cold space dead volume, m^3

V_{DH} Hot space dead volume, m^3

V_{DR} Regenerator dead volume, m^3

W Output work, J

x Dryness fraction

y Extraction rate of steam turbine

Z Displacer stroke, m

Abbreviations

ANN Artificial neural network

CCHP Combined cooling, heating and power

CFD Computational fluid dynamics

CPC Compound parabolic collector

CRTEn Research and technologies centre of energy in Borj Cedria

DSG Direct Steam Generation

HTF Heat Transfer Fluid

ISCC Integrated Solar Combined Cycle

LFC Linear Fresnel Collector

LM Levenberge Marguardt

LSSVM Least squares support vector machine

MCRT Monte Carlo Ray Tracing

ORC Organic Rankine Cycle

PCG Pola-Ribiere Conjugate Gradient

PTC Parabolic Trough Collector

PTSTPP Parabolic Trough Solar Thermal Power Plant

SCG Scaled Conjugate Gradient

SNL Sandia National Laboratory

SRC Steam Rankine Cycle

Greek Symbols

δ Thickness, m

ϵ Emissivity

$\eta_{shading}$ Shading factor

γ Intercept factor; compression ratio

γ_H Space ratio in process 12

γ_L Space ratio in process 34

λ Thermal conductivity, W·m^{-1}·K^{-1}

μ Viscosity, kg·m^{-1}·s^{-1}

ρ Reflectivity

θ_{dc} Dish aperture angle (0° is horizontal, 90° is vertically down)

Subscripts

c Cooling fluid

cd Condenser

cw Cooler wall

g General solution

h Heating fluid

h Homogeneous solution

hw Heater wall

i Inlet

$insu$ Insulating layer

o Outlet

p Particular solution

p Piston

pu Pump

r Regenerator

s Stand-alone systems

th Theoretical

w Tube wall

x Stirling engine in column x

List of Figures

List of Tables

Chapter 1 Introduction

Saving our planet, lifting people out of poverty, advancing economic growth... these are one and the same fight. We must connect the dots between climate change, water scarcity, energy shortages, global health, food security and women's empowerment. Solutions to one problem must be solutions for all.

Ban Ki-moon

This dissertation considers a way to solve the global problems of energy shortage and environment problem.

1.1 Research background and significance

REN21, a global renewable energy policy multi-stakeholder network, published the most comprehensive annual overview of renewable energy of 2016.[3] Renewables are now established around the world as mainstream sources of energy. Rapid growth, particularly in the power sector, is driven by several factors, including the improving cost-competitiveness of renewable technologies, dedicated policy initiatives, better access to financing, energy security and environmental concerns, growing demand for energy in developing and emerging economies, and the need for access to modern energy.

Solar energy, which has the advantages of widely distribution, huge amount, inexhaustible and no pollution, has received much attention by many countries and been regarded as the best potential candidate of the fossil energy. The International Energy Agency projected in 2014 that under its ”high renewables” scenario, by 2050, solar photovoltaics and concentrating solar power would contribute about 16 and 11 percent, respectively, of the worldwide electricity consumption, and solar would be the world's largest source of electricity.[4]

Concentrating solar thermal power generation is another form of power generation technology except solar photovoltaic power generation. Concentrating Solar Power (CSP) energy system uses mirrors to converge sunlight onto a receiver that absorbs the solar energy and transfer it to a heat transfer fluid (HTF) such as a synthetic oil, molten salt or air. The HTF then directly or indirectly used as the heat source in a power cycle. Compared to solar photovoltaic, solar thermal power is gaining more attention for its advantages as higher energy density, smooth power generation, good grid compatibility, easy to integrate with existing fossil power plant.

Concentrating solar power technologies use different mirror configurations to concentrate the sun's light energy onto a receiver and convert it into heat. The heat can then be used to create steam to drive a turbine to produce electrical power or used as industrial process heat. There are three types of CSP technologies being commercially applied: parabolic trough, parabolic dish and power tower.

A parabolic trough is a type of solar thermal collector whose mirror type is straight in one dimension and curved as a parabola in the other two. The reflector follows the sun during the daylight hours by tracking along a single axis. The energy of sunlight is reflected by the mirror and focused on the pipe positioned at the focal line. HTF (e.g. synthetic oil) runs through the pipe to absorb the heat generated by the focused sunlight, then used as the heat source for heating process or power generation. Figure 1-1 shows a parabolic trough product made by Alpha-E. A parabolic dish is a type of solar thermal collector whose mirror type is part of a circular paraboloid, that can converging the incoming sunlight traveling along the axis to the focus. A receiver or Stirling engine is put at the focal point to absorb the converged energy. Figure 1-2 shows a 38 kW prototype Stirling engine product of Xiangtan Electric Manufacturing Group Co., Ltd. (XEMC). A solar power tower is a type of solar furnace using a tower to receive the focused sunlight. It uses an array of flat, movable mirrors (called heliostats) to focus the sun's rays upon a collector tower (the target). Figure 1-3 shows the Solar Two power tower.

Among the three solar thermal power technologies, parabolic trough is the most mature and commercially deployed technology. However, it has a low concentration ratio, the receiver's temperature is relatively low, the solar-to-electric efficiency is relatively low. Parabolic dish can obtain high temperature thermal energy, it's solar-to-electric can be higher than parabolic trough. Besides, one advantage of parabolic trough is that it requires much

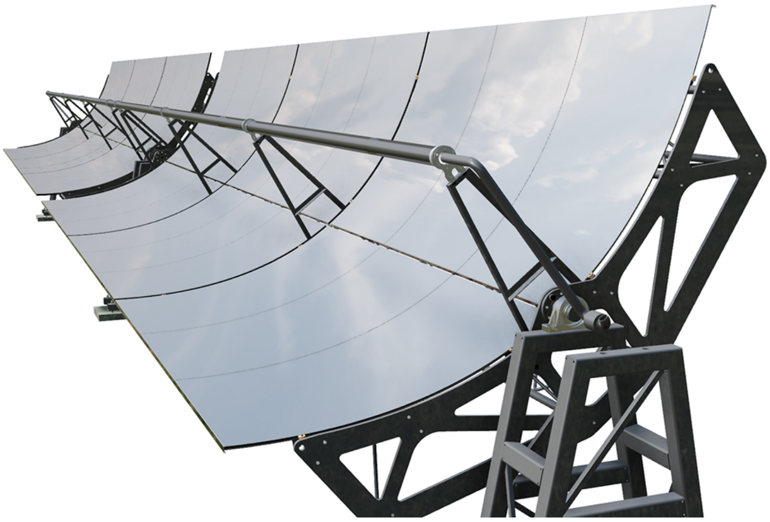

Figure 1-1 Alpha-Trough-350, a parabolic trough product made by Alpha-E

less water for power generation. However, solar parabolic dish is not a large-scale application, it's mainly applied for distributed power generation for its compact structure and easy installation. Solar power tower has a very high concentration ratio when more mirrors (also called heliostats) are used, the receiver's temperature can be very high and it can be applied for large-scale application. However, it has some disadvantages such as high investment. It is currently in rapid development stage.

It is very important to find out a way the utilize the advantages of existing solar thermal power technologies and overcome their disadvantages. In other words, to find out a new technology with higher efficiency lower cost is urgent. This research is trying to achieve this by proposing a cascade system that uses different collector power generation methods and different thermodynamic cycles, which may be a new and feasible technology to realize large-scale solar thermal power generation.

1.2 State of the art

1.2.1 Parabolic trough

Parabolic trough solar technology is the most proven and lowest cost large-scale solar power technology available.[5] Many researchers have done lots of work to research and investigate it.

Figure 1-2 A 38 kW prototype Stirling engine product of XEMC

Many of these works have concentrated on experimental work aimed at testing the mechanical and thermal performance of the parabolic trough collectors. Dudley et al.[6] tested the collector efficiency and thermal losses of the LS-2 type trough collector. Burkholder and Kutscher[7] tested the heat losses of Solel's UVAC3 and Schott's 2008 PTR70 parabolic trough collectors. A correlation to estimate the thermal efficiency of the collectors as a function of the absorber temperature was developed. Reddy et al.[8] developed and investigated six different receiver configurations for trough collectors for performance comparison. Experimental tests were carried out for a 15 m^2 collector according to ASHRAE 93-1986 test procedure. Li et al.[9] carried out experiments to verify the feasibility of proposed end loss

Figure 1-3 Overall view of Solar Two power tower

compensation methods. A fan-shaped plane mirror was put at one end of the trough collectors to compensate the end loss effect. Results prove that the compensation methods are feasible and effective. It is well known that experimental studies are the most accurate and convincing method for parabolic trough collector research. However, this method is not only investment required and also time consuming. In order to reduce the R&D cost and time, parabolic trough collectors are usually modeled.

Some researchers investigated the optical model of the parabolic trough solar collectors. Wang et al.[10] proposed a mathematical model for the optical efficiency of the trough collector and selected three typical regions of solar thermal utilization in China for the model. The model is validated by comparing the test results in parabolic trough power plant, with relative error range of 1% to about 5%. Zou et al.[11] investigated the influences of sunshape and incident angle on the optical performance of the trough collectors. It is found that the sunshape has significant effect on the optical efficiency and should be token into consideration in practice. Larger aperture with smaller absorber diameter leads to more end loss caused by incident angle. It is also found that optimal focal length exists for the optical efficiency. Lüpfert et al.[12] introduced the specific techniques to analyze the geometry and optical properties of trough collectors and summarized results in collector shape measurement, flux measurement, ray tracing, and thermal performance analysis for parabolic troughs. It is shown that the measurement methods and the parameter analysis give consistent results, which can provide references for the next generation trough collector relevant improvements. Xu et al.[13] analyzed the optical efficiency of a PTC with horizontal north-south axis and proposed a method to compensate the end loss effect of the PTC. The calculation formula of the optical end loss rate and the increased optical efficiency for the system using the compensation method were derived. A five-meter experimental system was built to verify the feasibility of the compensation method proposed. The increased thermal efficiency of the experimental system was measured, and it was proved that the proposed compensation method is feasible. Huang et al.[14] proposed an analytical model for optical performance which employed a modified integration algorithm to simulate the performance of trough collectors. The analytical equation of the optical efficiency of each point of the reflector was deduced to obtain the optical efficiency of the system by integration algorithm.

Some researchers investigated the exergy performance of the parabolic trough collectors. Padilla et al.[15] performed a comprehensive exergy balance of a parabolic trough collector based on the previous heat transfer model[16]. The results shown that inlet temperature of heat transfer fluid, solar irradiance, and vacuum in annulus have a significant effect on the thermal and exergetic performance, but the effect of wind speed and mass flow rate of heat transfer fluid is negligible. It was obtained that inlet temperature of heat transfer fluid cannot be optimized to achieve simultaneously maximum thermal and exergetic efficiency because they exhibit opposite trends. Finally, it was found that the highest exergy destruction is due to the heat transfer between the sun and the absorber while for exergy losses is due to optical error. Al-Sulaiman[17] presented the exergy analysis of selected thermal power systems driven by PTSCs. The power pf the thermal power system is produced using either a steam Rankine cycle (SRC) or a combined cycle, in which the SRC is the topping cycle and an organic Rankine cycle (ORC) is the bottoming cycle. Guo et al.[18] investigated the energy efficiency and exergy efficiency of the parabolic trough collector. The result shown that there exists an optimal mass flow rate of working fluid for exergy efficiency, and the thermal efficiency and exergy efficiency have opposite changing tendencies under some conditions.

Some researchers are dedicated to developing more accurate models using new methods. Behar et al.[19] developed and validated a novel parabolic trough solar collector model. The model has been compared with models made by Lab. SNL and NREL. The proposed model has a better accuracy of thermal performance prediction. Padilla et al.[16] performed a detailed one dimensional numerical heat transfer analysis of a PTC (Parabolic Trough Collector). To solve the mathematical model of heat transfer of the PTC model, the partial differential equations were discretized and the nonlinear algebraic equations were solved simultaneously. The numerical results was validated to the data from Sandia National Laboratory (SNL). Hachicha et al.[20] presented a detailed numerical heat transfer model based on the finite volume method for the parabolic trough collector. This model is based on finite volume method and ray trace techniques and takes into account the finite size of the Sun. The model is thoroughly validated with results from the literature and it shows a good agreement with experimental and analytical results. Guo and Huai[21] implemented a multi-parameter optimization of parabolic trough solar receiver based on genetic algorithm where Exergy and thermal efficiencies were employed as objective function. Boukelia et al.[22] investigated the feed-forward back-propagation learning algorithm with three different variants; Levenberge Marguardt (LM), Scaled Conjugate Gradient (SCG), and Pola-Ribiere Conjugate Gradient (PCG), used in artificial neural network (ANN) to find the best approach for prediction and techno-economic optimization of parabolic trough solar thermal power plant (PTSTPP) integrated with fuel backup system and thermal energy storage. Liu et al.[23] developed a mathematical model of PTC using the least squares support vector machine (LSSVM) method. Numerical simulations are implemented to evaluate the feasibility and efficiency of the LSSVM method, where the sample data derived from the experiment and the simulation results of two solar collector systems with 30 m^2 and 600 m^2 solar fields, and the complicated relationship between the solar collector efficiency and the solar flux, the flow rate and the inlet temperature of the heat transfer fluid (HTF) is extracted. Lobon et al.[24] introduced a computational fluid dynamic simulation approach to predict the behavior of a solar steam generating system, which is located at the Plataforma Solar de Almeria, Spain. The CFD package STAR-CCM+ code has been used to implement an efficient multiphase model capable of simulating the dynamics of the multiphase fluid in parabolic-trough solar collectors. Numerical and experimental data are compared in a wide range of working conditions.

To understand the thermal performance of the collector and identify the heat losses from the collector, Mohamad et al.[25] analyzed the temperature variation of the working fluid, tube and glass along the collector. It is found that using double glazing cover enhances the thermal efficiency of the collector operating at high temperature. However, when the collector length is 10 m or less, it is more economical to use a single glass cover for the collector than a double glazing cover. Also, it is clear shown that increasing the diameter of absorbing tube enhances the rate of heat transfer losses, consequently decreasing the thermal efficiency of the collector. Guo et al.[26] developed a nonlinear distribution parameter model to model the dynamic behaviors of direct steam generation parabolic trough collector loops under either full or partial solar irradiance disturbance.

Some researchers have proposed some new types of solar trough systems. Ashouri et al.[27] coupled a small scale parabolic trough collector and a thermal storage tank along with an auxiliary heater to a Kalina cycle to study the performance of the system throughout the year, both thermodynamically and economically. Bader et al.[28] developed a numerical model of a tubular vavity-receiver that uses air as the heat transfer fluid. Four different receiver configurations are considered, with smooth or V-corrugated absorber tube and single- or double-glazed aperture window. The different types of energy loss by the collector have been quantified, and the temperature distribution inside the receiver has been studied. The pumping power required to pump the HTF through the receiver has been determined for a 200 m long collector row. Good et al.[29] proposed solar trough concentrators using air as heat transfer fluid at operating temperatures exceeding 600°C. It consists of an array of helically coiled absorber tubes contained side-by-side within an insulated groove having a rectangular windowed opening. Secondary concentrating optics are incorporated to boost the geometric concentration ratio to 97×. Kaloudis et al.[30] investigated a PTC system with nanofluid as the HTF in terms of Computational Fluid Dynamics (CFD). Syltherm 800 liquid oil was used as the HTF, and Al_2O_3 nanoparticles with the concentrations ranges from 0% to 4% was investigated. A boost up to 10% on the collector efficiency was reported for Al_2O_3 concentration of 4%. Tan et al.[31] proposed a two-stage photovoltaic thermal system based on solar trough concentration, in which the metal cavity heating stage is added on the basis of the PV/T stage, and thermal energy with higher temperature is output while electric energy is output. The experimental platform of the two-stage photovoltaic thermal system was established, with a 1.8 m^2 mirror PV/T stage and a 15 m^2 mirror heating stage, or a 1.8 m^2 mirror PV/T stage and a 30 m^2 mirror heating stage. The results showed that with single cycle, the long metal cavity heating stage would bring lower thermal efficiency, but temperature rise of the working medium is higher, up to 12.06°C with only single cycle. With 30 min closed multiple cycles, the temperature of the working medium in the water tank was 62.8°C, with an increase of 28.7°C, and thermal energy with higher temperature could be output. Al-Sulaiman et al.[32] proposed a novel system based on PTC and ORC for combined cooling, heating and power (CCHP). Performance assessment, including efficiency, net electrical power, and electrical to heating and cooling ratios, of the system shown that when CCHP is used, the efficiency increases significantly. This study reveals that the maximum electrical efficiency for the solar mode is 15%, for the solar and storage mode is 7%, and for the storage mode is 6.5%. The maximum CCHP efficiency for the solar mode is 94%, for the solar and storage mode is 47%, and for the storage mode is 42%.

1.2.2 Parabolic dish

The solar parabolic dish system is a point focusing solar system and known as the most efficient solar thermal technology. Two-axis tracking system keeps it always directly towards the sun without cosine losses. It can obtain high concentration ratio and hence high temperature.

Many researchers conducted experiments to investigate the solar parabolic dish system or to validate proposed models. To investigate the heat loss of semi-spherical cavity receiver applied for solar parabolic dish system, Tan et al.[33] conducted experiments with different fluid inlet temperatures, receiver inclination angles and aperture sizes. Correlations of Nusselt number as a function of Grashof number were developed by the experiment results. Chaudhary et al.[34] investigated a solar cooker based on dish collector with phase change thermal (PCM) storage unit. Three cases have been considered for the investigation: ordinary solar cooker, solar cooker with outer surface painted black, and solar cooker with outer surface painted black along with glazing. It was observed that the last case shows the best performance, which can store 32.3% and 26.8% more heat for the PCM compared with the first and second cases respectively. Mawire and Taole[35] investigated the thermal performance of a cylindrical cavity receiver for an SK-14 parabolic dish concentrator. The receiver exergy rates and efficiencies are found to be appreciably smaller than the receiver energy rates and efficiencies. The exergy factor is found to be high under conditions of high solar radiation and under high operating temperatures. An optical efficiency of around 52%

for parabolic dish system is determined under high solar radiation conditions. Zhu et al.[36] conducted an experimental investigation of a coil type solar dish receiver. The solar irradiance is about 650 W/m^2, while the concentrated solar flux at the aperture is approximately 1000 kW/m^2. The energy and exergy performance of the receiver was analyzed and the experimental results show that, at steady state, the energy efficiency is maintained around 80%, and the exergy efficiency is around 28%. CRTEn developed a solar dish system using four types of absorbers: flat plat, disk, water calorimeter and solar heat exchanger.[37] For the different types of absorbers, experiments were conducted to obtain the mean concentration ratio and both energy and exergy efficiency. Results shown that thermal energy efficiency of the system varies from 40% to 77%, the concentrating system reaches an average exergy efficiency of 50% and a concentration factor around 178. Thirunavukkarasu et al.[38] carried out an experimental study to investigate the thermal performance of a cavity receiver for a dish concentrator. The overall system efficiency of the solar collector is 69.47%. The average exergy efficiency of the receiver is found to be 5.88% with a peak value of 10.35%. Pavlovic et al.[39] performed the experimental study of a solar dish system. In this system, different working fluids (water, thermal oil and air) were used to validate the numerical models developed in EES (Engineering Equation Solver). It was found that water is the most appropriate working fluid for low-temperature applications, while thermal oil is the most appropriate working fluid for higher-temperature applications.

Some researchers focused on the dish concentrator, many proposed different shapes of concentrators. The perfect concentrator has a parabolic shape, but for some considerations (better production, safer transportation, lest cost and so on), some solar concentrators are composed of multiple spherically shaped mirrors. A large dish solar concentrator, SG3, which is about 400 m^2, was designed and demonstrated in Australian National University (ANU) in 1994 as shown in Figure 1-4.[40] It successfully proved the technical viability of a concentrator that is approximately three times bigger than any other produced. Berumen et al.[41] developed a refector consists of 12 facets made of fiberglass with a reflecting surface made of aluminum sheet with reflectance of 86%. Pavlovic et al.[42] presented a procedure to design a square facet concentrator for laboratory-scale research on medium-temperature thermal processes. A parabolic collector made up of individual square mirror panels (facets) were investigated. These facets can deliver up to 13.604 kW radiative power over a 250 mm radius dish receiver with average concentrating ratio exceeding 1200. Hijazi et al.[43] de-

Figure 1-4 The SG3 400 m^2 dish in ANU

signed a low cost parabolic solar dish concentrator with small-to moderate size for direct electricity generation and special attention is given to the selection of the appropriate dimensions of the reflecting surfaces. Ma et al.[44] designed a solar dish concentrator based on triangular membrane facets. A 600-facet concentrator with focal-diameter ratio of 1.1 will achieve 83.63% of radiative collection efficiency over a 15 cm radius disk located in the focal plane, with a mean solar concentration ratio exceeding 300. A 3.6-meter diameter stretched-membrane optical facet for a parabolic dish has been successfully designed and demonstrated under contract with Sandia National Laboratories.[45] Twelve facets identical to them will be used to make the lightweight reflector of the dish. The project goal of 2.5 mrad surface accuracy was met with each of the two full-sized prototypes, and accuracies of as low as 1.1 mrad were achieved.

Many researches investigated the flux distribution and thermal performance of the solar dish receiver. Shuai et al.[46] developed a flux distribution measurement system for dish concentrators. A charge coupled device camera was applied to obtain the contours of the flux distribution for target placements with different location. Further, the measured flux distributions are compared with a Monte Carlo-predicted distribution. The results can be a valuable reference for the design and assemblage of the solar collector system. Flux distribution of the receiver is simulated successfully by Mao et al.[47] using MCRT method. The impacts of incident solar irradiation, aspect ratio (the ratio of the receiver height to the receiver diameter), and system error on the radiation flux of the receiver are investigated. Li et al.[48] used the Monte-Carlo ray-tracing method for the radiation flux distribution of the solar dish receiver system. The result was validated by experiment and used as the boundary conditions of a CFD receiver model. The fluid flow and conjugate heat transfer in the receiver was numerically simulated and validated by experiments. Wang and Laumert[49] used the ray-tracing methodology to investigate the effects of cavity surface materials on the flux distribution for an impinging receiver. Five cavity surface materials and their combinations have been studied. The results show that the flux distribution and the total optical efficiency are much more sensitive to the absorptivity on the cylindrical surface than on the bottom. Blazquez et al.[50] studied the optimization of the concentrator and receiver cavity geometry of parabolic dish system. Ray-tracing analysis has been performed with the open source software Tonatiuh, a ray-tracing tool specifically oriented to the modeling of solar concentrators. Reddy et al.[51?] performed the theoretical thermal performance analysis of a fuzzy focal solar parabolic dish concentrator with modified cavity receiver. Total heat loss from the modified cavity receiver is estimated considering the effects of wind conditions, operating temperature, emissivity of the cavity cover and thickness of insulation. Time constant test was carried out to determine the influence of sudden change in solar radiation at steady state conditions. The daily performance tests were conducted for different flow rates. Vikram and Reddy[52] investigated the total heat losses of modified cavity receiver of solar parabolic dish with three configurations using 3D numerical model. The effects of various parameters such as diameter ratio, angle of inclination, operating temperature, insulation thickness and emissivity of the cavity cover on the heat losses from the modified vavity receiver are investigated. An ANN model is developed to predict the heat loss for a large set of influencing parameters. Based on ANN modeling, improved Nusselt number correlations are proposed for convective, radiative and total heat losses from the modified cavity receiver. The convective heat losses are greatly influenced by receiver inclination whereas the radiation heat losses are influenced by the cavity cover emissivity. The diameter ratio also plays a major role in heat losses from the cavity receiver. The present method predicts the heat losses more accurately compared with the existing models.

Some researchers focused on the solar tracking system. Patil et al.[53] described the development of automatic dual axis solar tracking system for solar parabolic dish. Five light dependent resistors were used to sense the sunlight and Two permanent magnet DC motors are used to move the solar dish. A controller software were developed to control the motors using the data sensed by the resistors.

1.2.3 Power tower

Besarati and Yogi[54] developed a new and simple method to improve the calculation speed and accuracy for shading and blocking computation of the heliostat field. The Sassi method[55] is used for the shading and blocking efficiency. A 50 MWth heliostat field in Dagget, California, USA was used as a case study for the proposed method.

Haroun[56] proposed a novel system combines both solar chimney and solar tower. The solar tower receiver was installed at the top of the chimney. Theoretical study of this novel system was conducted. The results shown that the new system generates more power than conventional system with the same parameters of solar irradiance, collector radius, height of chimney, and height of solar tower. The inlet air speed of the chimney is higher than that of the conventional, and it increases with the solar irradiance. Moreover, the results indicated that there exists a optimum ratio of solar tower height to solar chimney height for the maximum overall power.

Franchini et al.[57] developed a computing procedure for solar tower system under both nominal and part load conditions. A Siemens gas turbine product, SGT-800, was considered as a study case for the solar tower system. The turbine has a dual pressure heat recovery steam generator, which can be used for the Integrated Solar Combined Cycle (ISCC) plant. A model of Solar Rankine Cycle (SRC) driven by PTCs was also developed for comparison. A highest solar-to-electric efficiency of 21.8% can be achieved by the designed ISCC plant. And in all conditions, the global solar energy conversion efficiency of the ISCC is higher than that of the SRC.

Kim et al.[58] investigated the heat loss of solar central receiver. Numerical simulations using CFD (Computational Fluid Dynamics) with the consideration of four different receiver shapes were carried out to get the influence on convection and radiation heat losses. Different opening ratio between cavity aperture area and receiver aperture area, receiver temperatures, wind velocities and wind directions (head-on and side-on) were considered for the simulations. Results were used to get a simplified correlation model which gets the fraction of convection heat loss. The correlation obtained showed good agreements with the simulation results. The correlation was also validated with experimental data from three central receiver systems (Martin Marietta, Solar One and Solar Two).

Lara et al.[59] presented a novel modeling tool for calculation of central receiver concentrated flux distributions. The modeling tool is based on a drift model that includes different geometrical error sources in a rigorous manner and on a simple analytic approximation for the individual flux distribution of a heliostat. The model is applied to a group of heliostats of a real field to obtain the resulting flux distribution and its variation along the day. The distributions differ strongly from those obtained assuming the ideal case without drift or a case with a Gaussian tracking error function. The time evolution of peak flux is also calculated to demonstrate the capabilities of the model. The evolution of this parameter also shows strong differences in comparison to the case without drift.

Wei et al.[60] proposed a new method for the design of the heliostat field layout for solar tower power plant. In the new method, the heliostat boundary is constrained by the receiver geometrical aperture and the efficiency factor which is the product of the annual cosine efficiency and the annual atmospheric transmission efficiency of heliostat. With the new method, the annual interception efficiency does not need to be calculated when places the heliostats, therefore the total time of design and optimization is saved significantly. Based on the new method, a new code for heliostat field layout design (HFLD) has been developed and a new heliostat field layout for the PS10 plant at the PS10 location has been designed by using the new code. Compared with current PS10 layout, the new designed heliostats have the same optical efficiency but with a faster response speed. In addition, to evaluate the feasibility of crops growth on the field land under heliostats, a new calculation method for the annual sunshine duration on the land surface is proposed as well.

Wei et al.[61] developed a new code for the design and analysis of the heliostat field layout for power tower system. In the new code, a new method for the heliostat field layout is proposed based on the edge ray principle of non-imaging optics. The heliostat field boundary is constrained by the tower height, the receiver tilt angle and size and the heliostat efficiency factor which is the product of the annual cosine efficiency and the annual atmospheric transmission efficiency. With the new method, the heliostat can be placed with a higher efficiency and a faster response speed of the design and optimization can be obtained. A new module for the analysis of the aspherical heliostat is created in the new code. A new toroidal heliostat field is designed and analyzed by using the new code. Compared with the spherical heliostat, the solar image radius of the field is reduced by about 30% by using the toroidal heliostat if the mirror shape and the tracking are ideal. In addition, to maximize the utilization of land, suitable crops can be considered to be planted under heliostats. To evaluate the feasibility of the crop growth, a method for calculating the annual distribution of sunshine duration on the land surface is developed as well.

Xu et al.[62] created a model of the 1 MW Dahan solar thermal power tower plant using the modular modeling method. The dynamic and static characteristics of the power plant are analyzed based on these models. Response curves of the system state parameters are given for different solar irradiance disturbances. Conclusions in this paper are good references for the design of solar thermal power tower plant.

Xu et al.[63] built the thermal energy storage model of Badaling 1 MW solar power tower plant using the modular modeling method. This model can accurately simulate the recharge and discharge processes of thermal energy storage system. The dynamic and static characteristics of the thermal energy storage system are analyzed based on the model response curves of the system state parameters that are obtained from different steam flow disturbances. Conclusions of this paper are good references for the design, operating, and control strategy of solar thermal power plant.

1.2.4 Cascade solar system

There are mainly two directions of the research of cascade solar systems. One is cascade collection, the other is cascade utilization.

1.2.4.1 Cascade collection

Some researchers have investigated the combination of different types of collectors for CSP to achieve cascade solar collection. Suzuki[64] analyzed the solar thermal systems with two different types of collectors connected in series. A key value of the collectors was revealed to be the key factor to determine whether a cascade system is better than either one of the collectors alone. The value is the product of the collector efficiency factor and the optical efficiency. If the value of the lower concentration ratio collector is lager than that of the higher concentration ratio, the cascade system is more effective. Furthermore, to obtain the maximum energy gain, there exists the optimum operating conditions.

Kribus et al.[65] proposed an idea of using separate aperture stages for different irradiance distribution. The working fluid is gradually heated when it flow through the receiver elements with increasing irradiance levels. A two-stage system was set up to demonstrate this principle at the Weizmann Institute's Solar Tower. Air was used as the HTF to obtain 750°C after the low-temperature stage and 1000°C after the high-temperature stage. Figure 1-5 shows the two-stage receiver system.

Gordon and Saltiel[66] presented an analytic method for predicting the long-term performance of solar energy systems with more than one collector brand (“multi-stage” systems). This procedure enables the designer to determine the most cost-effective method of combining different collector brands for a given load. Although our derivations pertain to solar systems for constant load applications and/or near constant collector operating threshold, they can also be used for conventional multi-pass designs. The problems of excess energy delivery, and of various collector on/off control strategies, are taken into account. Our results are simple closed-form expressions whose evaluation requires readily-available average climatic data, and load and collector characteristics. The analytic method is illustrated by a solved example which shows that significant savings can be realized by combining different collector brands for a given application (multi-staging).

Oshida and Suzuki[67] presented the idea of optical cascade heat collection of solar energy. Two absorbers, one warm and the other hot, are used in the cascade system. The warm absorber is heated by the Fresnel lenses and the hot absorber is heated by CPC. HTF flows into the warm absorber firstly and then flows into the hot absorber. The temperature of HTF can increase more effectively.

Desai et al.[68] presented an integrated CSP plant configuration with the combination of both PTC and LFC. Thermo-economic comparisons between PTC-based, LFC-based and integrated CSP plant configurations, without hybridization and storage, were analyzed. Figure 1-6 shows a simplified schematic of a proposed integrated CSP plant configuration. It is demonstrated that the cost of energy of an integrated CSP plant is 9.6% cheaper than PTC-based CSP plant and 13.5% cheaper than LFC-based CSP plant.

Coco et al.[69] developed four different line-focusing solar power plant configurations integrated both direct steam generation and Brayton power cycle. In these configurations, collectors are divided into different solar fields to supply different heat demands. This provides the ability to use different types of collectors (parabolic trough and linear Fresnel) in

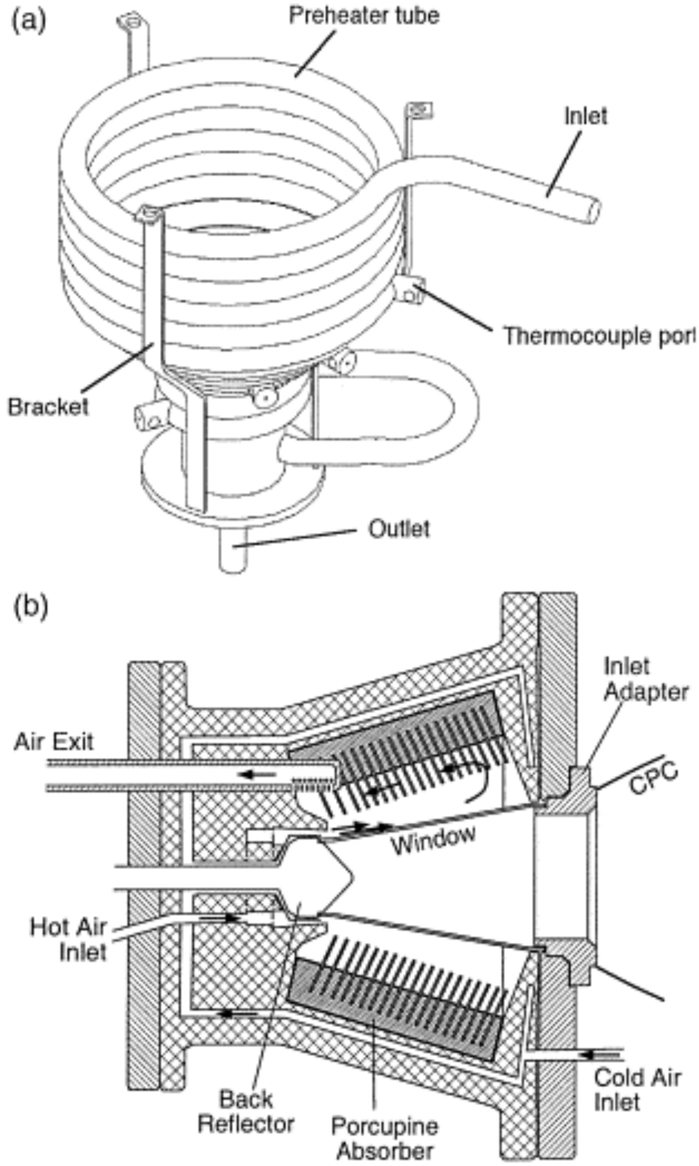

Figure 1-5 Two-stage receiver system. (a)Low temperature receiver (preheater) (b)High-temperature receiver.

the systems.

1.2.4.2 Cascade utilization

Many researchers have done the work on the combination of different thermodynamic cycles for CSP. Lots of the work focused on integrated solar combined cycle (ISCC) with

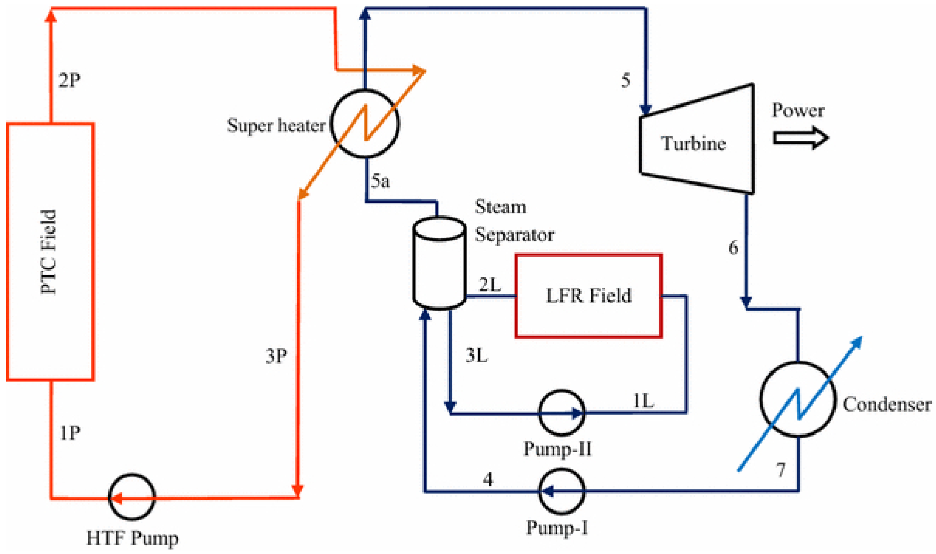

Figure 1-6 Simplified schematic of a proposed integrated CSP plant configuration

parabolic trough, where Rankine cycle is used as the bottom cycle.

Li and Yang[70] proposed a novel two-stage ISCC system that could reach up to 30% of the net solar-to-electricity efficiency as shown in Figure 1-7. In their research, the impact on the system overall efficiencies of how and where solar energy is input into ISCC system was investigated.

Behar et al.[71] reviewed the R&D activities and published studies since the introduction of such a concept in the 1990s. One of the conclusions is that the higher the solar radiation intensity the better is the performance of the ISCCS than those of conventional CSP technologies.

Gulen [72] used the exergy concept of the second law of thermodynamics to distill the complex optimization of ISCCS to its bare essentials. After the exergy analysis, physics-based, user-friendly guidelines were provided to help direct studies involving heavy use of time consuming system models in a focused manner and evaluate the results critically to arrive at feasible ISCC designs.

Shaaban [73] introduced a novel ISCC with steam and organic Rankine cycles. The ORC was used in order to intercool the compressed air and produce a net power from the received thermal energy. The proposed cycle performance was studied and optimized with different ORC working fluids. Figure 1-8 shows the schematic of the proposed ISCC.

Alqahtani and Dalia[74] quantified the economic and environmental benefits of an ISCC

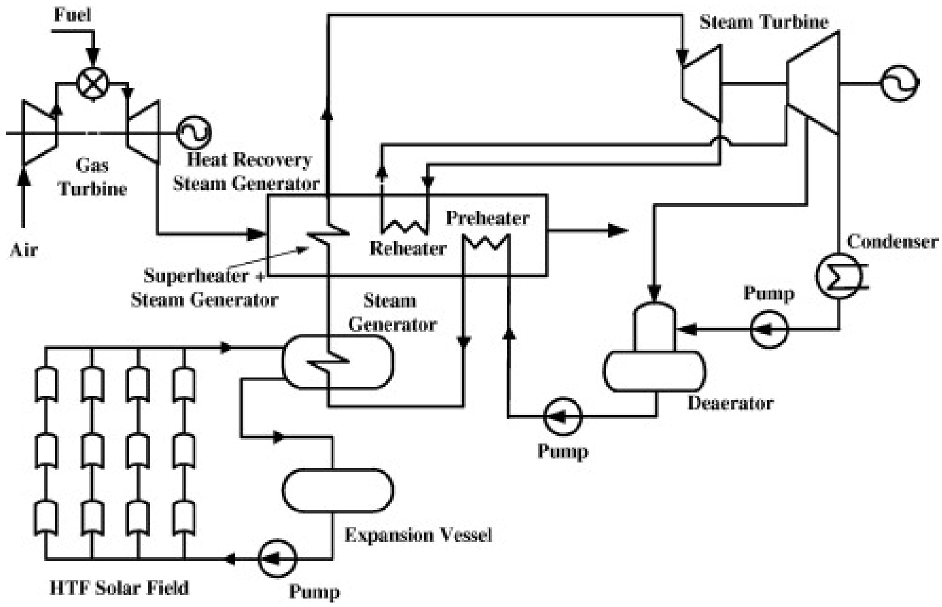

Figure 1-7　The proposed ISCC scheme

power plant relative to a stand-alone CSP with energy storage, and a natural gas-fired combined cycle plant. Results show that integrating the CSP into an ISCC reduces the LCOE of solar-generated electricity by 35-40% relative to a stand-alone CSP plant, and provides the additional benefit of dispatch ability.

Manente[75] developed a 390 MWe three pressure level natural gas combined cycle to evaluate different integration schemes of ISCC. Both power boosting and fuel saving operation strategies were analyzed in the search for the highest annual efficiency and solar share. Result shown that, compared to power boosting, the fuel saving strategy shows lower thermal efficiencies of the integrated solar combined cycle due to the efficiency drop of gas turbine at reduced loads.

Compared with traditional ISCC design, two new conceptual hybrid designs for ISCC with parabolic trough were represented by Turchi et al.[76]. In the first design, gas turbine waste heat is supplied for both heat transfer fluid heating and feed water preheating. In the second design, gas turbine waste heat is supplied for a thermal energy storage system.

Mukhopadhyay and Ghosh[77] presented a conceptual configuration of a solar power tower combined heat and power plant with a topping air Brayton cycle. The conventional gas turbine combustion chamber is replaced with a solar receiver. A simple downstream Rankine cycle with a heat recovery steam generator and a process heater have been considered for

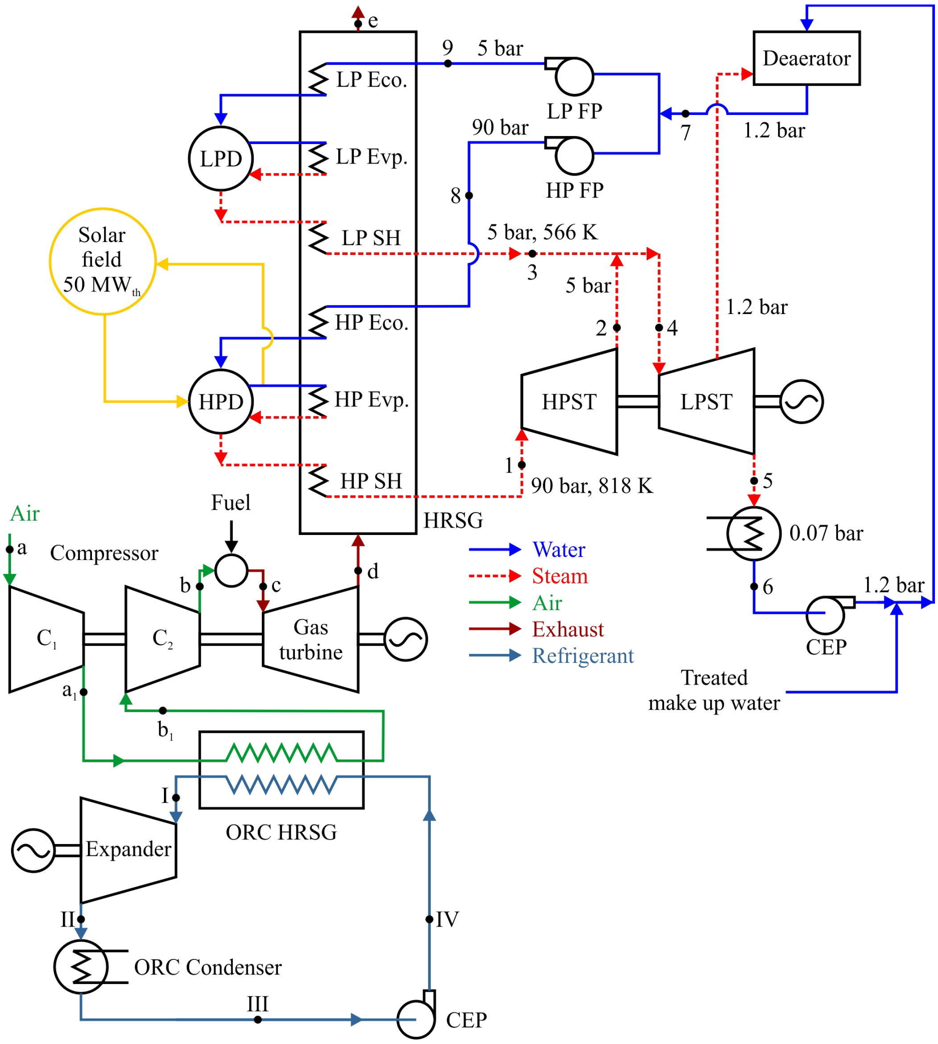

Figure 1-8 Schematic of the proposed ISCC with two bottoming cycles

integration with the solar Brayton cycle.

Li et al.[78] presented a novel cascade system using both steam Rankine cycle and organic Rankine cycle. Screw expander is employed in the steam Rankine cycle for its good applicability in power conversion with steam-liquid mixture. The heat released by steam condensation is used to drive the organic Rankine cycle.

Al-Sulaiman[17] compared the produced power of an SRC-ORC combined cycle with traditional SRC cycle. The SRC is driven by parabolic trough solar collectors, and the ORC cycle is driven by the condensation heat of the SRC.

Bahari et al.[79] considered the optimization of an integrated system using organic Rankine cycle to utilize the heat released by the Stirling cycle. However, the integrated system is a primitive design and it takes no consideration of the application in CSP field.

1.3 Research content

The research is based on the national cooperation project ”Collaborative research on key technologies to produce electricity by cascade utilization solar thermal energy” as the background. The objective of this project is to research the equipment of solar thermal power generation system, to propose, develop and optimize a solar thermal cascade system depending on the advantages and disadvantages of the solar thermal power generation systems, and to explore a new feasible technology for large-scale solar thermal power generation. The main contents and conclusions of this thesis are as follows:

Firstly, mechanism models were established for the components of solar thermal power generation system. The mechanism mathematical models were developed according to the operation mechanism of the target object and physical equations. The key components in the system, such as collectors, steam generating system, steam turbine and Stirling engine, were modeled with details. The mathematical model of each component is a model verified by the classical theory or a large number of experimental data, which is the basic of the model of the cascade solar thermal power generation system. Heat loss models were established for the receivers of trough collector and dish collector. For the Stirling engine, based on the reasonable simplification and hypothesis, the model of the Stirling machine considered various losses and irrevisibilities was developed. The component models were developed in MATLAB by using object-oriented method. It makes full use of inheritance and polymorphism to ensure both the independence and the relevance of the components.

Secondly, the topological structure of solar thermal cascade power generation system was proposed. According to the analysis of thermal characteristics and the working characteristics of each component in the system, rationally arranged topological structures of cascade system were proposed. These systems use different thermodynamic cycles to utilize energy in different temperature zones. A reasonable cascade generation system can make full use of the mechanism models of the power generation system and provide the foundation for higher efficiency solar thermal cascade generation systems. In this thesis, several schemes of feasible topological structures of solar thermal cascade system were set up according to the mechanism model of each component. After system evaluation, parameter selection, preliminary calculation and scheme comparison, two representative typical schemes were determined. In one scheme, both Rankine cycle (water as the working fluid) and Stirling cycle are used for power generation. Cooling water of the Rankine cycle is used to cool the hot end of the Stirling engines to recover the released heat. In the other scheme, multiple organic Rankine cycles are used for power generation. Condensation heat of upper cycle is absorbed by lower cycle for energy cascade utilization.

Thirdly, the solar thermal cascade generation system models were developed. Based on the selected solar thermal cascade generation systems, solar thermal cascade generation system models were established based on the model of each component in the systems. The object-oriented features of inheritance, combination and polymorphism were used for the model development. The change rules of the main parameters and the performance indexes under the coupling of external and internal factors were studied. The change mechanism was studied and the calculation method of its performance characteristics was established. After setting up the components, setting the parameters and compiling the environment, the thesis completes the system construction of each system scheme, and finally completes the simulation system of solar thermal cascade generation based on MATLAB with the copyright of independent computer software. The system components are relatively independent, easy to replace or improve the parts model; the results of the calculation of the system model can be a single object to easily view the various components of the system key parameters.

Then, simulation and optimization of cascade solar thermal power generation system model. Based on the study of the performance characteristics of solar thermal cascade generation system, the system is optimized and the structure is reconstructed. In particular, by analyzing the steam generation system of the system, a method of staged heating is proposed to reduce the heat transfer temperature difference in the steam generating system by changing the mass flow rate of the heat conduction oil, effectively reducing the heat generated during the heat exchange process in the steam generating system. Which can improve the efficiency of the whole system. Based on Stirling unit in cascade system, five kinds of basic arrangement forms of Stirling unit are summarized, and the difference of unit efficiency and output power under various arrangement forms is analyzed, and a given cold and heat source fluid Stirling unit under the conditions of the best arrangement.

Finally, the operating parameters of solar thermal cascade power generation system are optimized. According to the specific structural scheme and operation mode, the performance parameters and economic indexes of the cascade generation system are taken as the objective function, reasonable adjustable parameters are selected, various constraints are established, and modern optimization methods such as genetic algorithm and ant colony algorithm are used to complete the system Parameter optimization analysis, as well as the independent system for comparative analysis. The results show that solar thermal cascade power generation system has higher overall solar-to-electric conversion efficiency under certain parameter conditions than its corresponding independent system. Under the condition of direct solar radiation intensity of 700 W/m^2 and dish type collector outlet air temperature of 800°C, the solar thermal cascade power generation system of Scheme 1 is better than the corresponding The efficiency of stand-alone system is increased by 5.2%. The solar thermal cascade power generation system selected in Scheme 2 is 15.3% more efficient than the corresponding independent system.

Chapter 2 System topology

2.1 System topology design

The objective of this research is to research the equipment of solar thermal power generation system, to propose, develop and optimize a solar thermal cascade system depending on the advantages and disadvantages of the solar thermal power generation systems. The research is based on the national cooperation project "Collaborative research on key technologies to produce electricity by cascade utilization solar thermal energy" as the background. There are three kinds of mature technologies been applied commercially – parabolic trough, parabolic dish and solar tower. Considering the future deployment of solar cascade demo system, two solar thermal technologies, parabolic trough and parabolic dish, are chosen as the basic systems for the design of cascade solar thermal power system. For the cascade utilization of the high temperature of the parabolic receiver, air (or nitrogen) is used as the HTF to transfer the heat collected. Figure 2-1 shows the schematic diagrams of a parabolic trough system and a parabolic dish system. To make the system structure diagrams in this paper more clearly and consistent, legends of the components that may appear in solar power systems are listed in Figure 2-2.

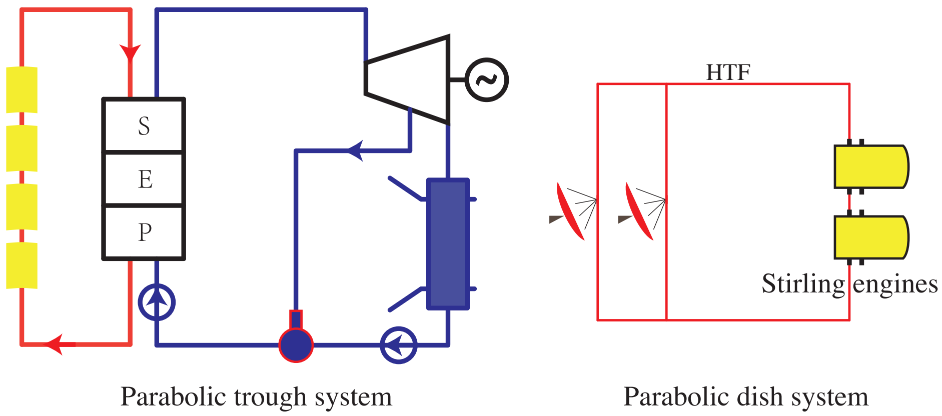

Figure 2-1 Schematic diagrams of a parabolic trough system and a parabolic dish system

With different considerations (such as water Rankine cycle or ORC, combination of different systems, connection types of collectors, etc) of the cascade system topology, multiple

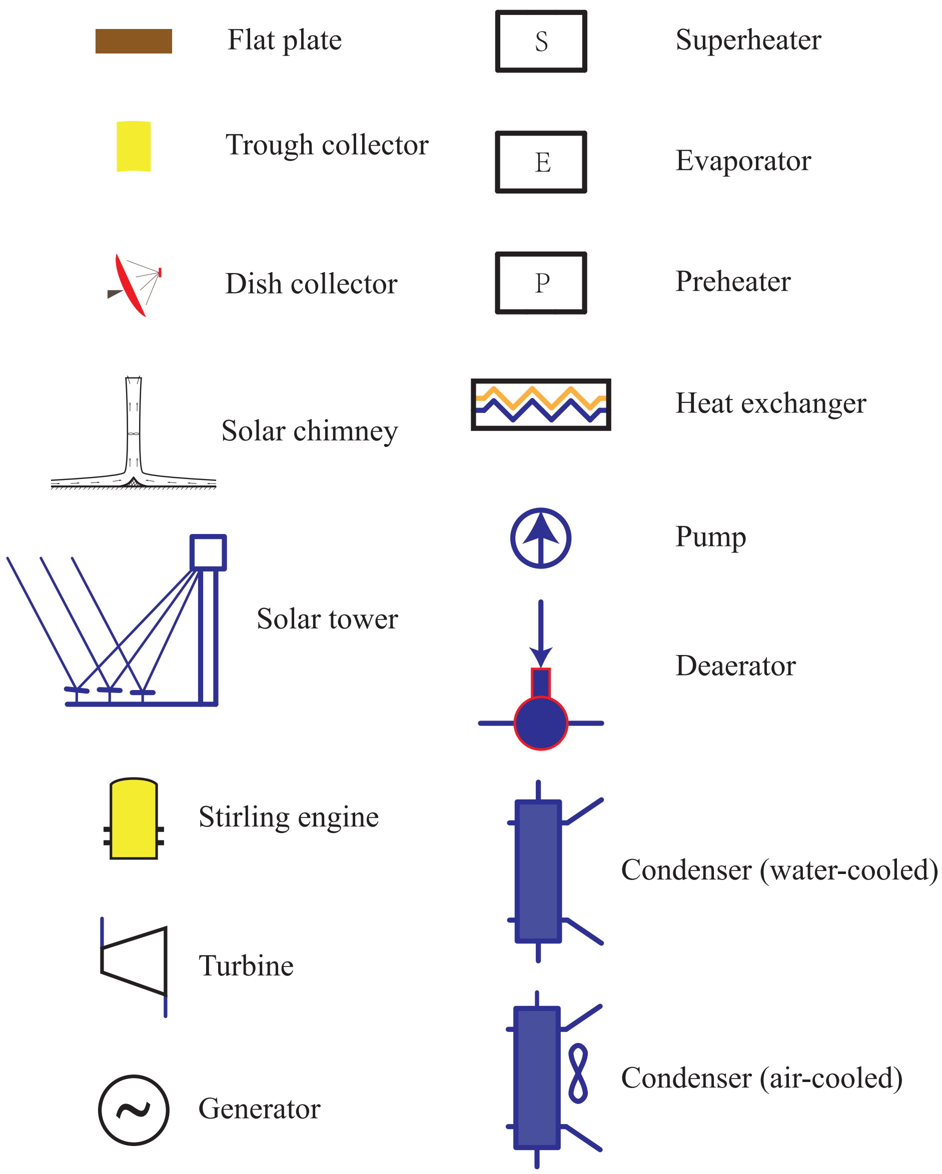

Figure 2-2   Components in solar power systems

combination topologies may be used for cascade systems. To get the most suitable system topology, these considerations will be analyzed in the following sections.

2.1.1 Rankine cycle fluid

An ideal working fluid would have the temperature entropy diagram given in Figure 2-3. The following characteristics listed by Abbin and Leuenberger[80] describe this fluid:

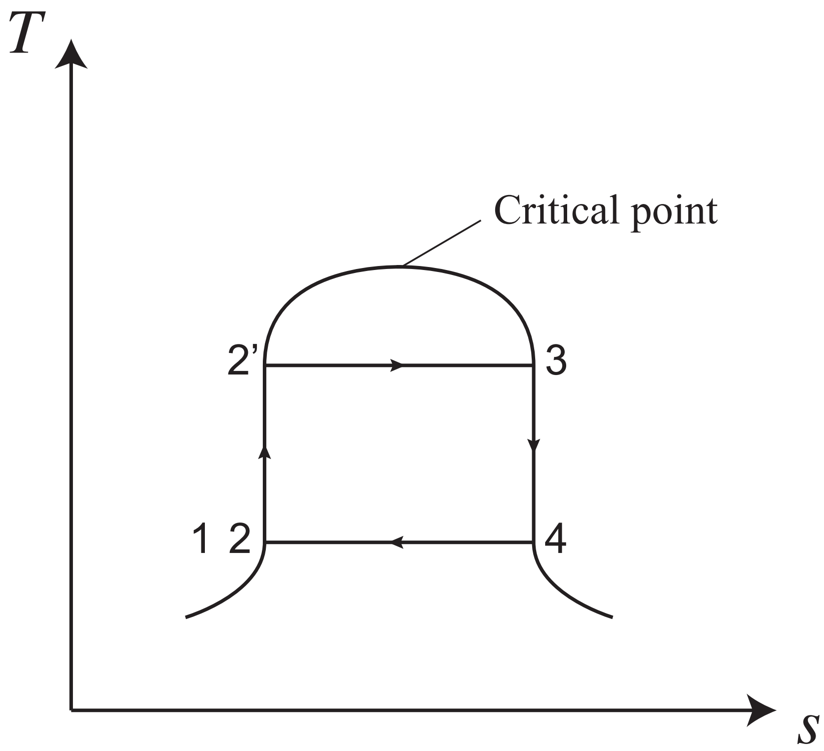

Figure 2-3 Collector and Rankine cycle efficiency variation with operating temperature

- The heat capacity of the liquid phase should be small. This makes the curve 22' in Figure 2-3 almost vertical.
- The critical point should be above the highest operating temperature to allow all heat to be added at that temperature.
- The vapor pressure at the highest operating temperature should be moderate for safety reasons and to reduce the cost of the equipment.
- The vapor pressure at the condensing temperature should be above atmospheric pressure to prevent air leakage into the system.
- The specific volume of the vapor at state 4 should be small to avoid large-diameter turbine wheels, casings, and heat exchangers.
- The saturated vapor curve 3-4 in Figure 2-3 should be vertical to avoid expansion into the wet vapor region (negative ds/dT) or expansion into the superheat region (positive ds/dT).
- For low-power turbine applications, the fluid should have a high molecular weight to

minimize the rotational speed and/or the number of turbine stages and to allow for reasonable mass flow rates and turbine nozzle areas.

- The fluid should be liquid at atmospheric pressure and temperature for ease of handling and containment.
- The freezing point should be lower than the lowest ambient operating temperature.
- The fluid should have good heat-transfer properties, be inexpensive, thermally stable at the highest operating temperature, nonflammable, noncorrosive, nontoxic, and so on.

Water is the most commonly used fluid for Rankine cycle, it is mare mature to design Rankine cycle components for steam systems than any other liquid. It is inexpensive to use (although boiler-grade water must be highly distilled and thus costs more than tap water), sealing of the high-pressure portions of a Rankine cycle using steam is not critical. Nonflammability and ready availability of steam are additional advantages. Because it has a critical temperature and pressure of 374°C / 22.1MPa, it can be used for systems operating at fairly high temperatures with most of the heat addition (at constant temperature) and at moderate pressure. Figure 2-4a shows the schematic diagram of a typical steam Rankine cycle solar system.

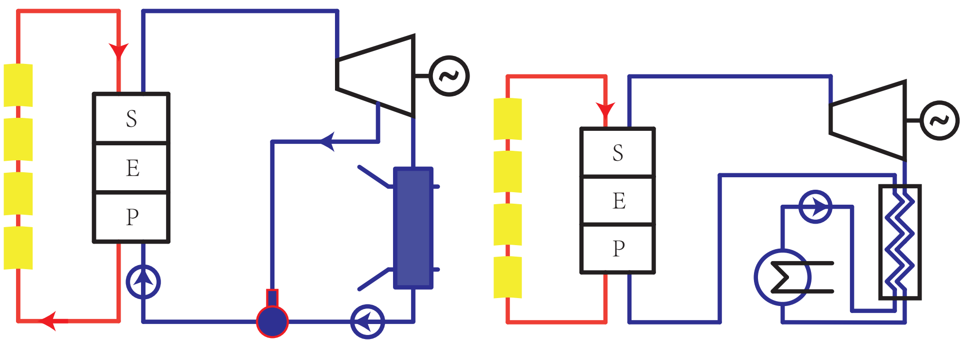

(a) (b)

Figure 2-4 Schematic diagrams of two types of Rankine cycle solar system

There are some disadvantages for steam as the Rankine cycle fluid. The low temperature characteristics of steam are not ideal because the steam has a low vapor pressure (see Table 2.1) and a very low density at ambient temperature. Therefore, sealing air from low pressure components is a major design problem.

Table 2.1 Saturated steam pressure at the corresponding temperature

T(K)	373.15	363.15	353.15	343.15	333.15	323.15	313.15	303.15	293.15
p(Pa)	101322	70117	47373	31176	19932	12344	7381	4246	2339

The organic Rankine cycle can be used in the solar parabolic trough technology in place of the usual steam Rankine cycle. The ORC allows power generation at lower capacities and with a lower collector temperature, and hence the possibility for low-cost, small scale decentralized CSP units. Most organic fluids used in organic Rankine cycle are drying fluids. The vapor leaving the expander still contains heat that can be transferred to the compressed liquid stream because the turbine outlet temperature is above the condenser temperature. A vapor-to-liquid heat exchanger, known as a regenerator, is typically used for this purpose. Figure 2-4b shows the schematic diagram of a typical organic Rankine cycle solar system.

Compared with steam for the Rankine cycle, it has the following advantages:

- Small turbine head allows for moderate shaft speed and a single- or two-stage design.
- Low volume ratio facilitates the flow path design.
- High volume flow and low velocity of sound results in reasonable flow areas.
- Low temperature drop during expansion reduces thermal stress problems.
- Dry expansion avoids blade erosion caused by vapor wetness.
- Low system pressure facilitates housing design.

2.1.2 Solar chimney

Solar chimney, also known as solar updraft tower, directly (without concentration) uses the sun's heat to generate power. It uses solar radiation to increase the internal air temperature to form a flow to the chimney located at the middle of the roof. Figure 2-5 shows the schematic of a typical solar chimney power plant. In this plant, air is heated by the green house effect under the translucent roof. As the roof is open at its periphery, air flows into the plant due to different density distribution. Hot air flows into the chimney because of buoyancy. An electricity-generating turbine is set in the path of the air current to convert the kinetic energy of the flowing air into electricity.

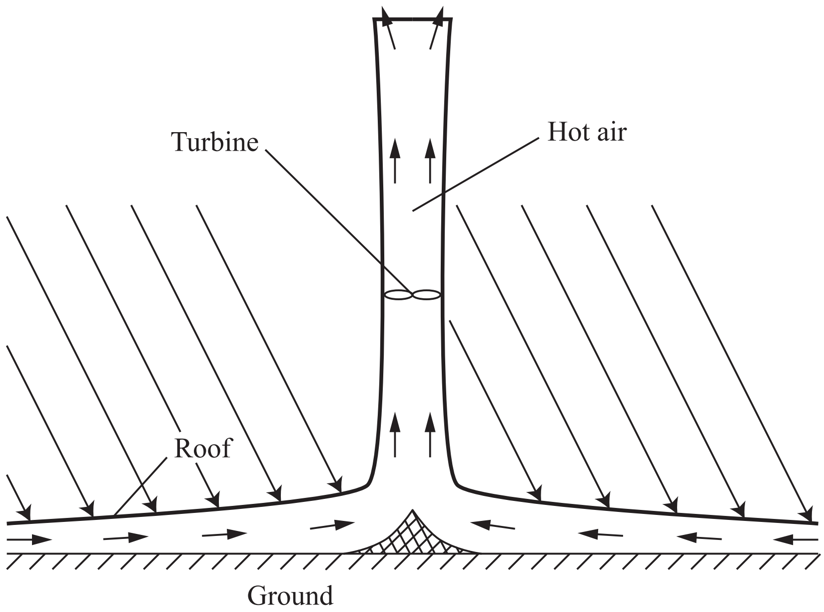

Figure 2-5 Schematic diagram of a solar chimney power plant

The solar chimney can use the low temperature (low grade energy) for power generation. So the combination of parabolic trough system and solar chimney is considered an effective way for energy cascade utilization. In the combined system, the condenser in the Rankine cycle is air cooled. The fan blows the hot air that has cooled the condenser into the solar chimney power plant from its periphery. The hot air stream converges at the bottom of chimney, flows upward with the action of buoyancy and drives the turbine in the chimney. Energy of the hot air can be utilized by the solar chimney. Figure 2-6 shows an example of the combined system.

2.1.3 Collector series connection

Considering different heat collecting temperatures of different types of collectors, series connection of different types of collectors can be a feasible choice for solar cascade collection. Trough collectors and Fresnel collectors have better performance for lower temperature heat collection. Dish collectors and solar towers are more suitable for higher temperature heat collection. Serial connection utilize the advantages of different types of collectors. Figure 2-7 shows an example of a cascade system using collector series connection. In this

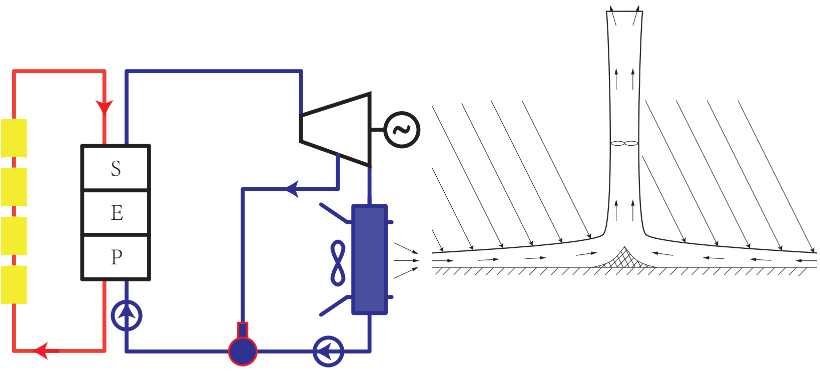

Figure 2-6　Schematic diagram of a combined solar trough and chimney power system

system, air, the HTF, is preheated by parabolic collectors before it flows into the parabolic dish collectors.

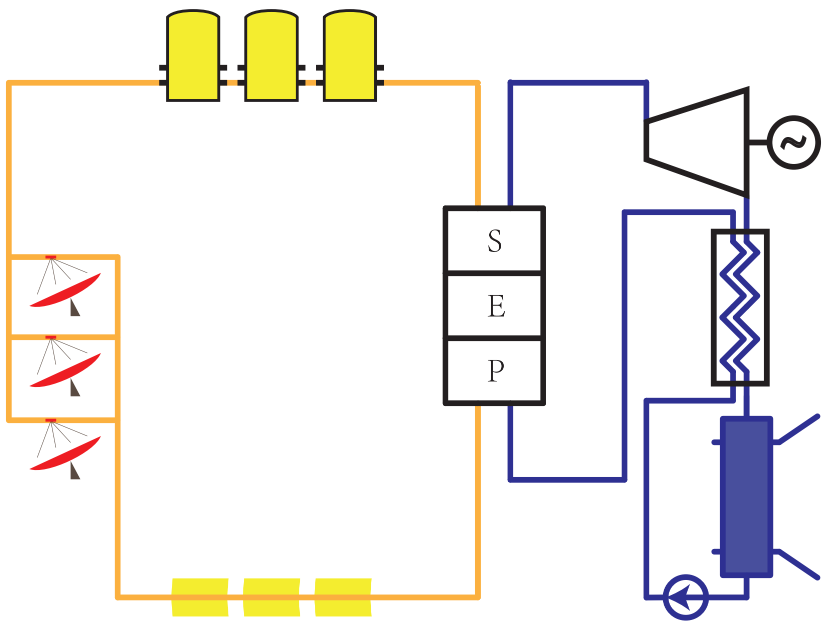

Figure 2-7　Schematic diagram of a cascade system using collector series connection

2.1.4　Direct steam generation

All commercial parabolic trough solar plants implemented to date use heat-transfer fluid (typically synthetic oil or melton salt) in the solar field. It leads to high pressure drop, limits the oil (or salt) related equipment operation, maintenance and cost. Besides, the highest temperature of the Rankine cycle is limited by the oil (or salt) temperature. So generating steam in the receiver tubes (direct steam generation, DSG) of the solar collector is one of the directions to reduce the cost and increase the efficiency of the PTC systems. Figure 2-8 shows the schematic diagram of a typical DSG solar system.

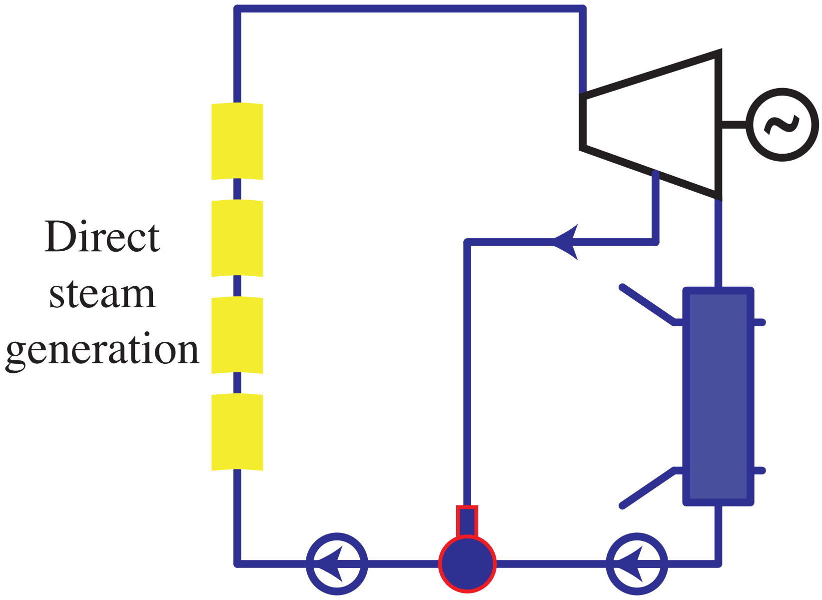

Figure 2-8 schematic diagram of a typical solar system using receiver vapor generator

2.1.5 Heat exchanger between circuits

Heat transfer between different circuits can be applied for cascade utilization of the heat collected. Depending on the two basic solar system in 2-1, there are two types of heat exchangers that can be applied in the solar system.

In the first type, air-oil heat exchanger is applied to transfer heat between the air circuit and the oil circuit. Figure 2-9 shows an example of solar system using this type of heat exchanger. In this system, after providing heat for the Stirling engines, the hot air flows through the air-oil heat exchanger and provides heat for the oil.

In the second type, air-water heat exchanger is applied to transfer heat between the air circuit and the oil circuit. Figure 2-10a and Figure 2-10b show two different kinds of solar systems using this type of heat exchanger. In Figure 2-10a,

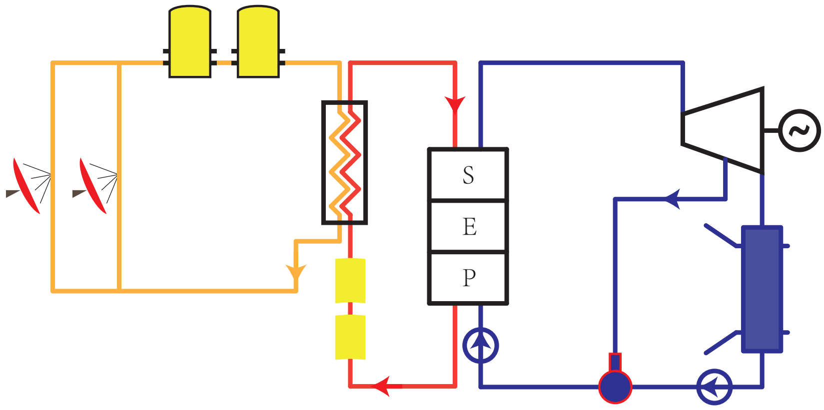

Figure 2-9   Schematic diagram of a solar system using air-oil heat exchanger

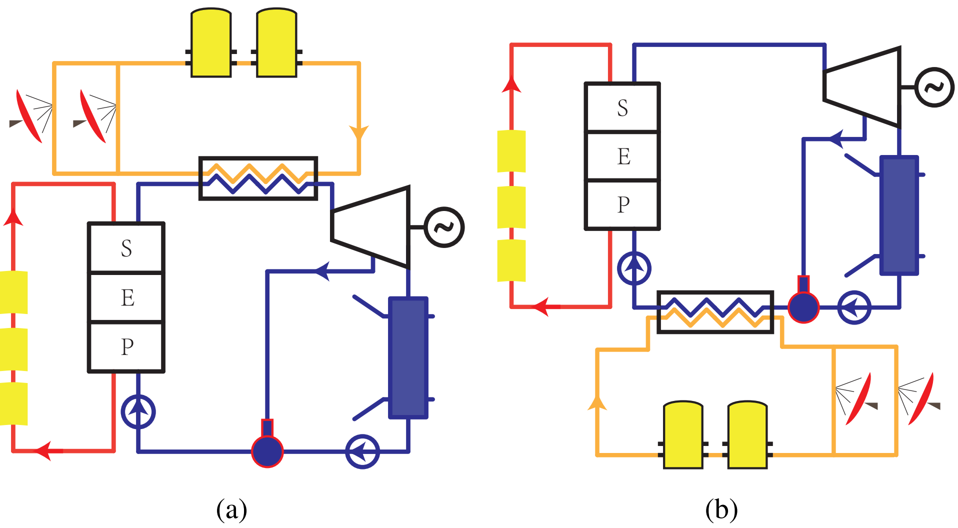

Figure 2-10   Schematic diagrams of two kinds of solar systems using air-water heat exchanger

2.1.6   Heat recovery between cycles

According to the second law of thermodynamics, it is impossible for any device that operates on a cycle to receive heat from a single reservoir and produce a net amount of work. For a heat engine, it requires both a hot source and a cold sink to convert heat energy to mechanical energy. Figure 2-11 shows the diagram of a typical heat engine. In a thermodynamic cycle, heat is absorbed from the hot source, only part of it can be converted into mechanical work by the engine. The ratio related to the temperatures of hot source and cold sink is fundamentally limited by Carnot's theorem.

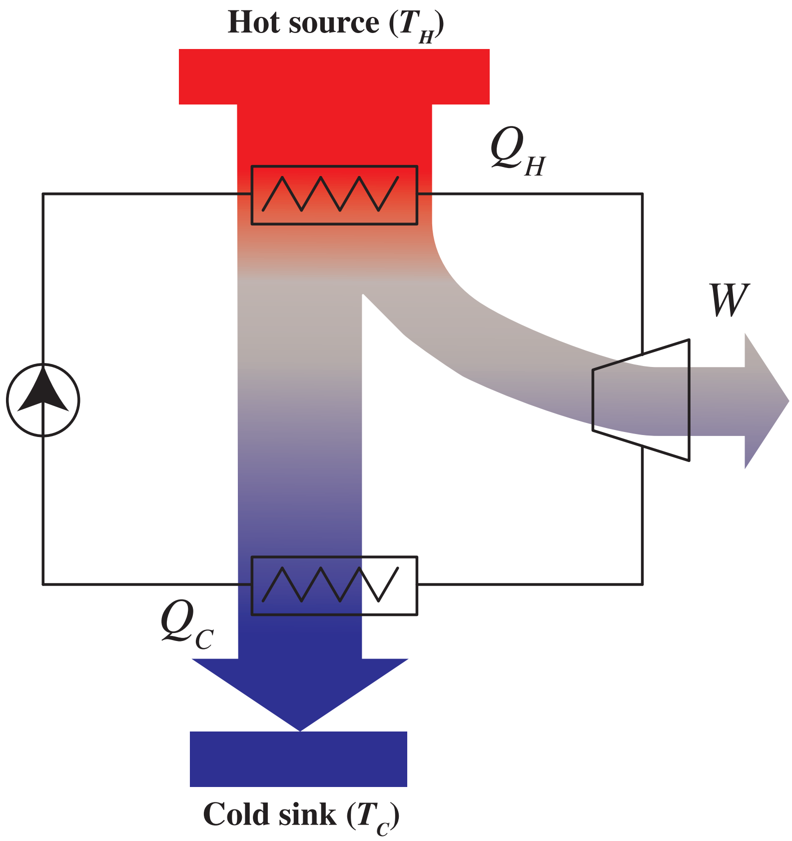

Figure 2-11 Diagram of a typical heat engine

Engines that only suitable for external heating are usually considered for solar applications. Unlike an internal combustion engine that generates heat within the working fluid, an externally heated engine needs external heat to be added to the working fluid by a heat exchanger.

Three types of engines are designed to accept external heat and have been used for solar heat sources: the Rankine, the Stirling, and the Brayton cycles[81]. The Rankine and Brayton cycles are both suitable for constant-pressure heat-addition. The original Brayton engine uses piston compressors and piston expanders, but more modern gas turbines and airbreathing jet engines also follow the Brayton cycle. Although the cycle is usually an open system, in order to carry out thermodynamic analysis, usually it is assumed that exhaust gases are reused as the intake so that the whole process can be analyzed as a closed cycle. The Stirling machine uses a reciprocating piston design that allows external heating to be combined into its constant-temperature heat-addition process. In a Rankine cycle, the pressurized liquid enters a boiler (or a heat exchanger) where it is heated at constant pressure by an external heat source to become a dry saturated vapor.

These three kinds of cycles work at different optimum operating temperatures. Rankine cycle works with the lowest hot source temperature and Brayton works with the highest. Figure 2-12 shows the diagram of the three cycles used in solar energy. The heat released by these cycles may be recovered by another cycle (bottom cycle).

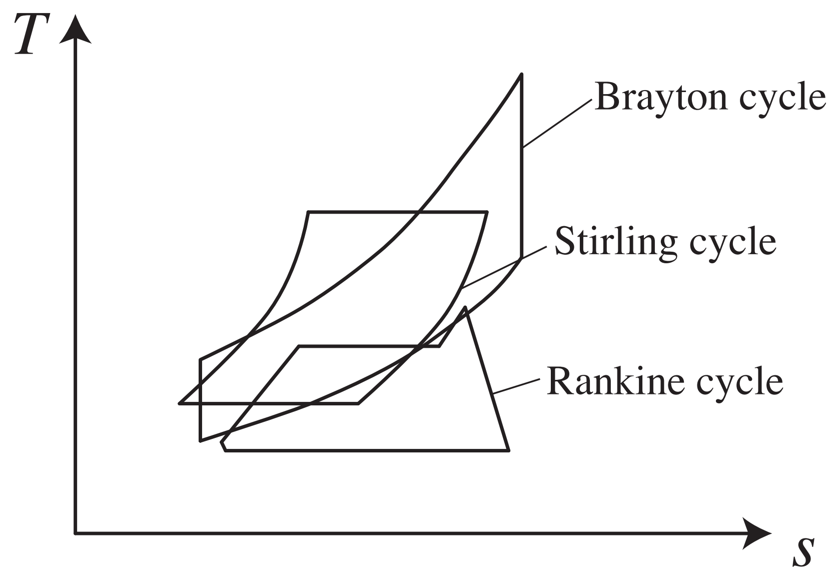

Figure 2-12 Diagram of three cycles used in solar energy

Some researchers have proposed combined cycles for power generation. Dunham and Lipi[82] proposed a single Brayton and a combined Brayton-Rankine power cycle for distributed solar power generation and compared its theoretical efficiency to a single Brayton cycle. In the combined power cycle, exhaust gas of the turbine is used to provide heat for Rankine cycle. Working fluids including air, Ar, CO_2, He, H_2, and N_2 are examined for the topping Brayton cycle. C6-fluoroketone, cyclohexane, n-pentane, R-141b, R-245fa, and HFE-7000 are examined as working fluids in the bottoming Rankine cycle. It is found that the combination of the Brayton topping cycle using carbon dioxide and the Rankine bottoming cycle using R-245fa gives the highest combined cycle efficiency of 21.06%, while a single Brayton cycle is found to reach a peak cycle efficiency of 15.31% with carbon dioxide at the same design point conditions. Bahrami et al.[83] proposed a combined Stirling-organic Rankine cycle (ORC) power cycle. An ORC was used as the cold-side heat rejector of a

Stirling engine. The operating temperatures of the ORC are between 80°C and 140°C and the combined system can achieve 4% to 8% higher efficiency compared with a standard Stirling cycle. Li et al.[78] proposed a novel solar electricity generation system (SEGS) using both SRC and ORC. Screw expander (SE) is employed in the SRC for its good applicability in power conversion with steam-liquid mixture. The heat released by steam condensation is used to drive the ORC. Simulation results show that efficiency of 13.68–15.62% for the proposed system can be achieved. Thierry et al.[84] proposed a nonlinear optimization formulation of multistage Rankine cycle with two types of configurations. Both cascade style and series style of the ORC are considered. The results show that for some cases the multistage configurations can achieve higher efficiency at low temperature.

2.2 System topology selection

2.2.1 Rankine cycle fluid

There are two important aspects to consider when selecting the working fluid of the Rankine cycle solar power system:

1. Select the working fluid that is conducive to the optimization of the cycle efficiency
   For a Rankine cycle solar system, the collector efficiency reduces with operating temperature, and the Rankine cycle efficiency increases with operating temperature, there exists an optimal operating temperature as illustrated in Figure 2-13. The working fluid should be conducive to achieve the optimal operating temperature.
2. The working fluid state matches the heat transfer fluid state, if heat transfer fluid is used.
   On the one hand, the operating temperature of the working fluid should be lower than the collecting temperature of the HTF. On the other hand, the operating temperature of the working fluid should not be much lower than the collecting temperature of the HTF to avoid large exerge loss during the heat exchange process.

Based on the advantages and disadvantages of water and organic fluid as the working fluid of Rankine cycle, it is clear that, for low operating temperature and small capacity distribution power generation, organic fluid will be a better choice, otherwise water is the better one. Bao and Zhao[85] presented a comprehensive review of working fluid selection (including pure fluids and mixtures). In this review, many factors such as operating conditions,

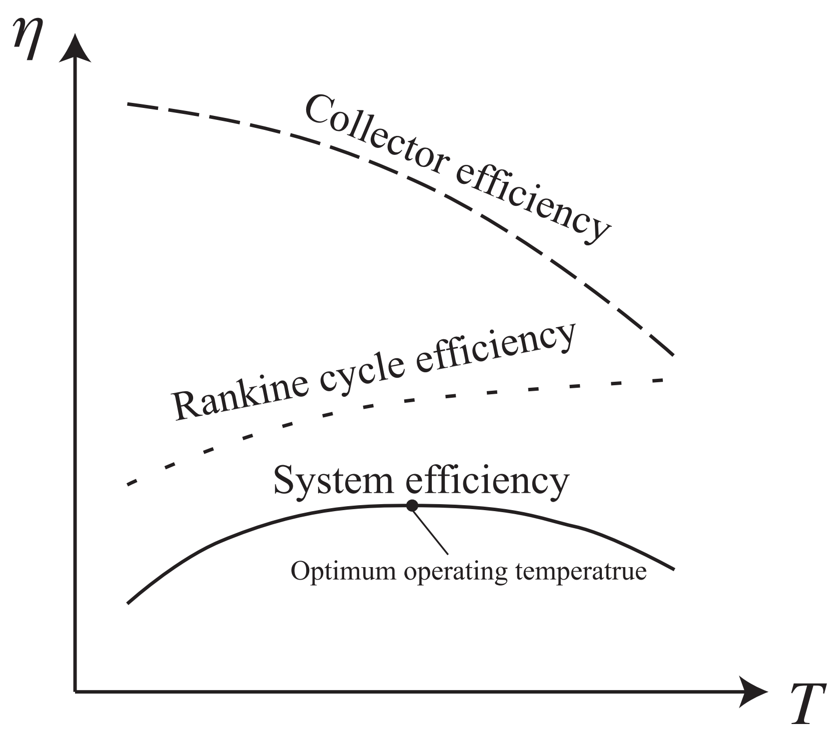

Figure 2-13 Collector and Rankine cycle efficiency variation with operating temperature

working fluid characteristics, equipment structures and environmental safety considerations were considered. It has to be mentioned that the types of working fluids (mainly dry or wet) will affect the operation and layout of the system.

2.2.2 Solar chimney

Section 2.1.2 shows the idea of coupling solar chimney to concentrated solar thermal power generation technologies. However, the efficiency of current solar chimney system is still very low. Primary design data of solar chimney power plants with different location, different chimney height and collector height are shown in Table 2.2[86]. The preliminary design parameters in Table 2.2 are selected and determined for a nominal solar intensity of $1000\,\mathrm{W/m^2}$ and the nominal plant power of 5 MW. From the table, it can be found that the chimney efficiency and total efficiency are very low and the technology is still in the development stage.

Besides, a solar chimney is costly and requires vast land, which is adverse to the future deployment of solar cascade demo system. With these considerations, the solar chimney

Table 2.2 Results of SEA models under specified parameters

	Ottawa	Winnipeg	Edmonton	Schlaich
Collector diameter (m)	-	-	-	1110
Collector area (m^2)	950000	950000	950000	950000
Chimney height (m)	123	60	35	547
Collector height (m)	848	975	1024	-
Chimney diameter (m)	54	54	54	54
Temperature rise in collector (°C)	25.9	25.9	25.9	25.9
Updraft velocity (m/s)	9.1	9.1	9.1	9.1
Total pressure head (Pa)	518.3	518.3	518.3	383.3
Average efficiency				
Collector (%)	56.00	56.00	56.00	56.24
Chimney (%)	1.82	1.82	1.82	1.45
Turbine (%)	77.0	77.0	77.0	77.0
Whole system (%)	0.79	0.79	0.79	0.63

plans are not adopted.

2.2.3 Collector series connection

Each type of collector has its own suitable temperature range. It is feasible to heat the HTF step by step using different types of collectors with series connection.

It can be a good choice to apply flat plate solar collectors and parabolic trough collectors in traditional solar tower power plant that uses water as the HTF (such as Solar One). As demonstrated in Figure 2-14, condensed water is heated by the flat plate solar collectors and feedwater is heated by the parabolic trough collectors. Flat plate collectors and parabolic trough collectors have much lower unit thermal cost compared to solar tower. The addition of flat plate collectors and parabolic trough collectors can effectively reduce the cost of the system.

A collector series connection is proposed in Section 2.1.3 (see Figure 2-7) depending

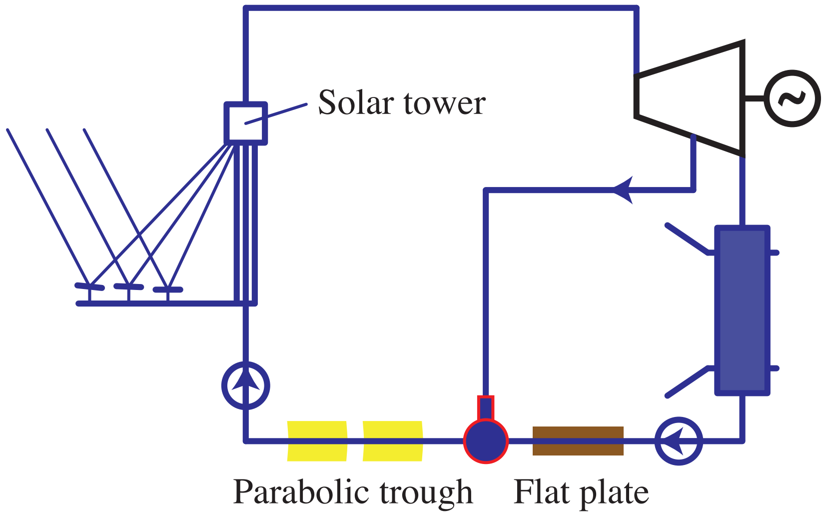

Figure 2-14 Schematic diagram of a cascade system using collector series connection

on the basic systems. In this configuration, air is heated in the trough collectors and dish receivers consequently. After providing heat for the Stirling engines, the hot air flows into the heat exchanger to provide heat for the Rankine cycle. However, this topology is not adopted due to the parabolic trough collectors. In this collectors, air is used as the HTF, which will lead to low efficiency due to low conductivity and low heat capacity.

2.2.4 Direct steam generation

Direct steam generation for solar thermal power generation has the advantage of having fewer components and no loss of temperature required with an intermediate transfer. Besides, it is clear that water is characterized by lower environmental risk than thermal oil so that leakages in a DSG power plant do not represent an environmental hazard [87]. Water has a lower freezing temperature than thermal oil and above all than solar salt: the efforts required to ensure adequate anti-freezing protection are significantly reduced. Water is also less corrosive than solar salt[88]. With both liquid and vapor in a receiver, however, extreme care must be taken in the design of the receiver to ensure that the radiant flux incident on that portion of the receiver containing vapor is less than the flux incident in the regions with liquid and where boiling is taking place. This is because the heat-transfer coefficient into a liquid is significantly higher than into superheated vapor. For similar values of solar flux, burnout of the receiver walls could occur in the regions where vapor exists on the other side of the receiver wall.

Many concentrating collector designs require that the receiver change attitude while the collector tracks the sun. This change of attitude increases the chances of high flux on portions of the receiver containing vapor. Two examples of solar Rankine power systems where the engine working fluid vapor is generated directly in the receiver are the Solar One Pilot Plant at Barstow, CA and the solar organic Rankine cycle module built by Ford Aerospace and Communications Corporation. Because Solar One is a central receiver system, the vertical-tube receiver remains stationary and liquid level control is relatively easy. The vertical tubes of the receiver are made of a material with a high melting point and thus can withstand high temperatures in the upper regions where vapor is being superheated. Tube burnout is avoided in the Ford Aerospace receiver design because the inner wall of the receiver is a copper shell with tubes wound around its exterior. The high thermal conductivity of the copper shell provides an averaging effect on receiver temperature, and superheat is attained without burnout of the receiver walls.

All the CSP commercial plants already built apply indirect steam generation, with the exception of the 5 MWe DSG Thai Solar One (TSE-1) plant in Thailand (Thailand, 2012)[89]. The reason for this universally accepted choice must be found in the difficulties related to the flow control and manufacturing of equipment to be used in the presence of a two-phase flow in the absorber tubes. The behavior of the two-phase flow inside the absorber tubes of a parabolic-trough collector forces the implementation of a complex and expensive control system and the use of fast water streams in order to avoid stratified flow.

Another problem related to the DSG is the high value of the steam pressure inside the receiver tubes that must match the turbine inlet pressure for less than pressure losses. Indeed, handling the moveable and flexible components forming the receiver tube of the collector in case of high-pressure values was one of the main problems to be faced at the early stages of the DSG concept technology.

Apply direct steam generation may be a better choice in the cascade system, however, it is not adopted for the cascade system for its immaturity.

2.2.5 Heat exchanger between circuits

Section 2.1.5 introduces two types of heat exchangers that may be applied in the solar thermal cascade system – the air-oil heat exchanger (see in Figure 2-15) and the air-water heat exchanger (see in Figure 2-16).

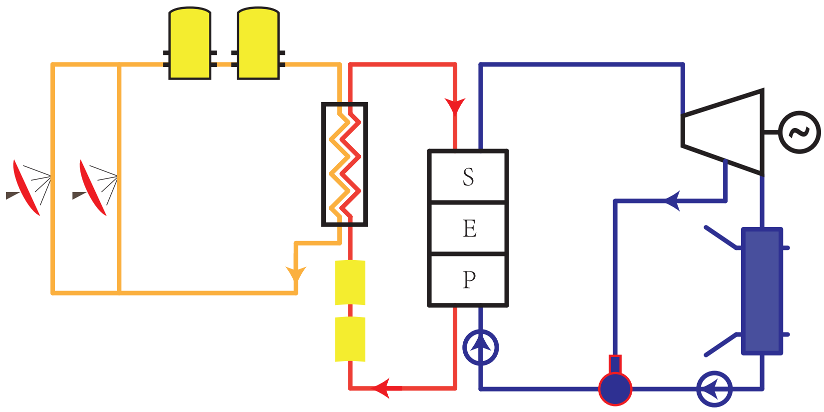

Figure 2-15　Schematic diagram of a solar system using air-oil heat exchanger

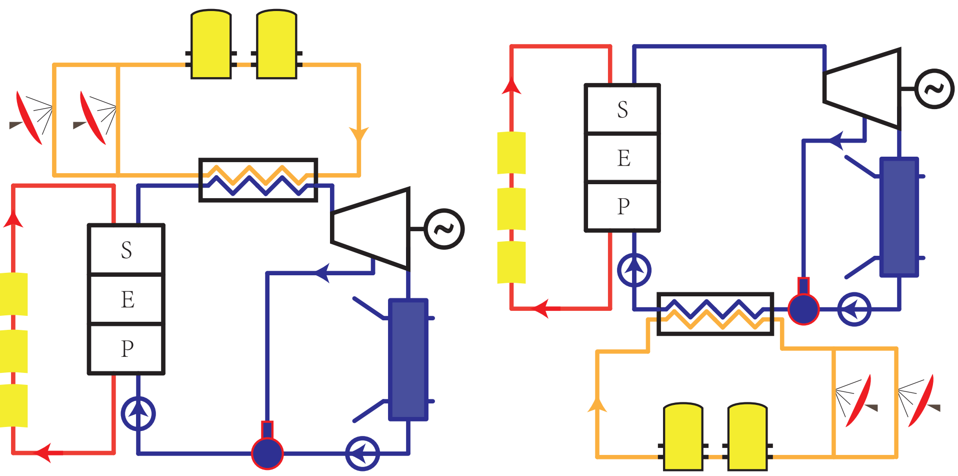

(a)　　　　　　　　　　　　　　(b)

Figure 2-16　Schematic diagrams of two kinds of solar systems using air-water heat exchanger

For the first type, air provides heat for oil. It is not economic for several reasons. First, The temperature of the heat transfer oil can not be further increased. The temperature of the oil is not limited by the parabolic trough collectors. The temperature of the oil is constrained by the oil properties and heat collecting temperature of the trough collectors can exceed this value. In high temperature conditions, oil may deterioration, evaporation, decompose, which has a negative impact on the stable and safe operation of the system. Second, using dish to provide heat for the oil is not suitable since the dish is designed for higher temperature collections and it's less cost-effective compared with parabolic trough.

For the second type, air provides heat for water. Two kinds of solar systems using air-water heat exchanger can be found in Figure 2-16. Figure 2-16a shows the scheme that air after the Stirling engine is used to overheat the steam. It's feasible since the air can increase the average temperature of the endothermic process of the water to increase the efficiency of Rankine cycle. On the other hand, in the traditional solar trough system, the main steam temperature is limited by the oil, which is not conductive to Rankine cycle efficiency. In this proposed cascade system, the main steam temperature of the Rankine cycle can be raised to be higher than 400°C to eliminate the negative effect of the oil. This is the scheme that will be discussed in detail in the next few chapters. Figure 2-16b shows the scheme that air after the Stirling engine is used to preheat the feed water. It is not a good choice since the temperature difference of the heat transfer process is large and it provides no benefits to increase the inlet temperature of the steam turbine.

2.2.6 Heat recovery between cycles

As it is mentioned in section 2.1.6, different thermodynamic cycles work at different optimum working temperatures. Since each thermodynamic cycle has endothermic and exothermic processes, a bottoming cycle may use the released heat of a topping cycle.

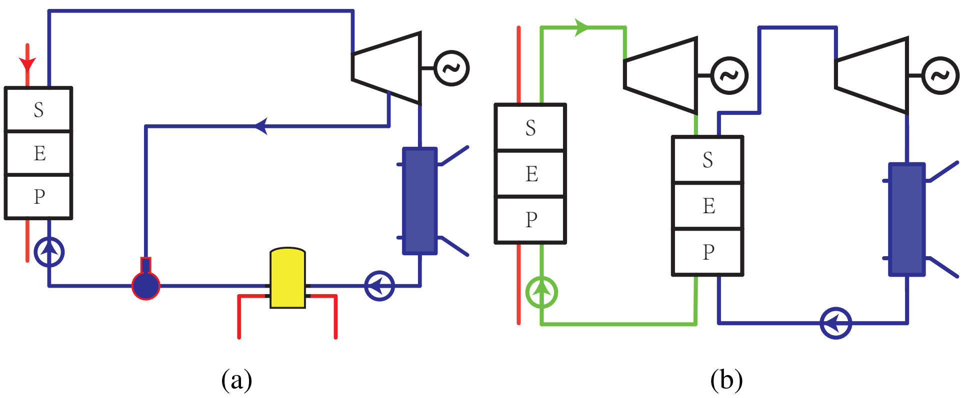

Figure 2-17 Two configurations with heat recovery between thermodynamic cycles

In our basic systems (see Figure 2-1), Rankine cycle and Stirling cycle can be coupled for cascade usage. Figure 2-17 shows two configurations of the cascade systems with heat recovery between cycles. For a traditional Stirling engine, to enhance the performance, cooling water is used to absorb the heat released by the engine. The absorbed heat is wasted without reuse. In Figure 2-17a, condensate of the Rankine cycle is used to cool the Stirling engine. Rejected heat of the Stirling cycle can be reused by Rankine cycle. For organic Rankine cycles, different working fluids determine the working temperature zones. It is feasible to reuse the condensation heat of an organic Rankine cycle by another organic Rankine cycle. In Figure 2-17b, two organic Rankine are coupled together for power generation. The bottoming cycle uses the condensation heat of the topping cycle for preheating, evaporation and superheating.

2.3 Selected system topology

Considered all the conditions in section 2.1 and section 2.2, two system topologies are chosen for this research as shown in Figure 2-18.

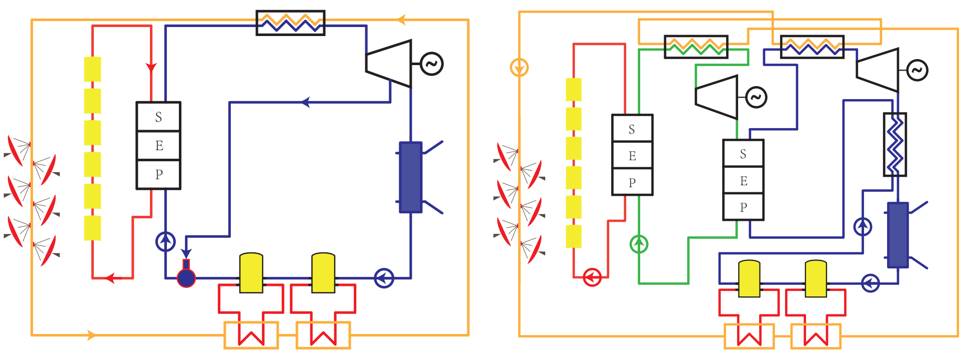

(a) (b)

Figure 2-18 Two selected typical cascade system

In Figure 2-18a, the cascade system has the following features:

- *Multiple types of collectors.* Trough collectors are applied for lower temperature heat collection and Dish collectors are applied for higher temperature heat collection. This helps to reduce the cost and improve the efficiency.
- *Multiple types of thermodynamic cycles.* Rankine cycle is applied for lower tempera-

ture heat utilization. Stirling cycle is applied for higher temperature heat utilization.

- *Air-water heat exchanger.* An extra air-water heat exchanger is applied to increase the temperature of the main steam, which helps to improve the efficiency of Rankine cycle. On the other hand, it can overcome the disadvantage of low limit temperature of heat transfer oil in traditional solar trough systems, which helps to achieve higher main steam parameters than traditional solar trough systems.
- *Condensate for Stirling engine cooling.* Condensate of the Rankine cycle is used to cool the Stirling engine. Rejected heat of the Stirling cycle can be reused by Rankine cycle, which helps to improve the overall system efficiency.

In Figure 2-18b, the cascade system also has the features mentioned above. Besides, it uses different kinds of organic fluid as the working fluid, which adapts more general working temperature for solar energy systems. Figure 2-19 shows a calculation example of the cascade system.

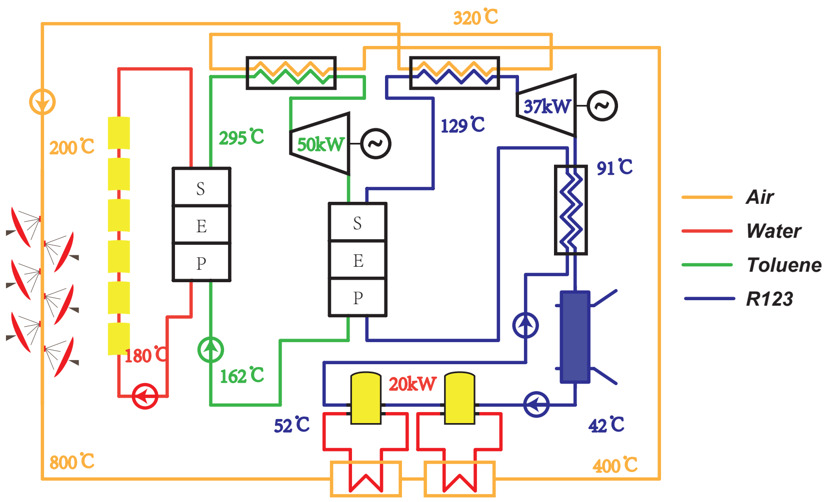

Figure 2-19 A calculation example of cascade system in Figure 2-18b

Both cascade systems are modeled for investigation, however, considering the more extensive application of the steam Rankine cycle, the system as described in Figure 2-18a will be used as the main research content in the following chapters.

Chapter 3 Modeling

To investigate the performance of the proposed cascade systems, mechanism models of the systems were developed with EES (Engineering Equation Solver) and MATLAB. Bottom-up design method was used for the system modeling. Firstly, the mechanism models of the developed in EES to validate the theoretical relationships of the models. Secondly, the component models were developed in MATLAB by using object-oriented method. It makes full use of inheritance and polymorphism to ensure both the independence and the relevance of the components. Three circuits, air circuit, water circuit and oil circuit, were developed with some specific state parameters in some key components. Energy-based models of these key components were created on the basis of their thermodynamic behavior, heat transfer and the second law.

The following parts introduce models of some key components.

3.1 Component modeling

3.1.1 Parabolic trough collector

Parabolic trough collector consists of a reflector and a receiver. The reflector (mirror) reflects direct solar radiation and concentrates it onto a receiver tube located in the focal line of the parabola. The receiver is typically a metal absorber tube with high absorption rate coating. An outer glass tube is used outside the absorber tube to reduce thermal losses and the space between the absorber tube and the glass tube is usually drawn into a vacuum to further reduce the thermal losses.

Optical loss exists in the reflection process due to optical efficiency terms. The reflection terms can be listed as bellow[5]:

- Shadowing factor
- Tracking error
- Geometry error
- Clean mirror reflectance
- Dirt on mirrors

- Unaccounted errors

Another term, incident angle modifier $K(\theta)$, should be concerned when the solar irradiation is not normal to the collector aperture. It is a function of the solar incidence angle to the normal of the collector aperture (θ).

The equation was determined from trough collector testing conducted at SNL[6].

$$K(\theta) = \cos\theta + 0.000884\theta - 0.00005369\theta^2 \tag{3.1}$$

The optical losses are associated with five parameters (see Figure 3-1):

(1) Reflectivity, ρ: only a fraction of the incident radiation is reflected towards the receiver. The fraction is determined by the reflector type and dirt condition. Reflectivity of commercial parabolic trough mirrors can be assumed to be 0.9 for washed mirrors.

(2) Intercept factor, γ: a fraction of the direct solar radiation reflected by the mirrors does not reach the glass cover of the absorber tube due to either microscopic imperfections of the reflectors or macroscopic shape errors in the parabolic trough concentrators (e.g., imprecision during assembly). These errors cause reflection of some rays at the wrong angle, and therefore they do not intercept the absorber tube. These losses are quantified by an optical parameter called the intercept factor, γ, that is typically 0.95 for a collector properly assembled.

(3) Transmissivity of the glass tube, τ: only a fraction of the direct solar radiation reaching the glass cover of the absorber pipe is able to pass through it. The ratio between the radiation passing through the glass tube and the total incident radiation on it, gives transmissivity τ, which is typically 0.93.

(4) Absorptivity of the absorber selective coating, α_{abs}: this parameter quantifies the amount of energy absorbed by the steel absorber pipe, compared with the total radiation reaching the outer wall of the steel pipe. This parameter is typically 0.95 for receiver pipes with a cermet coating, whereas it is slightly lower for pipes coated with black nickel or chrome.

(5) Soiling factor, F_e: because of the dirt on reflectors will reduce the reflectivity, it needs to concern the soiling factor. The soiling factor F_e takes into account the progressive soiling of mirrors and glass tubes after washing.

The energy pass through the glass tube to the receiver can be obtained by

$$P = I_r w_{tc} L_{tc} \rho\gamma\tau F_e K(\theta) \tag{3.2}$$

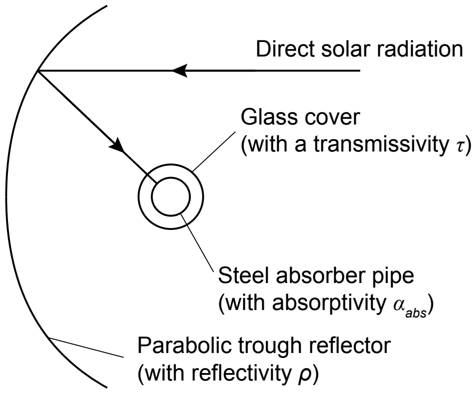

Figure 3-1 Some of the optical parameters of a parabolic trough

The solar energy absorbed by the absorber occurs very close to the outer surface, to simplify the absorption process, it is treated as a uniform heat flux q''.

$$q'' = \frac{P}{\pi d_o L_{tc}} = \frac{I_r w_{tc} \rho \gamma \tau F_e K(\theta)}{\pi d_o} \tag{3.3}$$

Assume overall heat transfer coefficient $U(T_{abs})$ is uniform for whole length of the collector, and the heat transfer correlation in Appendix B can be used. Figure 3-2 shows the schematic diagram of the thermal analysis of the absorber pipe.

$$\frac{T_o - T_{amb} - \dfrac{q''}{U(T_{abs})}}{T_i - T_{amb} - \dfrac{q''}{U(T_{abs})}} = \exp(-\frac{U(T_{abs})PL}{\dot{m}c_p}) \tag{3.4}$$

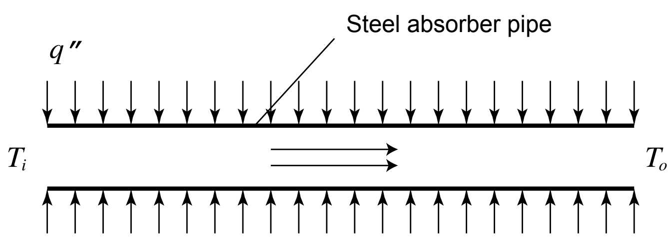

Figure 3-2 Schematic diagram of the absorber pipe

Since the Nusselt number Nu in the pipe is very large (about 1×10^4), small temperature difference exists between the absorber and oil. So the average fluid temperature $(T_i + T_o)/2$ can be used as the average value of T_{abs}, and $U(T_{abs})$ can be obtained by the a second-order polynomial function given by Romero and Zarza[90]. The length L required to get the required number of trough collectors in a row can be obtained from Equation 3.4.

3.1.2 Parabolic dish collector

Parabolic dish collector consists of a reflector and a receiver. The reflector (mirror) tracks the sun to reflect direct solar radiation and concentrates it onto a receiver located at the focal point of the reflector. Two axes tracking system needs to be applied for the reflector to continuously follow the daily path of the sun.

In a traditional dish-Stirling system, a Stirling engine is located at the focal point. The Stirling engine has a receiver to absorb the thermal energy from the concentrated sunlights. The receiver consists of an aperture and an absorber. The aperture in a Stirling receiver is located at the focal point of the reflector to reduce the radiation and convection losses. The absorber absorbs the solar radiation and transfers the thermal energy to the working gas of the Stirling engine. An electrical generator, directly connected to the crankshaft of the engine, converts the mechanical energy into electricity.

In the proposed cascade system, a volumetric receiver is located on the focal point. Spiral tube is located in the receiver to absorb the concentrated solar energy. Air (or nitrogen, is used as the heat transfer fluid) flows trough the tube to transfer the absorbed energy as the heat source of Stirling engine(s).

The reflector is a key element of the systems. The curved reflective surface can be manufactured by attached segments, by individual facets or by a stretched membranes shaped by a continuous plenum. In all cases, the curved surface should be coated or covered by aluminum or silver reflectors.

Two different methods[91] are applied for the sun tracking systems:

- Azimuth elevation tracking by an orientation sensor or by calculated coordinates of the sun performed by the local control.
- Polar tracking, where the concentrator rotates about an axis parallel to the earth’s axis rotation.

A dish reflector product of SES (Stirling Energy System) is used in this cascade system, and its key parameters can be found in Table 3.1. The structure of the receiver is shown in Figure 3-3.

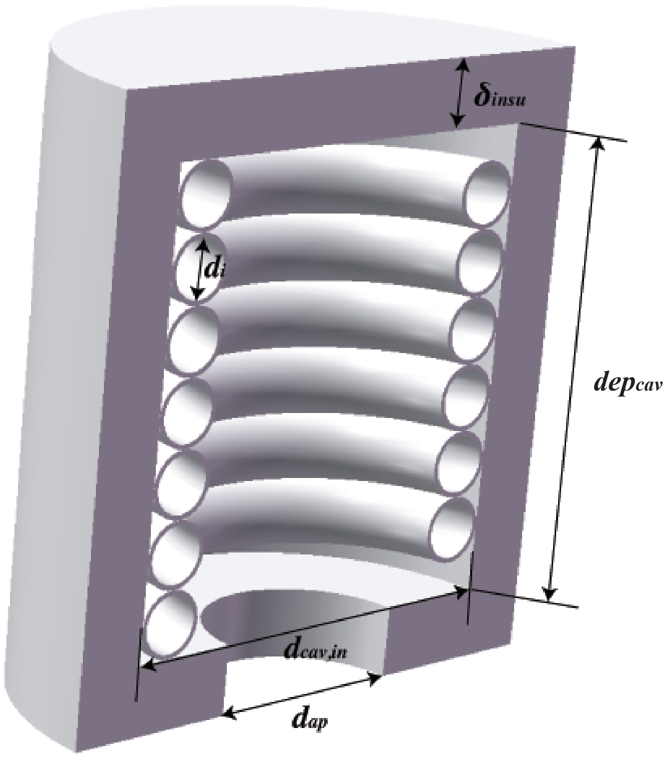

Figure 3-3 The structure of the dish receiver

The dish receiver model concerns the losses include: collector losses due to mirror reflectivity, receiver intercept losses, losses due to shading, and thermal losses. Thermal losses take the largest portion of all those losses, which are due to conduction, convection and radiation. Figure 3-4 shows the thermal network of dish receiver, which concerns the losses:

- Radiation losses reflected off of the receiver cavity surfaces and out of the receiver through the aperture. ($q_{rad,ref}$)
- Conductive losses through the receiver insulating layer. ($q_{cond,tot}$)
- Free convection from the cavity in the absence of wind. ($q_{conv,free}$)
- Forced convection in the presence of wind. ($q_{conv,forc}$)
- Emission losses due to thermal radiation emitted from the receiver aperture. ($q_{rad,emit}$)

To solve the thermal network in Figure 3-4, correlations and relationships of the heat fluxes should be clear.

Table 3.1 Key parameters of the dish collector

Parameter	Value	Parameter	Value	Parameter	Value
d_{cav}	0.46 m	ϵ_{insu}	0.6	θ_{dc}	45°
δ_{insu}	0.075 m	α_{cav}	0.87	γ	0.97
dep_{cav}	0.23 m	δ_a	0.005 m	$\eta_{shading}$	0.95
d_{ap}	0.184 m	$d_{i,1}$	0.07 m	ρ	0.91
λ_{insu}	0.06 W/(m · K)	A_{dc}	87.7 m^2		

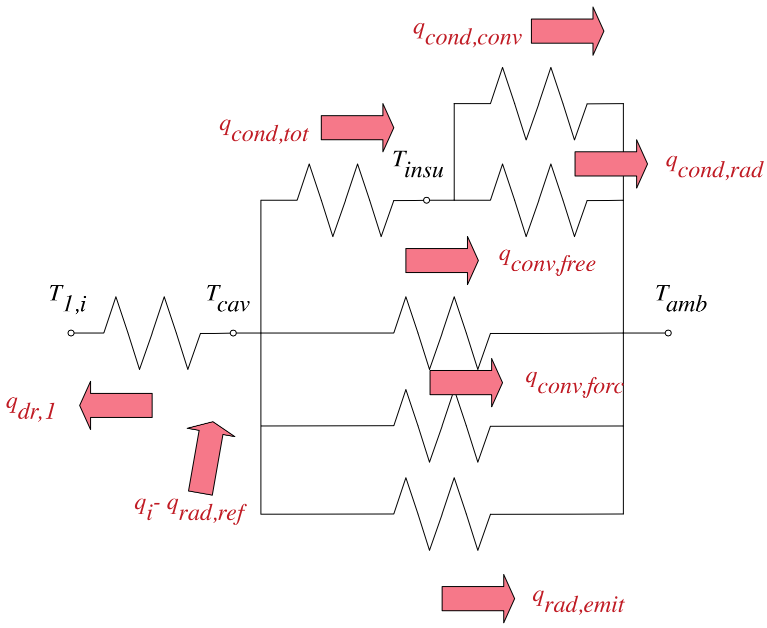

Figure 3-4 Thermal network of dish receiver

(1) *Inlet energy from the reflector,* q_i

To simplify the model, influences made by receiver blocking and imperfection track are ignored.

$$q_i = I_r A_{dc} \gamma \eta_{shading} \rho \tag{3.5}$$

In Equation 3.5, γ is the intercept factor, $\eta_{shading}$ is the shading factor between different collectors, ρ is the reflectivity of the reflector.

(2) *Heat exchange between the HTF and the dish absorber,* $q_{dr,1}$

The heat transfer process between the HTF and the dish absorber is simplified to a heat exchange process of a flow in a uniform temperature heat pipe. So $q_{dr,1}$ can be written as

$$q_{dr,1} = h_{dr,1} A_{dr,1} \Delta T_{ln,dr,1} \tag{3.6}$$

where

$$h_{dr,1} = Nu_{tube} \lambda_{dr,1} / d_{i,1} \tag{3.7}$$

$$Nu_{tube} = c_r Nu'_{tube} \tag{3.8}$$

For helical spiral pipe, multiplier c_r based on curvature ratio can be written as[92]

$$c_r = 1 + 3.5 \frac{d_{i,1}}{d_{cav} - d_{i,1} - 2\delta_a} \tag{3.9}$$

Nu'_{tube} is the Nusselt number of straight circular tube, which can be obtained by[93]

$$Nu'_{tube} = 0.027 Re_{tube}^{0.8} Pr_{tube}^{1/3} (\mu_{tube}/\mu_{tube,w})^{0.14} \tag{3.10}$$

and the logarithmic mean temperature difference $\Delta T_{ln,dr,1}$ can be written as

$$\Delta T_{ln,dr,1} = \frac{(T_{cav} - T_{dc,i}) - (T_{cav} - T_{dc,o})}{\ln \dfrac{T_{cav} - T_{dc,i}}{T_{cav} - T_{dc,o}}} \tag{3.11}$$

(3) *Radiation losses reflected off the receiver,* $q_{rad,ref}$

$$q_{rad,ref} = (1 - \alpha_{eff}) q_i \tag{3.12}$$

where α_{eff} is the effective absorptivity of the receiver.

$$\alpha_{eff} = \frac{\alpha_{cav}}{\alpha_{cav} + (1 - \alpha_{cav}) \dfrac{A_{ap}}{A_{cav}}} \tag{3.13}$$

α_{cav} is the absorptivity of the cavity, A_{cav} is the cavity area, A_{ap} is the aperture area.

(4) *Conductive losses through the receiver insulating layer,* $q_{cond,tot}$

$$q_{cond,tot} = 2\pi\lambda_{insu} dep_{cav} \frac{T_{cav} - T_{insu}}{\ln((d_{cav} + 2\delta_{insu})/d_{cav})} \tag{3.14}$$

where T_{cav} is the temperature of the cavity wall, T_{insu} is outside temperature of the insulation wall.

(5) *Convection losses from the receiver insulating layer,* $q_{cond,conv}$

$$q_{cond,conv} = h_{insu} A_{insu}(T_{insu} - T_{amb}) = \frac{k_{insu} Nu_{insu} A_{insu}(T_{insu} - T_{amb})}{d_{cav} + 2\delta_{insu}} \tag{3.15}$$

where Nu_{insu} can be obtained by the correlation for flow over a circular cylinder.[94]

(6) *Radiation losses from the receiver insulating layer,* $q_{cond,rad}$

$$q_{cond,rad} = \epsilon_{insu} A_{insu} \sigma (T_{insu}^4 - T_{amb}^4) \tag{3.16}$$

(7) *Free convection from the cavity in the absence of wind,* $q_{conv,free}$

Ma[95] conducted tests to determine the free convection losses from the receiver for alternative setups, and the data were consistent with Stine and McDonald's free convection correlation. It is assumed that forced convection is independent of free convection in the receiver, so the total convection losses can be represented as the total of the free and forced convection losses as shown in Figure 3-4.

$$q_{conv,free} = h_{free} A_{cav}(T_{cav} - T_{amb}) \tag{3.17}$$

where $h_{free} = k_{film} Nu_{free}/\overline{d_{cav}}$, $\overline{d_{cav}}$ is the effective diameter of the cavity, $\overline{d_{cav}} = d_{cav} - 2d_i - 4\delta_a$. $d_i =$0.066 m

(8) *Force convection from the cavity in the presence of wind,* $q_{conv,forc}$

$$q_{conv,forc} = h_{forc} A_{cav}(T_{cav} - T_{amb}) \tag{3.18}$$

Wu et al.[96] present a comprehensive review and systematic summarization of convection heat loss from cavity receiver in parabolic dish solar thermal power system. And we choose the correlation presented by Leibfried and Ortjohann[97]. This correlation gives an extended model of Koenig and Marvin[98] and Stine and Diver[99] with better results.

For forced convection loss, side-on wind convection loss model given by Ma[95], which is independent of the aperture orientation, is used

$$h_{forc} = 0.1967 v_{wind}^{1.849} \tag{3.19}$$

(9) *Emission losses due to thermal radiation emitted from the receiver aperture,* $q_{rad,emit}$
The emissivity is set equal to the effective absorptivity of the cavity (gray body),

$$\epsilon_{cav} = \alpha_{eff} \tag{3.20}$$

$$q_{rad,emit} = \epsilon_{cav} A_{ap} \sigma (T_{cav}^4 - T_{amb}^4) \tag{3.21}$$

From Figure3-4, it can be found that

$$q_{dr,1} = q_i - q_{rad,ref} \tag{3.22}$$

$$q_{dr,1} = q_{cond,tot} + q_{conv,free} + q_{conv,forc} + q_{rad,emit} \tag{3.23}$$

$$q_{cond,tot} = q_{cond,conv} + q_{cond,rad} \tag{3.24}$$

So the temperature nodes in the thermal network can be solved by these equations. $q_{dr,1}$ can be obtained by Equation 3.6.

3.1.3 Stirling engine

3.1.3.1 Theoretical Stirling cycle

In a Stirling cycle, there are two isothermal processes that exchange heat with heating and cooling fluids, two isochoric processes that exchange heat with regenerator. In Figure 3-5, the heat absorbed by regenerator in process 4-1 is reused in process 2-3, but only able to heat the working gas from 2 to 3' due to the imperfect regeneration. e is defined as the regenerator effectiveness[100,101], $e = \frac{T_R - T_L}{T_H - T_L}$, where T_H is the temperature in the hot space, T_L is the temperature in the cold space, T_R is the effective working fluid temperature in the regenerator.

In order to obtain a simplified analytical model, several simplifications were made:

- The working gas in Stirling engines obeys the idea gas law.
- No heat loss to the environment for Stirling engines.
- Overall heat transfer coefficients of the fluids are constant.

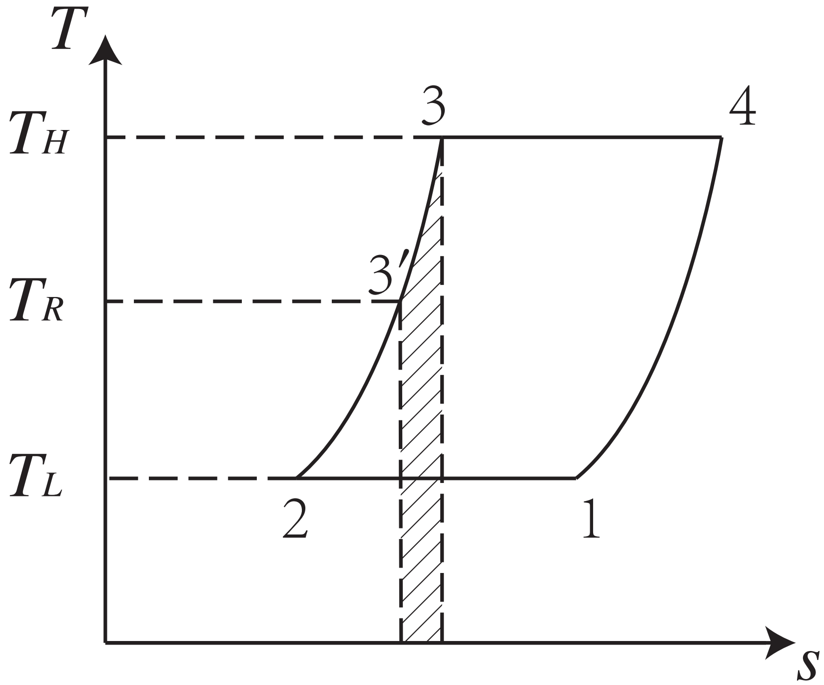

Figure 3-5 T-s diagram of a Stirling cycle

- A symmetrical regenerator behavior is assumed[100,101] so that a simple effectiveness can be obtain by $T_R = \frac{T_H - T_L}{\ln(T_H/T_L)}$.

To consider internal irreversibilities in Stirling cycle made by dead volumes, total dead volume V_D can be divided into heater dead volume V_{DH}, regenerator dead volume V_{DR} and cooler dead volume V_{DC}.[102], There exists a factor K to describe the dead volumes under different temperatures. K is relevant with temperatures in the process and regenerator effectiveness.

$$K = \frac{V_{DH}}{T_H} + \frac{V_{DR}}{T_R} + \frac{V_{DC}}{T_L} \tag{3.25}$$

For the isothermal compression process 1-2, the output work

$$W_{12} = \int_{V_E+V_C}^{V_E} p_{12} dV = -mRT_L \ln \frac{V_E + V_C + KT_L}{V_E + KT_L} \tag{3.26}$$

For the isothermal expansion process 3-4, the output work

$$W_{34} = \int_{V_E}^{V_E+V_C} p_{34} dV = mRT_H \ln \frac{V_E + V_C + KT_H}{V_E + KT_H} \tag{3.27}$$

Define $\gamma_H = \frac{V_E+V_C+KT_H}{V_E+KT_H}$, and $\gamma_L = \frac{V_E+V_C+KT_L}{V_E+KT_L}$, so in a cycle, the theoretical output work

$$W_{th} = W_{12} + W_{34} = mR(T_H \ln \gamma_H - T_L \ln \gamma_L) \tag{3.28}$$

For the isochoric heating process 3'-3, the absorbed heat

$$Q_{3'3} = nc_v(T_H - T_R) = \frac{1-e}{k-1} mR(T_H - T_L) \tag{3.30}$$

For the the isothermal expansion process 3-4, the absorbed heat

$$Q_{34} = W_{34} = mRT_H \ln \gamma_H \tag{3.31}$$

In a cycle, the theoretical absorbed heat

$$Q_{th} = Q_{3'3} + Q_{34} = \frac{1-e}{k-1} mR(T_H - T_L) + mRT_H \ln \gamma_H \tag{3.32}$$

3.1.3.2 Irrevisibilities and losses

(1) Non-ideal heat transfer effect

Because of non-ideal heater and cooler, the working fluid temperature (T_H/T_L) in these two heat exchangers is less/higher than the wall temperature (T_{hw}/T_{cw}), respectively. And T_H and T_L can be corrected by the wall temperatures as follows:

$$T_H = T_{hw} - \frac{Qs_{se}}{h_h A_{hw}} \tag{3.33}$$

$$T_L = T_{cw} + \frac{(Q-W)s_{se}}{h_c A_{cw}} \tag{3.34}$$

The heat transfer coefficient can be obtained using the following correlation[1]:

$$h_{h,c} = \frac{\mu c_p f_{Re}}{2D_{h,c} Pr_{h,c}} \tag{3.35}$$

where f_{Re} is a Reynolds friction factor defined as:

$$f_{Re} = 0.0791 {Re_{h,c}}^{0.75} \tag{3.36}$$

$Re_{h,c}$, $Pr_{h,c}$ and $D_{h,c}$ are Reynolds number, Prandtl number and hydraulic diameter of the heater/cooler exchanger.

(2) Effect of pressure drop

Pressure drops in the heat exchangers cause power losses of the Stirling engine. The pressure drops can be obtained by[103]:

$$\Delta p = -\frac{2 f_{Re} \mu u V}{d^2 A} \tag{3.37}$$

where u is the working gas speed, V is volume, A is flow cross-section area.

The net power loss of the Stirling engine due to pressure drop of the heat exchangers can be evaluated by:

$$W_{pd} = \oint \sum_{i=E,C} (\Delta p_i \frac{dV_i}{d\theta}) d\theta \tag{3.38}$$

(3) Effect of finite speed of piston and mechanical friction

Due to the finite speed of piston, the pressure on the piston surface is different from the pressure of expansion and compression spaces. It has been demonstrated that the pressure on the piston surface in the expansion process is less than the mean pressure in the expansion space. Similarly, the pressure on the piston surface in the compression process is greater than the mean pressure in the compression space. This means the output work is less than the theoretical value. Besides, The output work also reduces due to mechanical friction. The output work loss due to finite speed of piston and mechanical friction can be obtained as follows[1]:

$$W_{fs} = \oint p(\pm \frac{a u_p}{c} \pm \frac{\Delta p_f}{p}) dV \tag{3.39}$$

where the sign (+) is used in the compression space, and the sign (-) is used in the expansion space. p is the mean pressure in the compression/expansion space, u_p is velocity of the piston, c is the average speed of molecules and Δp_f is the pressure loss due to mechanical friction. Δp_f, a and c can be obtained by[104]:

$$\Delta p_f = 0.97 + 0.009 s_{se} \tag{3.40}$$

$$a = \sqrt{3k} \tag{3.41}$$

$$c = \sqrt{3RT} \tag{3.42}$$

(4) Energy losses due to internal conduction

The temperature differs from the heater and cooler, heat losses from heater to cooler exists due to internal conduction through the walls of regenerator.[105] The internal conduction loss in a cycle can be obtained by follows:

$$Q_{id} = \frac{k_r A_r}{L_r s_{se}}(T_{hw} - T_{cw}) \tag{3.43}$$

where, k_r, A_r and L_r denote the regenerator matrix conductivity, regenerator length, and regenerator conductive area respectively.

(5) Energy losses due to shuttle conduction

The displacer shuttles between the expansion and compression space. It absorbs heat during the hot end of its stroke and releases it during the cold end of its stroke. This heat loss can be estimated as[106]:

$$Q_{sc} = 0.4\frac{Z^2 k_p D_p}{J L_d s_{se}}(T_H - T_L) \tag{3.44}$$

where, Z, k_p, D_p, J and L_d denote the displacer stroke, piston thermal conductivity, displacer diameter, gap between the displacer and the cylinder, and length of the displacer respectively.

So, in a Stirling engine, the total absorbed heat in a cycle

$$Q = Q_{th} + Q_{id} + Q_{sc} \tag{3.45}$$

the output work

$$W = W_{th} - W_{pd} - W_{fs} \tag{3.46}$$

Power of the Stirling engine

$$P = W s_{se} \tag{3.47}$$

Efficiency of the Stirling engine

$$\eta = W/Q \tag{3.48}$$

3.1.3.3 Model validation

Evaluation of the developed thermal model was performed by considering the GPU-3 Stirling engine as a case study. Design specifications of the GPU-3 Stirling engine are indicated in Table 3.2. The thermal efficiency and power of the proposed Stirling engine model was compared with previous thermal models and experimental data as shown in Table 3.3 and Table 3.4.

It can be found that the proposed model has much better agreement with the experimental results than previous thermal models at various rotation speeds and mean effective pressures. It is required to mention that in all thermal models both power W and input heat Q were determined by the thermal process of heat transfer between the wall and working gas. In the proposed model, W and Q are obtained by Equation 3.33 and 3.34. Therefore all the three parameters W, Q and η are determined by the thermal model and input parameters to the model. These input parameters includes heater, cooler, mean effective pressure, type of working gas and geometrical specification of the engine.

Table 3.3 and 3.4 indicate that when mean effective pressure of the engine increases from 2.76 MPa to 6.90 MPa, best performance (efficiency and power) prediction of the proposed model exists. When rotation speed increases from 16.67 Hz to 58.33 Hz, error in prediction of performance of the proposed model increases. The proposed model may have the best performance prediction at a low rotation speed, with mean effective pressure between 4.14 MPa and 5.52 MPa.

However, there is still some discrepancy between the the simulation results of proposed model and the experimental data. In the future researches, more accurate models of Stirling engine may be developed by considering other irreversibilities such as heat loss to the environment, gas spring hysteresis, and etc. It is worth pointing that there are more accurate Stirling engine models. For example, polytropic simulation models of Stirling engine show higher accuracy than our proposed model[1,107]. However, the model needs more costly calculations and the polytropic indexes are engine-specific.

3.1.3.4 Heat transfer between the engine and the fluids

For a Stirling engine thermal process, the wall temperatures of the heater and cooler are considered to be uniform and constant. The heat transferred between the wall and the fluids

Table 3.2 Design specifications of the GPU-3 Stirling engine[1,2]

Parameter	Value
Engine type	β
Working gas	Helium
Mass of the working gas	1.136 g
Heater	
Number of tubes	40
Tube external diameter	4.83×10^{-3} m
Tube internal diameter	3.02×10^{-3} m
Tube length (cylinder side)	0.1164 m
Tube length (regenerator side)	0.1289 m
Cooler	
Number of tubes	312
Tube external diameter	1.59×10^{-3} m
Tube internal diameter	1.09×10^{-3} m
Average tube length	4.61×10^{-2} m
Regenerator	
Number of regenerator	8
Regenerator internal diameter	2.26×10^{-2} m
Regenerator length	2.26×10^{-2} m
Diameter of regenerator tube	4×10^{-5} m
Material	Stainless steel
Volume	
Swept Vol. (expansion/compression)	120.82/114.13 cm^3
Clearance Vol. (expansion/compression)	30.52/28.68 cm^3
Dead Vol. (heater/cooler/regenerator)	70.28/13.18/50.55 cm^3

Table 3.3 Thermal efficiency of the models and experimental data (at T_{hw} =922 K and T_{cw} =288 K)

Rotation speed (Hz)	Mean effective pressure (MPa)	The simple analysis (variable Pr[103])			The adiabatic analysis (simple II[105])			The proposed Stirling engine model			Experimental efficiency[1]
		Value (%)	Error (%)	Average error (%)	Value (%)	Error (%)	Average error (%)	Value (%)	Error (%)	Average error (%)	Actual value (%)
16.67	2.76	38.72	18.22	17.90	32.48	11.98	12.85	28.16	7.66	12.10	20.50
25.00		36.16	15.46		31.21	10.51		27.75	7.05		20.70
33.33		33.79	15.79		29.45	11.45		27.43	9.43		18.00
41.67		31.48	16.28		27.45	12.25		27.17	11.97		15.20
50.00		29.12	17.32		25.21	13.41		26.94	15.14		11.80
58.33		29.74	24.34		22.89	17.49		26.74	21.34		5.40
25.00	4.14	35.65	10.85	11.46	32.29	7.49	8.28	27.29	2.49	6.65	24.80
33.33		33.52	9.62		30.40	6.50		26.94	3.04		23.90
41.67		31.48	10.18		28.39	7.09		26.65	5.35		21.30
50.00		29.45	11.25		26.33	8.13		26.39	8.19		18.20
58.33		27.40	15.40		24.21	12.21		26.17	14.17		12.00
41.67	5.52	31.20	8.70	10.82	28.59	6.09	8.11	26.24	3.74	7.48	22.50
50.00		29.33	10.53		26.62	7.82		25.97	7.17		18.80
58.33		27.44	13.24		24.62	10.42		25.73	11.53		14.20
50.00	6.90	29.07	10.37	11.73	26.61	7.91	9.19	25.62	6.92	9.05	18.70
58.33		27.29	13.09		24.67	10.47		25.37	11.17		14.20

Table 3.4 Output power of the models and experimental data (at T_{hw} =922 K and T_{cw} =288 K)

Rotation speed (Hz)	Mean effective pressure (MPa)	The simple analysis (variable Pr[103])			The adiabatic analysis (simple II[105])			The proposed Stirling engine model			Experiment (kW)[1]
		Value (kW)	Error (%)	Average error (%)	Value (kW)	Error (%)	Average error (%)	Value (kW)	Error (%)	Average error (%)	Actual value (kW)
16.67	2.76	1.796	119.02	272.03	1.772	116.10	254.71	0.861	4.98	104.84	0.82
25.00		2.555	128.13		2.500	123.21		1.253	11.88		1.12
33.33		3.215	165.70		3.117	157.60		1.632	34.88		1.21
41.67		3.769	211.49		3.615	198.76		2.001	65.37		1.21
50.00		4.195	303.37		3.973	282.08		2.362	127.12		1.04
58.33		4.505	704.46		4.203	650.54		2.715	384.82		0.56
25.00	4.14	3.844	114.75	259.70	3.761	110.11	158.41	1.818	1.56	39.83	1.79
33.33		4.856	120.73		4.708	114.00		2.362	7.36		2.20
41.67		5.734	136.94		5.501	127.31		2.890	19.42		2.42
50.00		6.462	174.98		6.126	160.68		3.405	44.89		2.35
58.33		7.030	306.36		6.573	279.94		3.908	125.90		1.73
41.67	5.52	7.645	133.08	180.02	7.334	123.60	164.91	3.742	14.09	43.68	3.28
50.00		8.655	163.87		8.206	150.18		4.401	34.18		3.28
58.33		9.470	243.12		8.858	220.94		5.045	82.79		2.76
50.00	6.90	10.788	174.50	287.04	10.223	160.13	263.63	5.362	36.44	97.75	3.93
58.33		11.840	399.58		11.071	367.13		6.140	159.07		2.37

is

$$(T_w - T)UdA = \dot{m}c_p dT \tag{3.49}$$

with $T(0) = T_i$, $T(A) = T_o$,

$$\frac{T_o - T_w}{T_i - T_w} = \exp(-\frac{UA}{\dot{m}c_p}) \tag{3.50}$$

For a Stirling engine, T_{hw} or T_{cw} can be used to substitute T_w to get the relationships between $T_{i,h}$, $T_{o,h}$ and T_{hw}, or $T_{i,c}$, $T_{o,c}$ and T_{cw} respectively.

$$\frac{T_{o,h} - T_{hw}}{T_{i,h} - T_{hw}} = \exp(-\frac{U_h A_h}{\dot{m}_h c_{p,h}}) \tag{3.51}$$

$$\frac{T_{o,c} - T_{cw}}{T_{i,c} - T_{cw}} = \exp(-\frac{U_c A_c}{\dot{m}_c c_{p,c}}) \tag{3.52}$$

Heat transferred from heating fluid to Stirling engine in a cycle

$$\dot{m}_h c_{p,h}(T_{i,h} - T_{o,h})/s_{se} = Q \tag{3.53}$$

Heat transferred from Stirling engine to cooling fluid in a cycle

$$\dot{m}_c c_{p,c}(T_{o,c} - T_{i,c})/s_{se} = Q - W \tag{3.54}$$

3.1.4 Steam generating system

The steam generating system can be divided into preheater, evaporator and superheater, they are collectively referred to as PES. They are all heat exchangers. It is assumed that, in these heat exchangers, the pressure of the fluid does not change significantly. It can be assumed to be equal to the pressure of the inlet pressure of the turbine. Besides, these heat exchangers do not exchange heat with the environment. To clearly understand the modeling process of these heat exchangers, an example of steam generating system as shown in Figure 3-6 is used for explanation. Figure 3-7 shows the T-Q diagram of the heat transfer process.

The modeling process of PES is the process of solving the unknown states of the state points. Notice that, the pressure of the fluids keeps constant in the heat transfer process. For

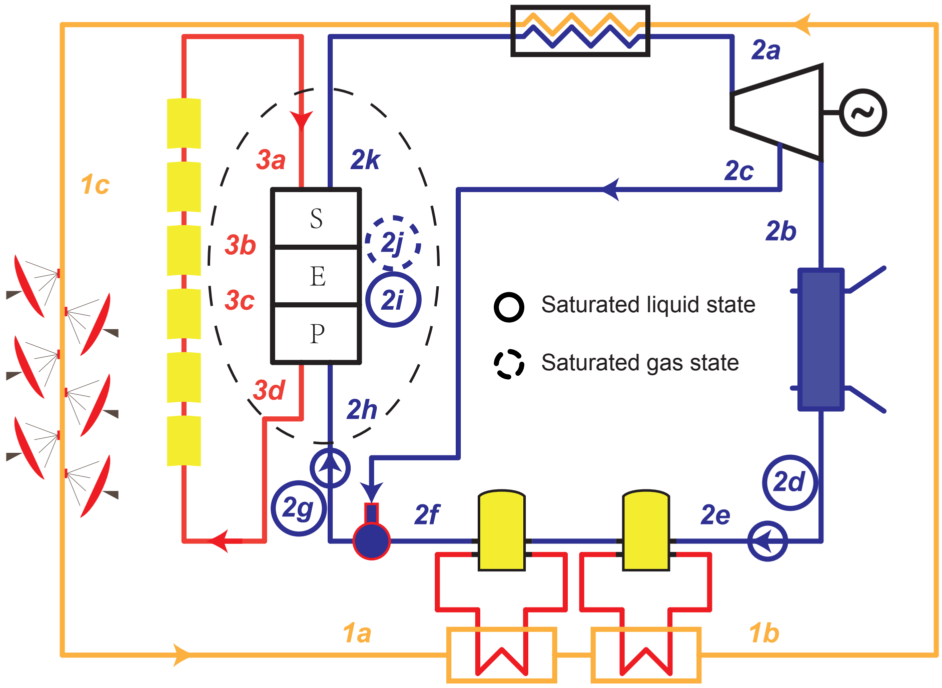

Figure 3-6 An example of steam generating system in a cascade system

an unsaturated state, known the temperature or enthalpy, the state is determined. This means, the temperature can be obtained by the enthalpy, and vice versa. For a saturated state, known the dryness (x) of the fluid, the state is determined.

For a typical PES modeling process as shown in Figure 3-6, $\dot{m}_2$, state $2h$ and state $2k$ are determined by the parameters of the turbine. State $3a$ is determined by the design parameters. State $2i$ and state $2j$ are determined by their dryness values.

(1) *Preheater*

The outlet of the heated fluid is saturated liquid ($x = 0$), so the outlet temperature T_{2i} and outlet enthalpy h_{2i} of the heated fluid are determined by the main pressure of the turbine, p_s.

$$\dot{m}_3(h_{3c} - h_{3d}) = \dot{m}_2(h_{2i} - h_{2h}) \tag{3.55}$$

(2) *Evaporator*

The outlet of the heated fluid is saturated gas ($x = 1$), so the outlet temperature T_{2j} and outlet enthalpy h_{2j} of the heated fluid are determined by the main pressure of the

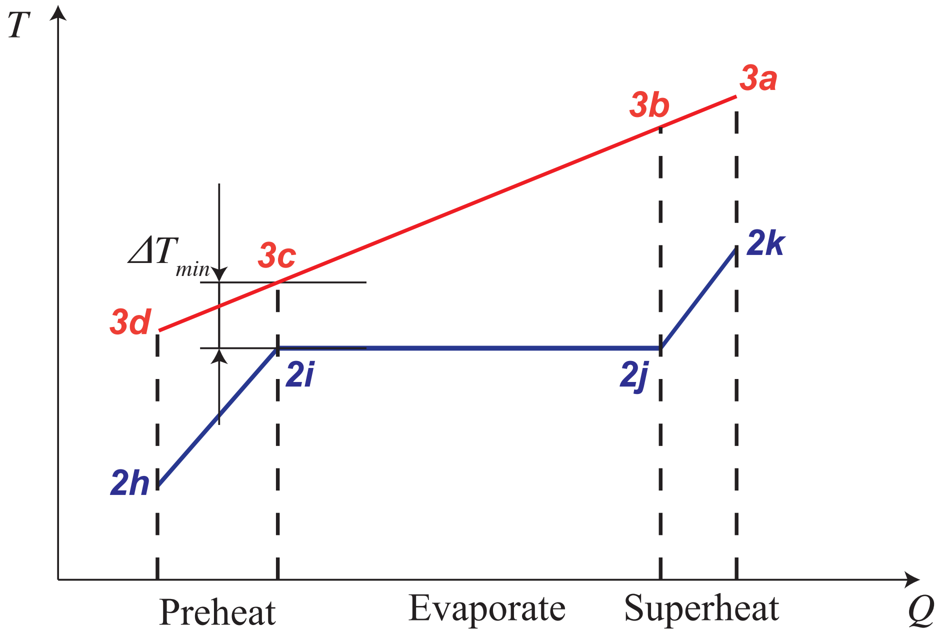

Figure 3-7 The steam generating process

turbine, p_s.

$$\dot{m}_3(h_{3b} - h_{3c}) = \dot{m}_2(h_{2j} - h_{2i}) \tag{3.56}$$

It has to be mentioned that, state $3c$ is determined by T_{3c}, which equals to $T_{2i} + \Delta T_{min}$. ($T_{3c} = T_{2i} + \Delta T_{min}$)

(3) *Superheater*

For the energy balance,

$$\dot{m}_3(h_{3a} - h_{3b}) = \dot{m}_2(h_{2k} - h_{2j}) \tag{3.57}$$

By solving the equations 3.55 to 3.57, $\dot{m}_3$, state $3b$ and $3d$ can be obtained.

3.1.5 Rankine power generation system

The Rankine power generation system consists of turbine, condenser, deaerator, generator and pumps. Based on different working fluids, there are two different kinds of Rankine power generation systems, steam Rankine power generation system and organic Rankine power generation.

3.1.5.1 Steam Rankine cycle

For steam Rankine cycle, deaerator is used to remove the oxygen and other non-condensable gases in the feedwater to steam generating system. Dissolved oxygen in feedwater will cause serious corrosion damage in steam generating system by forming oxides (rust) of the metal pipes. Dissolved carbon dioxide combines with water to form carbonic acid will cause further corrosion. The accumulation of the non-condensable gases will increase the heat transfer resistance, which is harmful for the heat exchangers. The extraction of the steam turbine provides heat for the deaerator.

Figure 3-8a shows the T-s diagram of the water circuit in the cascade system in Figure 3-6. Process $2a$-$2c$-$2b$ shows the heat process in the steam turbine. (see Figure 3-8b) State point $2b$ and $i, 2b$ have the same pressure, state point $2c$ and $i, 2c$. To simplify the inner process $2a$-$2c$-$2b$ of the turbine, same isentropic efficiency of steam turbine with different loads and in different stages is assumed, which means

$$\eta_{i,tb} = (h_{2a} - h_{2b})/(h_{2a} - h_{i,2b}) = (h_{2a} - h_{2c})/(h_{2a} - h_{i,2c}) \tag{3.58}$$

where $h_{i,2b}$ is determined by s_{2a} and p_c; $h_{i,2c}$ is determined by s_{2a} and p_e.

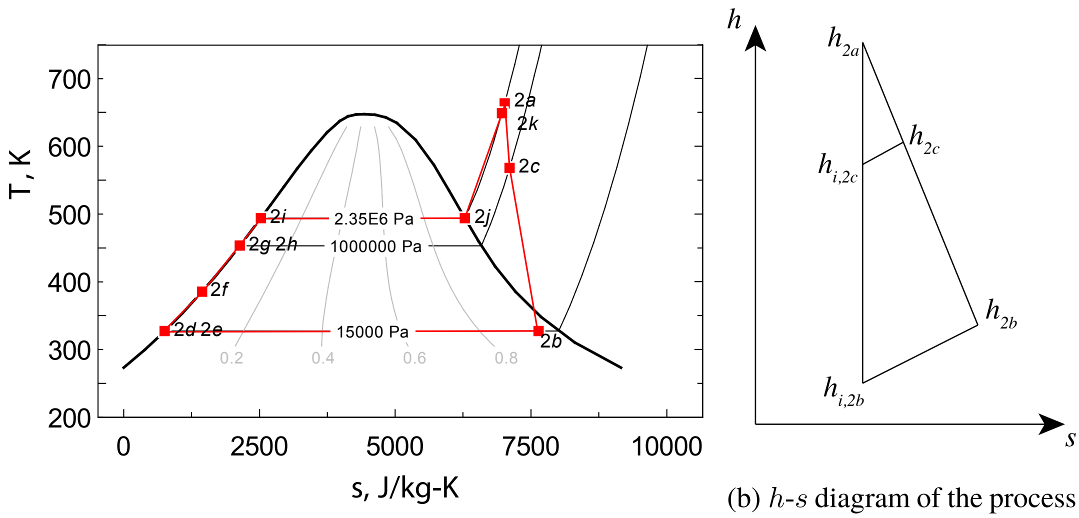

(a) T-s diagram of the water circuit

(b) h-s diagram of the process $2a$-$2c$-$2b$

Figure 3-8 T-s diagram of the water circuit and h-s diagram of the process $2a$-$2b$

The output power of the steam turbine

$$P_{tb} = (1-y)\,\dot{m}_2\,(h_{2a}-h_{2b}) + y\dot{m}_2\,(h_{2a}-h_{2c}) \tag{3.59}$$

Process $2b$-$2d$ shows the heat process in the condenser. The outlet water in the condenser is saturated water. The outlet temperature T_{2d} and outlet enthalpy h_{2d} are determined by the exhaust pressure of the turbine p_c. The released heat of the condenser

$$Q_{cd} = (1-y)\dot{m}_2(h_{2b}-h_{2d}) \tag{3.60}$$

State points $2c$, $2f$ and $2g$ have the same pressure (p_e, 1 MPa). The water at the outlet of the deaerator is saturated fluid, its enthalpy is determined.

$$yh_{2c} + (1-y)h_{2f} = h_{2g} \tag{3.61}$$

The total power of the pumps

$$P_{pu} = (1-y)\,\dot{m}_2\,(h_{2e}-h_{2d}) + \dot{m}_2\,(h_{2h}-h_{2g}) \tag{3.62}$$

where h_{2e} can be obtained by $\eta_{pu} = (h_{i,2e} - h2d)/(h_{2e} - h_{2d})$, h_{2h} can be obtained by $\eta_{pu} = (h_{i,2h} - h_{2g})/(h_{2h} - h_{2g})$. $h_{i,2e}$ is determined by s_{2d} and p_e, $h_{i,2h}$ is determined by s_{2g} and p_s.

The outlet water of the deaerator is saturated water ($x = 0$), so the outlet temperature T_{2g} and outlet enthalpy h_{2g} of the heated fluid is determined by pressure p_{2g}. For the deaerator, the outlet pressure equals to any of the inlet pressure.

$$p_{2g} = p_{2c} \tag{3.63}$$

Heat injected in the water circuit

$$Q_2 = (1-y)\,\dot{m}_2\,(h_{2f}-h_{2e}) + \dot{m}_2\,(h_{2a}-h_{2h}) \tag{3.64}$$

The efficiency of Rankine cycle can be expressed as

$$\eta_{rk} = (P_{tb} - P_{pu}/\eta_{ge})/Q_2 \tag{3.65}$$

3.1.5.2 ORC cycle

Compared with steam Rankine cycle, ORC has the following features:

(1) Organic fluid has lower boiling point, and higher evaporation pressure. It is suitable for the recovery of low temperature waste heat. Besides, it has small density and specific heat capacity, the required size of turbine, pipes and heat transfer areas are small, which is beneficial for cost saving.

(2) The exhaust fluid of the turbine is dry. So without overheat, the saturated gas can be used as the main gas for the turbine. The corrosion situation caused by the impact of the droplets to the high-speed rotating blades will not happen with ORC.

(3) Organic fluid has lower sound speed than vapor, the turbine can achieve favorable aerodynamic performance with lower wheel speed.

(4) Organic fluid has higher condensing pressure than water. It can condense under the pressure higher than the atmosphere. The system pressure can be maintained above the atmosphere pressure to prevent air leak into the system. This means a deaerator is no more necessary.

(5) Organic fluid has low freezing point, no anti-freezing treatment is required even in the cold area.

The shapes of curves in the T-s diagram of different fluids are different. According to the saturated vapor curve dT/ds in the T-s diagram, the working fluid can be divided into three types: $dT/ds > 0$ means dry fluid (moisture does not form when high-pressure saturated vapor expanded reversibly from a high pressure) , most of the organic fluid are dry fluids; $dT/ds < 0$ means wet fluid (moisture forms when high-pressure saturated vapor expanded reversibly from a high pressure), such as water; $dT/ds \to \pm\infty$ means isentropic fluid, such as R134a. For the high temperature high pressure dry fluid and isentropic fluid, since there is no droplets after work in the expansion turbine, no superheater is required. On the other hand, since the purpose of the ORC focuses on the recovery of low grade heat power, a superheated approach like the traditional Rankine cycle is not appropriate.

Figure 3-9 shows the T-s diagram of steam Rankine cycle and ORC cycle. Figure 3-10 shows the schematic diagram of the ORC system. For a dry fluid, the cycle can be improved by the use of a regenerator: since the fluid has not reached the two-phase state at the end of the expansion, its temperature at this point is higher than the condensing temperature. This higher temperature fluid can be used to preheat the liquid before it enters the evaporator. A counter-current heat exchanger is thus installed between the expander outlet and the evaporator inlet. The power required from the heat source is therefore reduced and the efficiency is increased.

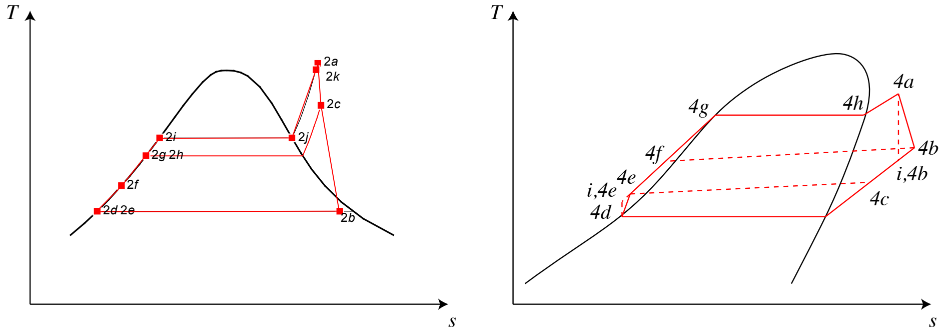

Figure 3-9 T-s diagram of water and a typical organic fluid

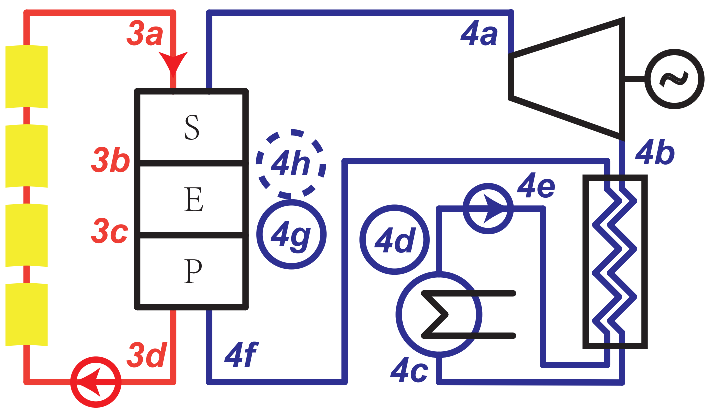

Figure 3-10 The schematic diagram of an ORC system with regenerator

The isentropic efficiency of the turbine

$$\eta_{i,tb} = (h_{4a} - h_{4b})/(h_{4a} - h_{i,4b}) \tag{3.66}$$

where $h_{i,4b}$ is determined by s_{4a} and p_c.

The output power of the turbine

$$P_{tb} = \dot{m}_4(h_{4a} - h_{4b}) \tag{3.67}$$

Process $4c$-$4d$ shows the heat process in the condenser. The outlet fluid in the condenser is saturated liquid. The outlet temperature T_{4d} and outlet enthalpy h_{4d} are determined by the exhaust pressure of the turbine p_c.

For the regenerator,

$$h_{4b} - h_{4c} = h_{4f} - h_{4e} \tag{3.68}$$

The released heat of the condenser

$$Q_{cd} = \dot{m}_4(h_{4c} - h_{4d}) \tag{3.69}$$

The power of the pump

$$P_{pu} = \dot{m}_4(h_{4e} - h_{4d}) \tag{3.70}$$

where h_{4e} can be obtained by $\eta_{pu} = (h_{i,4e} - h4d)/(h_{4e} - h_{4d})$. $h_{i,4e}$ is determined by s_{4d} and p_s.

Heat injected in the circuit

$$Q_4 = \dot{m}_4(h_{4a} - h_{4f}) \tag{3.71}$$

The efficiency of Rankine cycle can be expressed as

$$\eta_{rk} = (P_{tb} - P_{pu}/\eta_{ge})/Q_4 \tag{3.72}$$

3.1.5.3 Generator

The generator is relatively independent of the cascade system and its efficiency is assumed to be a constant, 0.975.

3.2 Stirling engine array modeling

Stirling engine array is used in the cascade system, Figure 3-11 shows the layout of the Stirling engine array. Each Stirling engine in the Stirling engine array has the identical parameters: $U_{se,1}$ =30 $\mathrm{W/(m^2 \cdot K)}$, $U_{se,2}$ =150 $\mathrm{W/(m^2 \cdot K)}$, $A_{se,1}$ =6 $\mathrm{m^2}$, $A_{se,2}$ =6 $\mathrm{m^2}$, k_{se} =1.4, γ_{se} =3.375, n_g =7.84×10^{-2} mol, s_{se} =10 $\mathrm{s^{-1}}$.

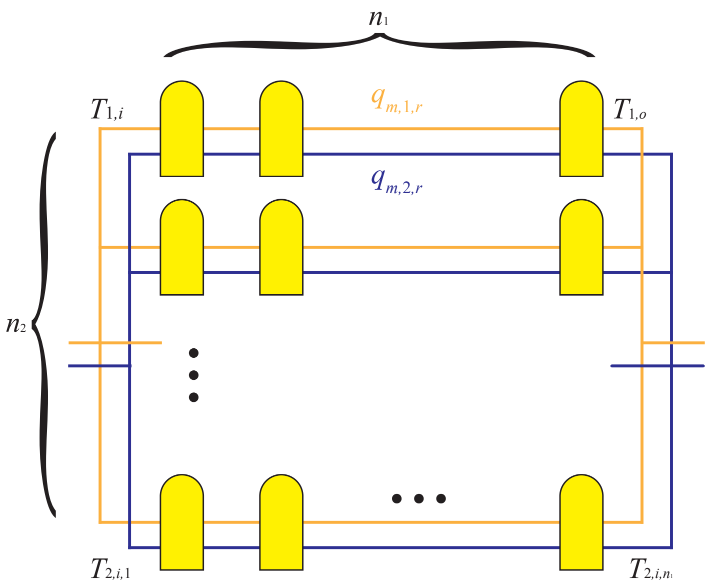

Figure 3-11 Layout of Stirling engines

Depending on the direction of heating and cooling flows, there are two possible flow types: parallel flow and counterflow. Figure 3-12 and Figure 3-12b show the heat transfer diagrams of the two flow types. n_1 is chosen to be 10 and can be optimized later.

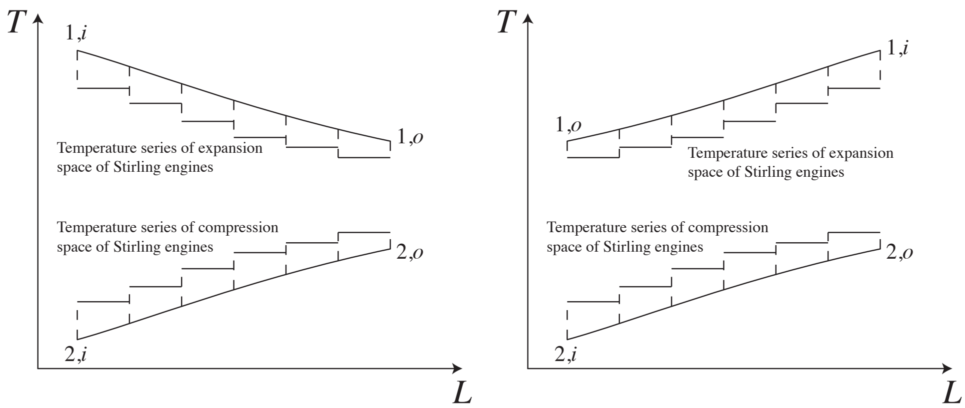

(a) Parallel flow (b) Counterflow

Figure 3-12 Heat transfer diagram of parallel flow and counterflow

In Figure 3-11, $T_{1,i,1} = T_{1,i}, \dot{m}_{1,r} = \dot{m}_1/n_2$. For x from 1 to $n_1 - 1$, where x is the column number of Stirling engines, $T_{1,i,x+1} = T_{1,o,x}, T_{2,i,x+1} = T_{2,o,x}$.

Assume that the positive flow direction is to the right, for parallel flow, $T_{2,i,1} = T_{2,i}$, $\dot{m}_{2,r} = \dot{m}_2/n_2$; for counterflow, $T_{2,o,n_1} = T_{2,i}$, $\dot{m}_{2,r} = -\dot{m}_2/n_2$.

Assume linear temperature profile across the regenerator, the mean effective temperature $T_{R,x} = \dfrac{T_{H,x} - T_{L,x}}{\ln(T_{H,x}/T_{L,x})}$ [108,109], and the symmetrical regenerator behaviour assumption $e_x = \dfrac{T_{R,x} - T_{L,x}}{T_{H,x} - T_{L,x}}$ [100,101]. For a Stirling engine in column x, x from 1 to n_1, according to Equation 3.33 and Equation 3.34,

$$T_{hw,x} = T_{1,i,x} - \frac{T_{1,i,x} - T_{1,o,x}}{1 - \exp(-\dfrac{U_{se,1}A_{se,1}}{\dot{m}_{1,r}c_{p,1,x}})} \tag{3.73}$$

$$T_{cw,x} = T_{2,i,x} - \frac{T_{2,i,x} - T_{2,o,x}}{1 - \exp(-\dfrac{U_{se,2}A_{se,2}}{\dot{m}_{2,r}c_{p,2,x}})} \tag{3.74}$$

The power of each Stirling engine in column x can be written as

$$P_{se,x} = W_{th,x} - W_{pd,x} - W_{fs,x} \tag{3.75}$$

The efficiency of each Stirling engine in column x can be written as

$$\eta_{se,x} = \frac{W_{th,x} - W_{pd,x} - W_{fs,x}}{Q_{th,x} + Q_{id,x} + Q_{sc,x}} \tag{3.76}$$

For energy balance,

$$\dot{m}_{1,r}(h_{1,i,x} - h_{1,o,x})(1 - \eta_{se,x}) = \dot{m}_{2,r}(h_{2,o,x} - h_{2,i,x}) \tag{3.77}$$

By using equations in 3.1.3 and the energy balance equations, key parameters of the Stirling engine array can be obtained.

The efficiency of the Stirling engine array

$$\eta_{sea} = 1 - \frac{\dot{m}_2(h_{2,o,n_1} - h_{2,i,1})}{\dot{m}_1(h_{1,i,1} - h_{1,o,n_1})} \tag{3.78}$$

The output power of each Stirling engine in column x

$$P_{se,x} = \dot{m}_{1,r}(h_{1,i,x} - h_{1,o,x})\eta_{se,x} \tag{3.79}$$

The output power of the Stirling engine array

$$P_{sea} = \eta_{sea}\dot{m}_1(h_{1,i,1} - h_{1,o,n_1}) \tag{3.80}$$

3.3 System modeling

Different components are connected to form a system by their interfaces (inlets and outlets). These interfaces are interacted with each other by ”streams”. For example, the steam turbine in Figure 3-6 is connected with the deaerator by a steam stream. This steam stream has its own properties such as fluid type, mass flow rate, temperature, pressure and so on. ”Steams” are defined as objects in the modeling language – MATLAB. Listing 3.1 shows the source code of the definition of the class – **Stream**.

Listing 3.1 The MATLAB source code of the definition of the class – Stream

```
classdef Stream < handle
    %Stream This class describes a fluid stream that has inherent
    %properties and dependent properties

    properties
        fluid;  % Fluid type
        q_m;    % Mass flow rate, kg/s
        T;      % Temperature, K
        p;      % Pressure, Pa
        x;      % Quality, [0, 1] for two phase stream; NaN for single
                %   phase stream
    end
    properties(Dependent)
        h;      % Mass specific enthalpy, J.kg
        s;      % Mass specific entropy, J/kg-K
        cp;     % Specific heat under constant pressure, J/kg-K
    end

    methods
        function obj = Stream
            obj.T = Temperature;
            obj.q_m = Massflow;
            obj.p = Pressure;
        end
        function flowTo(obj, st)
            st.fluid = obj.fluid;
            st.q_m = obj.q_m;
        end
        function st2 = mix(obj, st1)
            % Get the properties of a stream mixed by two streams
            % The two streams must have the same fluid type and pressure
            if obj.fluid == st1.fluid
                if  obj.p.v == st1.p.v
                    obj.p = st1.p;
                    st2.fluid = obj.fluid;
                    st2.p = obj.p;
```

```
                    st2.q_m.v = obj.q_m.v + st1.q_m.v;
                    h = (obj.q_m.v .* obj.h + st1.q_m.v .* st1.h)...
                        ./ (obj.q_m.v + st1.q_m.v);
                    st2.T.v = CoolProp.PropsSI('T', 'H', h, 'P',st2.p.v);
                else
                    error('The two streams have different pressures!');
                end
            else
                error('The two streams have different fluid types!');
            end
        end
        function convergeTo(obj, st, y)
            % Get another stream converged (or diverged)
            % from the original stream state.
            % If y < 1, the original stream is diverged
            % If y > 1, the original stream is converged
            st.fluid = obj.fluid;
            st.T = obj.T;
            st.p = obj.p;
            st.x = obj.x;
            st.q_m.v = obj.q_m.v .* y;
        end
    end
    methods
        % The dependent properties can be obtained by the inherent
        %   properties
        % If x is NaN, then the dependent properties are determined
        %   by T and P; otherwise, they are determined by P and x
        function value = get.h(obj)
            if isempty(obj.x)
                value = CoolProp.PropsSI('H', 'T', obj.T.v, ...
                    'P', obj.p.v, obj.fluid);
            else
                value = CoolProp.PropsSI('H', 'P', obj.p.v, 'Q', ...
                    obj.x, obj.fluid);
            end
        end
        function value = get.s(obj)
            if isempty(obj.x)
                value = CoolProp.PropsSI('S', 'T', obj.T.v, ...
                    'P', obj.p.v, obj.fluid);
            else
                value = CoolProp.PropsSI('S', 'P', obj.p.v, 'Q', ...
                    obj.x, obj.fluid);
            end
        end
        function value = get.cp(obj)
            if isempty(obj.x)
                value = CoolProp.PropsSI('C', 'T', obj.T.v, ...
                    'P', obj.p.v, obj.fluid);
```

```
            else
                value = inf;
            end
        end
    end
end
```

Some properties, **T**, **q_m** and **p**, of **Stream** are also objects. They belong to the classes **Temperature**, **Massflow** and **Pressure** separately.

Given the inherent properties of a **Stream**, its dependent properties, mass specific enthalpy (**h**), mass specific entropy (**s**) and pressure (**p**), can be obtained.

If the stream is a single phase stream, its dryness does not exist. Its dependent properties (h, s, c_p) can be obtained by its temperature (T) and pressure (p) by calling the open source MATALB wrapper CoolProp. If the stream is a two-phase stream, $0 \leqslant x \leqslant 1$. Its dependent properties (h, s, c_p) can be obtained by its pressure (p) and dryness (x). The reason of choosing pressure (p) instead of temperature (T) as the input value is that it is easier to be determined.

A **stream** can be used to record a state point since it contains all the information for a state point. Streams are defined in a system for component connection and system calculation. Different components are connected by streams to form a system. The Streams are passed as parameters to the components, completing the calculation of the methods in the components.

Components are connected each other by streams. Their inlets and outlets are used as interfaces for connection. Two interfaces are connected together by be assigned the same stream.

Systems are initialized by given parameters (design parameters). These parameters are assigned to corresponding properties of the streams and thus affect the state of the related components.

For system calculation, it has to be mentioned that, some parameters of a component are related with other components. In such situations, guess values are used for the calculation methods in the components. The guess values are set to be the properties of some streams. Each of these streams is assigned to two components (evaporator and superheater). These streams are assigned to corresponding components to accomplish the calculation methods in the components. These calculation methods will return solutions for the stream parameters. Then the parameters will be compared with the guess values for verification. If the differences between guess values and the calculated parameters are within permissible error, the guess values are accepted; otherwise, the guess values will be iteratively readjusted according to the Runge-Kutta method until accepted.

For example, the mass flow rate of oil of the evaporator ($\dot{m}_3$) is related with the superheater in a system as described in Figure 2-18a. A guess value of $\dot{m}_3$, $\dot{m}_{3,g}$, is required to determine it. $\dot{m}_{3,g}$ is assigned to the evaporator oil stream. This stream is assigned to both evaporator and superheater. In **evaporator**, the method **get_T_3b** will change the temperature of the stream (T_{3b}) from the default value. In **superheater**, the method **get_q_m_3** will return a solution of $\dot{m}_3$, $\dot{m}_{3,s}$, for verification. If $|\dot{m}_{3,g} - \dot{m}_{3,s}|$ is less than permissible error (10^{-4}), then $\dot{m}_{3,g}$ is accepted as the value of $\dot{m}_3$; otherwise, $\dot{m}_{3,g}$ will be iteratively readjusted according to the Runge-Kutta method until $|\dot{m}_{3,g} - \dot{m}_{3,s}| < 10^{-5}$.

Chapter 4 Optimization of Stirling engine array

4.1 Connection types of SEA

For a single Stirling engine, the heat transfer processes between fluids and engine are independent and irrelevant with the direction of the flows, which means the efficiency and power are not affected by the direction of fluids. However, for an SEA, the connection type will affect the temperature profiles through the array and the specific work production, both of which will determine the efficiency and power of the SEA. It is practically significant to investigate the influence of connection type of an SEA on its performance. Using parallel flow, on the one hand, will reduce the flow rate of the fluid, which will reduce the power of each engine; however, on the other hand, will take the advantage of higher inlet heating fluid temperature (or lower inlet cooling fluid temperature), which may increase the power of each engine. friend who is Using serial flow, on the one hand, will increase the flow rate of the fluid, which will increase the power of each engine; however, on the other hand, the inlet heating fluid temperature reduces with the flow direction (or the inlet cooling fluid temperature increases with the flow direction), which leads to lower engine power along the flow direction. Using the same order will lead to largest fluid temperature difference (temperature difference of the heating and cooling fluids) at the first engines and smallest fluid temperature difference at the last engines. Using the reverse order will lead to more averaged fluid temperature differences of the engines. For a heat exchanger, the reverse order (counterflow), which leads to a smaller fluid temperature difference, has a better heat transfer effect for its lower exergy loss. However, for a Stirling engine, the smaller fluid temperature difference leads to lower performance due to the lower temperature difference of the working gas in the hot space and cold space. To find out the influence of connection types on the performance of SEA, it is essential to classify the connection types.

Five basic connection types of SEA were summarized according to the direction-irrelevant feature of Stirling engine, as shown in Figure 4-1. Type 1 is parallel flow, Type 2 is serial flows in the same order, Type 3 is serial flows in the reverse order, Type 4 is heating fluid in serial flow and cooling fluid in parallel flow and Type 5 is heating fluid in parallel flow and cooling fluid in serial flow. All other connection types are the combination of these five basic connection types. For instance, an SEA in Figure 4-2 is the combination of Type 2 and Type 4.

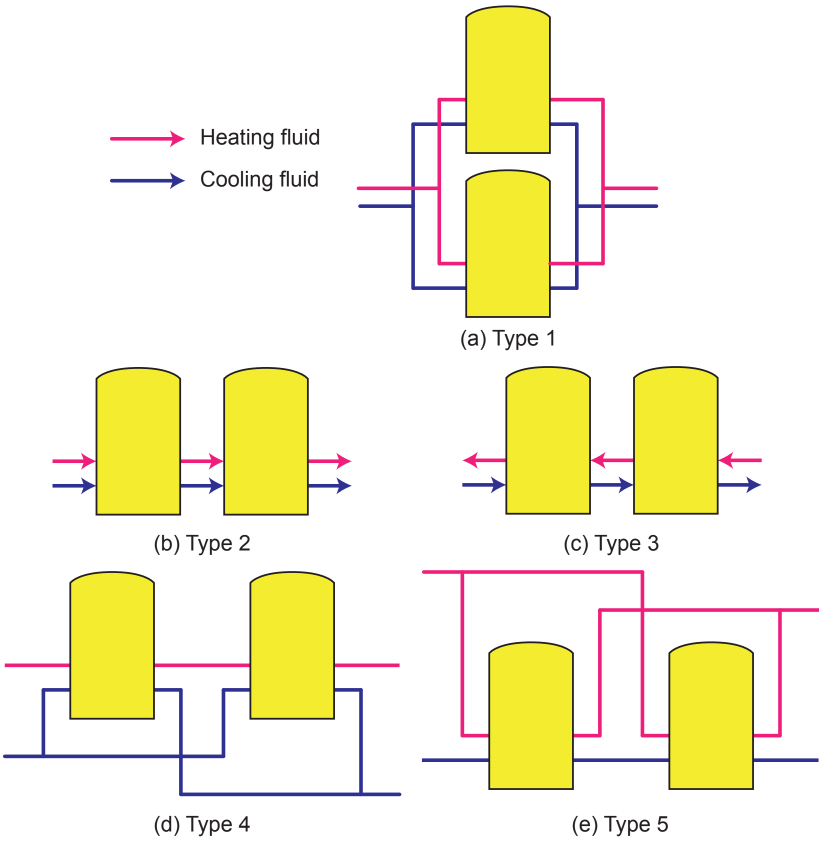

Figure 4-1 Five basic connection types of SEA

4.2 Modeling of the SEAs

As mentioned in Section 4.1, there are five basic connection types for an SEA. All other connection types are the combination of these five basic connection types. This thesis investigates the five basic connection types.

To determine the performance of an SEA, models of all the Stirling engines need to be built depending on their thermodynamic characteristic. Stirling engines are chosen to

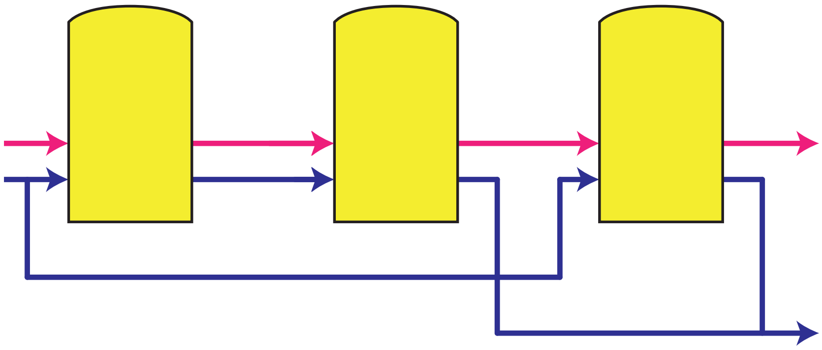

Figure 4-2 An instance of connection type of an SEA

have the same parameters including the same speed s_{se}. This is a reasonable assumption when using SEA for power generation, where the output power frequency should be constant. The speed of Stirling engine can be calibrated by speed controller system[110]. To eliminate interference of other factors, heating and cooling fluids are chosen to have same parameters for different connection types of SEAs. To clearly find out the performance differences of different SEAs, large temperature differences of the heating/cooling fluids after heat exchange with the engines are preferred. Air was chosen as the cooling fluid instead of commonly used water to avoid small temperature rise and evaporation in the cooling process. Design parameters of Stirling engines are the same as shown in Table 3.2. Other parameters of Stirling engines and heating/cooling fluids in SEAs are shown in Table 4.1. Rotation speed of the engines and mean effective pressure were chosen to be 25 Hz and 5 MPa respectively to get the best Stirling engine model for performance prediction, as pointed in Section 3.1.3.3.

In an SEA, there are 2 flows as shown in Figure 4-1. In a serial flow, each engine's mass flow rate is $\dot{m}$, and from the flow's direction, for $2 \leqslant x \leqslant n_{se}$, $T_{i,x} = T_{o,x-1}$. In a parallel flow, each engine's mass flow is $\dot{m}/n_{se}$, for $2 \leqslant x \leqslant n_{se}$, $T_{i,x} = T_{i,h}$.

$$T_{i,x} = T_{o,x-1} \tag{4.2}$$

$$T_{i,x} = T_{i,h} \tag{4.3}$$

According to the equations (Equation 3.51-4.3) , there are $6n_{se} - 2$ equations for $6n_{se}$ parameters for n_{se} engines. Other parameters of an SEA can be calculated by the given inlet

Table 4.1 Parameters of SEA models

Parameter	Value	Parameter	Value
Heating fluid	Air	$\dot{m}_h$	0.4 kg/s
Cooling fluid	Air	$T_{i,h}$	1000 K
n_{se}	6	$p_{i,h}$	5×10^5 Pa
s_{se}	25 Hz	$\dot{m}_c$	0.4 kg/s
p_{se}	5 MPa	$T_{i,c}$	300 K
U_hA_h	180 W/K	$p_{i,c}$	5×10^5 Pa
U_cA_c	180 W/K		

temperature of the heating and cooling fluids. The efficiency and power of each engine can be obtained from Equation 3.48, 3.47. The total efficiency and power of SEA can be obtained by powers of engines and outlet properties of the fluids.

MATLAB was used as the programming tool to build the model of SEAs, and CoolProp was used to provide fluid properties for MATLAB program. Five basic SEA models composed of the aforementioned Stirling engines and fluids were built. To compare SEA connection types under various conditions, several parameters are investigated to find out their effects on SEA performance.

Figure 4-3 shows the solution algorithm of the SEA model. Flowchart (a) shows the algorithm to solve a Stirling engine known inlet parameters of the fluids. Flowchart (b) shows the algorithm to solve a Stirling engine known inlet parameters of heating fluid and outlet parameters of cooling fluid. Flowchart (c) shows the algorithm to solve the SEA model iteratively depending on different connection types. The levenberg-marquardt algorithm is applied to numerically solve the non-linear equations in the flowcharts.

4.3 Result analysis

SEA models with specified parameters in Table 4.1 were built and calculated. Results of the performances of the SEAs are shown in Table 4.2, it can be found that under specified

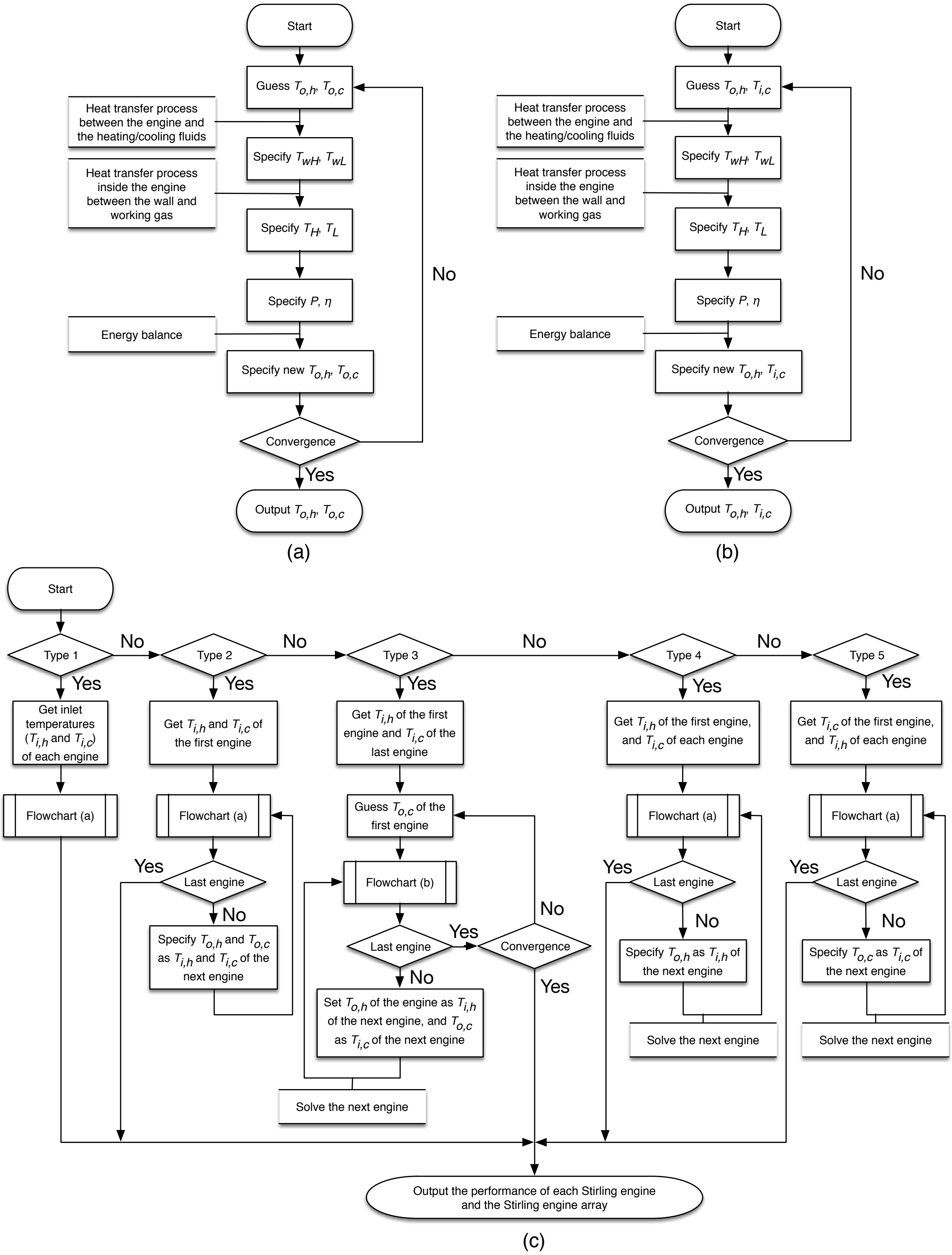

Figure 4-3 Flowcharts of the SEA model for performance analysis of the SEAs

parameters Type 3 has the highest efficiency and output power, while Type 1 has the lowest efficiency and output power.

Table 4.2 Results of SEA models under specified parameters

Parameter	Value	Parameter	Value
η_1	0.2215	P_1	8022 W
η_2	0.2273	P_2	8483 W
η_3	0.2277	P_3	8512 W
η_4	0.2227	P_4	8116 W
η_5	0.2263	P_5	8399 W

4.3.1 Effects of $T_{i,h}$

According to Carnot cycle efficiency formula, the temperature of heating fluid determines the efficiency of Stirling engine array. For a Stirling engine, lower temperature heating fluid leads to a lower efficiency. The efficiency and output power may drop to 0 due to its insufficient heating fluid temperature to drive the engine.

Curves of performance of SEAs and $T_{i,h}$ are shown in Figure 4-4. As it is shown, with the increase of $T_{i,h}$, both η and P increase for all SEAs. For some types of SEA, when $T_{i,h}$ is lower than a critical temperature, some of the engines in the SEA will not work and there will be turning points on the $\eta - T_{i,h}$, $P - T_{i,h}$ curves. For example, in SEA of Type 1, when $T_{i,h}$ is lower 820 K, all the engines stop working, turning points at 820 K can be found on the $\eta - T_{i,h}$, $P - T_{i,h}$ curves in Figure 4-4.

From curves in Figure 4-4, it can be concluded that Type 2 and Type 3 have the best performance, and Type 2 has the best adaptability for lower $T_{i,h}$. All engines in Type 2 work at 730 K.

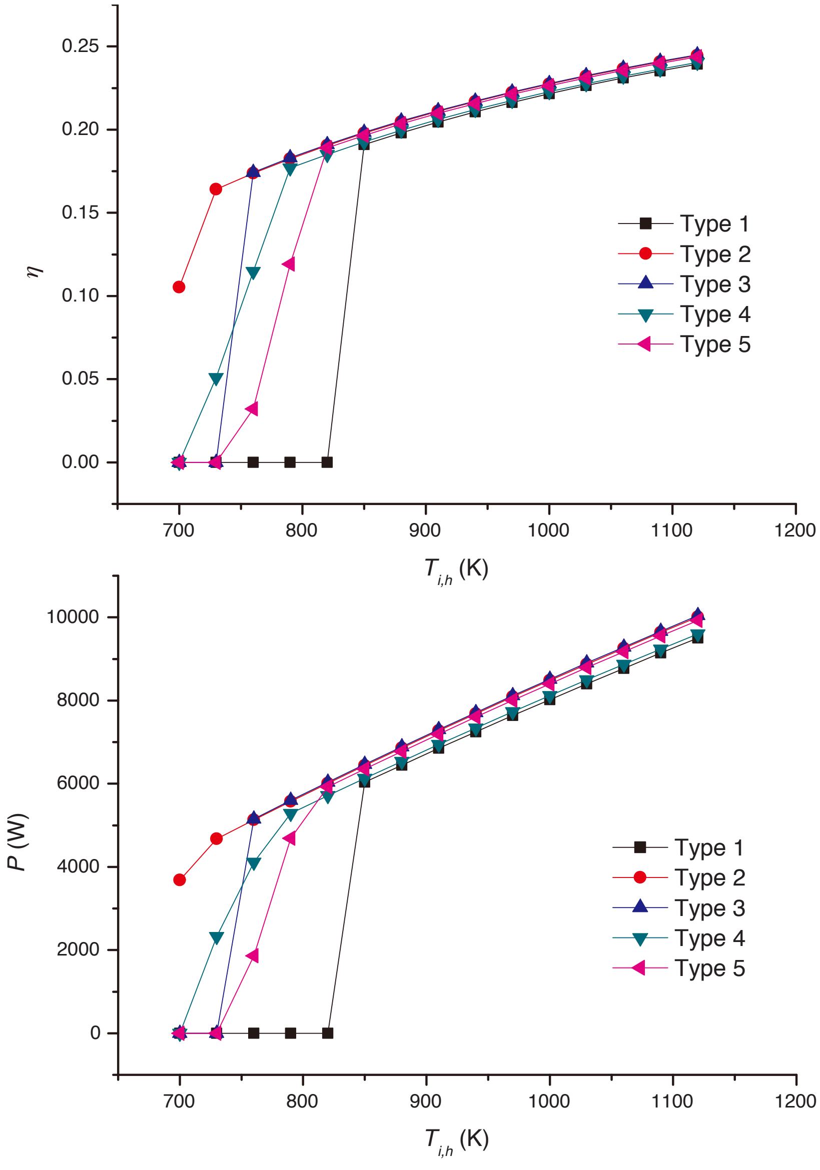

Figure 4-4 Influence of $T_{i,h}$ on efficiency and power of SEA

4.3.2 Effects of $\dot{m}c_p$

According to Equation 3.53, 3.54, $\dot{m}c_p$ (both $\dot{m}_h c_{p,h}$ and $\dot{m}_c c_{p,c}$) will affect the heat transfer process, which is one of the vital factor for the performance of SEA.

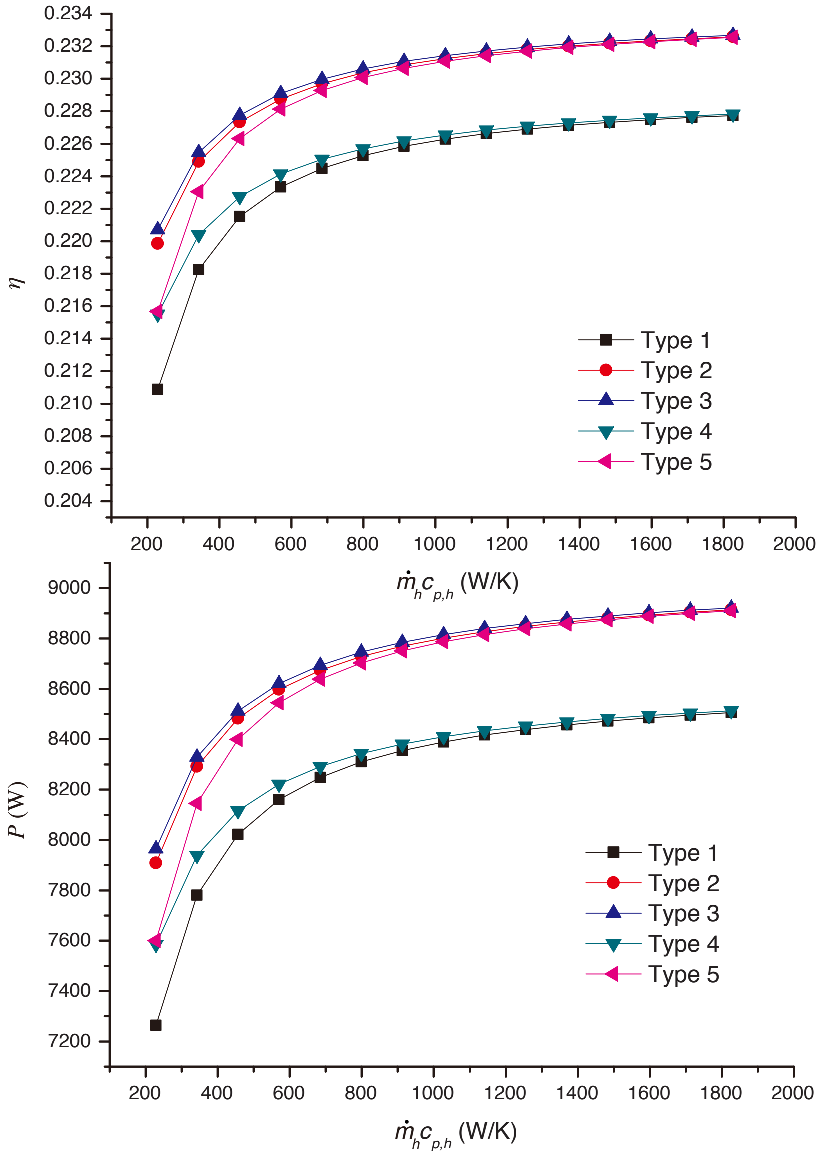

Figure 4-5 Influence of $\dot{m}_h c_{p,h}$ on efficiency and power of SEA

Curves of performance of SEAs and $\dot{m}_h c_{p,h}$ are shown in Figure 4-5. For a large $\dot{m}_h c_{p,h}$

(> 800 W/K), Type 2 , Type 3 and Type 5 have similar performance, which can be interpreted as the cooling fluid has the same properties for the two types of SEAs, and for a large $\dot{m}_h c_{p,h}$, the heating fluid has similar effect after diverged. Similar performance of Type 1 and Type 4 can be also interpreted for the same reason.

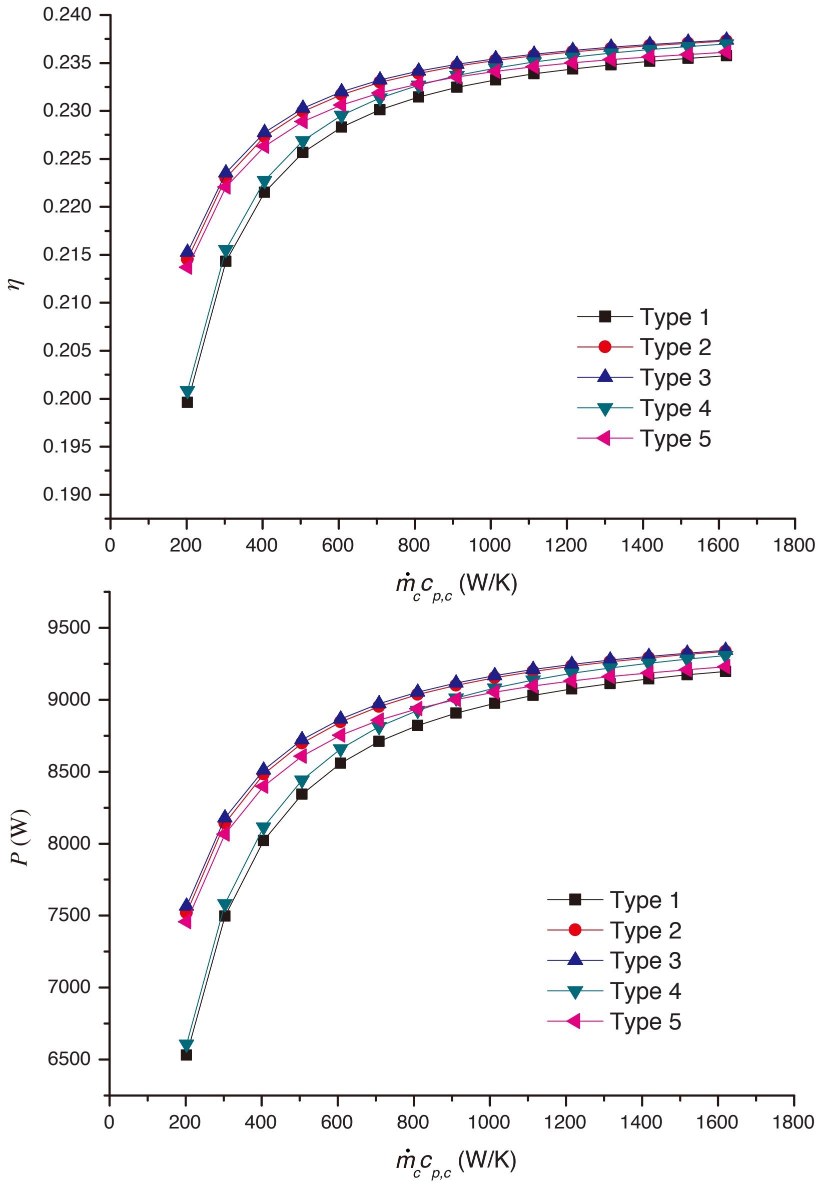

Figure 4-6 Influence of $\dot{m}_c c_{p,c}$ on efficiency and power of SEA

Curves of performance of SEAs and $\dot{m}_c c_{p,c}$ are shown in Figure 4-6. For a connection type of SEA, the performance improves with the increase of $\dot{m}_c c_{p,c}$. For a large $\dot{m}_c c_{p,c}$ (> 800 W/K), Type 2 and Type 3 have similar performance, which means the flow order doesn't affect the performance of SEA with a large $\dot{m}_c c_{p,c}$. There exists an intersection point (at 830 W/K) of curves of Type 4 and Type 5. For a larger $\dot{m}_c c_{p,c}$, Type 4 has a better performance, and vice versa. This can be interpreted that larger $\dot{m}_c c_{p,c}$ weaken the drawback of larger temperature rise of parallel flow, while for the heating fluid, temperature drop of serial flow is smaller than parallel flow.

4.3.3 Effects of n_{se}

By varying the number of engines in SEA, the performance levels changed accordingly. n_{se} may affect both the flow rates and temperatures of fluids of each engine. Figure 4-7 shows curves of performance of SEAs with different n_{se}. As it is shown, with an increase of n_{se} leads to a reduction of η for all SEAs due to smaller heating and cooling average temperature difference for more engines. For some types of SEA, when n_{se} is larger than a critical value, some of the engines in the SEA will not work and the curves will dive. E.g. for SEA of Type 1, when n_{se} is larger than 9, all the engines stop working, turning points at 9 can be found on the $\eta - n_{se}$, $P - n_{se}$ curves in Figure 4-7.

For Type 1, when $n_{se} \geqslant 10$, all engines stop working for given heating and cooling fluids due to small $\dot{m}c_p$. For Type 2 and Type 3, every engine in the SEAs works, by increasing n_{se}, η reduces due to smaller temperature difference of the fluids, and P increases due to more operating engines. For Type 4, by checking results, it can be found that when $n_{se} = 13$, the last engine doesn't work; when $n_{se} = 14$, only the first 10 engines will work; when $n_{se} = 15$, the working engine number drops to 9. For Type 5, by checking results, it can be found that when $n_{se} = 12$, the last 2 engines stop working; when $n_{se} = 13$, only the first 8 engines will work; when $n_{se} = 14$, the working engine number drops to 6; when $n_{se} = 15$, the working engine number drops to 4.

For a certain connection type, increase n_{se} will reduce the efficiency of SEA. For some connection types, increase n_{se} will reduce the output power P due to inoperative engines and smaller output power engines. It is important to choose the number of engines for some connection types of SEA.

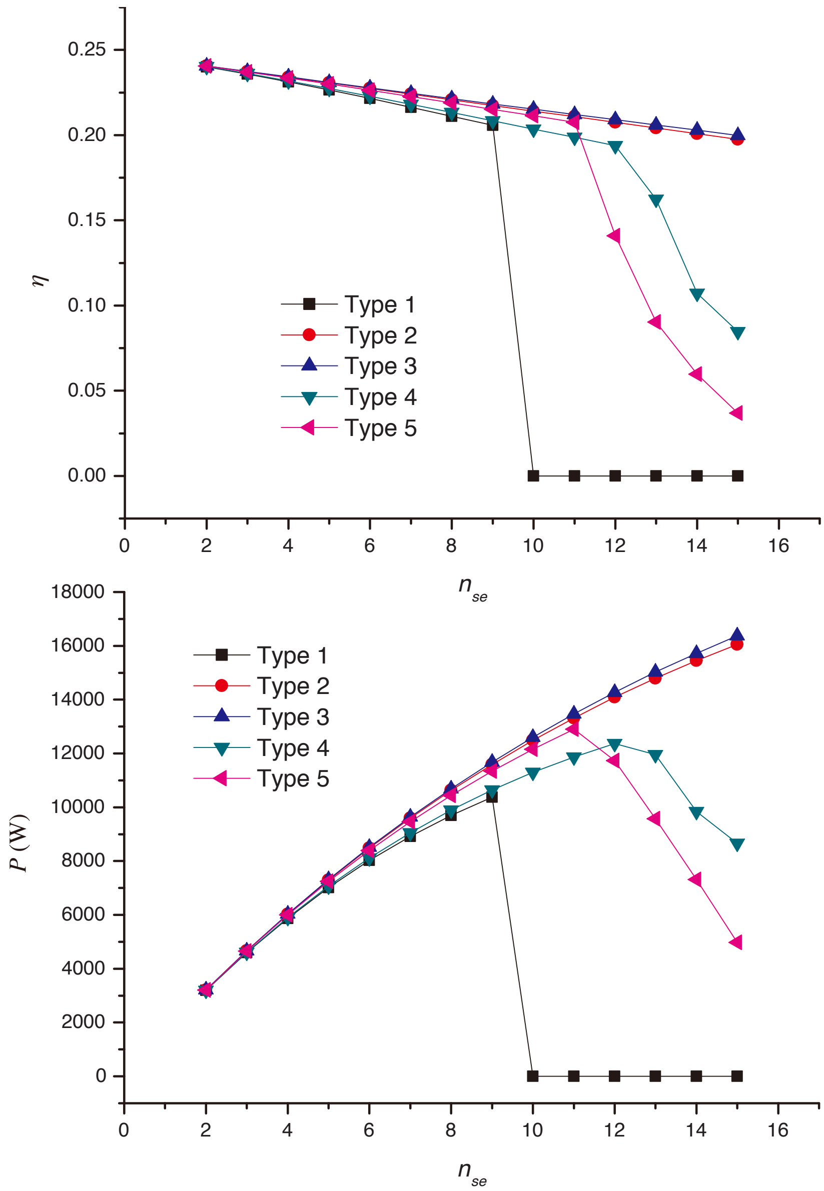

Figure 4-7　Influence of n_{se} on efficiency and power of SEA

4.4 Conclusion

A new layout scheme of the solar dish system by using SEA were proposed in this thesis. Connection type of the engines may change the flow rates and temperatures of the fluids, as a result the performance of the SEA will be different depending on the connection schemes. In order to compare performance of SEAs with different arrangements, five basic connection types of SEA were summed up according to flow type and flow order.

Analytical Stirling engine model was created to develop the SEA models for the investigation of influence of connection types. Imperfect regeneration and cycle irreversibility of Stirling engine cycle and heat exchange process between fluids and engine were considered in the model. Algorithm to numerically solve different connection types of SEA was developed. The model was evaluated by considering the prototype GPU-3 Stirling engine as a case study. Result shows that the proposed model predicted the performance with higher accuracy than Simple model[103] and Simple II model[105].

Models of SEAs were developed to calculated the performance under different parameters to find out the impacts of $T_{i,h}$, $\dot{m}_h c_{p,h}$, $\dot{m}_c c_{p,c}$ and n_{se} on different connection types. It was found that, as expected, decrease $T_{i,h}$ and $\dot{m}c_p$ will weaken the performance of SEA of all connection types. However, for some connection types, there exists a critical temperature below which some engines stop working. This needs to be considered for SEA connection type selection, especially when $T_{i,h}$ is low. For given heating and cooling fluids, Type 2 has the best performance and adaptability. Type 2 and Type 3 have similar performance under different parameters ($T_{i,h}$, $T_{i,c}$ and $\dot{m}c_p$), which means the flow order has little influence on the performance of an SEA. SEA of serial flows (Type 3) has the best performance and adaptability under different parameters. Given heating and cooling fluids, using serial flow is the best choice for the connection type of an SEA.

It is important to note that, in the future researches, the experiments of influence of connection type on SEA's performance can be carried out to verify the conclusions in this thesis.

Chapter 5 Optimization of steam generating system

5.1 Steam generator subsystem

In a solar parabolic trough power plant in which intermediate heat-transfer fluid (take oil for instance) is used, heat addition to the working fluid (take water for instance) takes place in three counterflow heat exchangers (steam generator subsystem, SGSS) as shown in Figure 5-1. The SGSS is consist of preheater, evaporator, superheater. The flow rates of both oil and water remains the same in the three heat exchangers. The water has phase change in the three heat exchangers, from liquid to vapor in the evaporator, however, oil remains liquid. The heat capacity of water in each heat exchanger differs a lot. The heat capacity of oil has no significant difference since no phase change. The heat transfer process is illustrated on Figure 5-2. Large temperature differences exist at the inlets and outlets of the heat exchangers, which makes large entropy production during the entire heat exchange process.

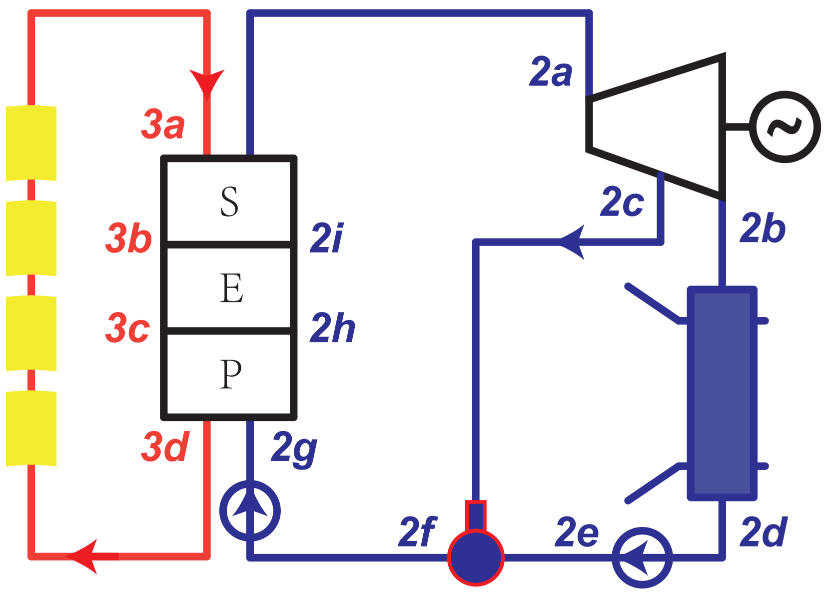

Figure 5-1 An typical solar parabolic trough system

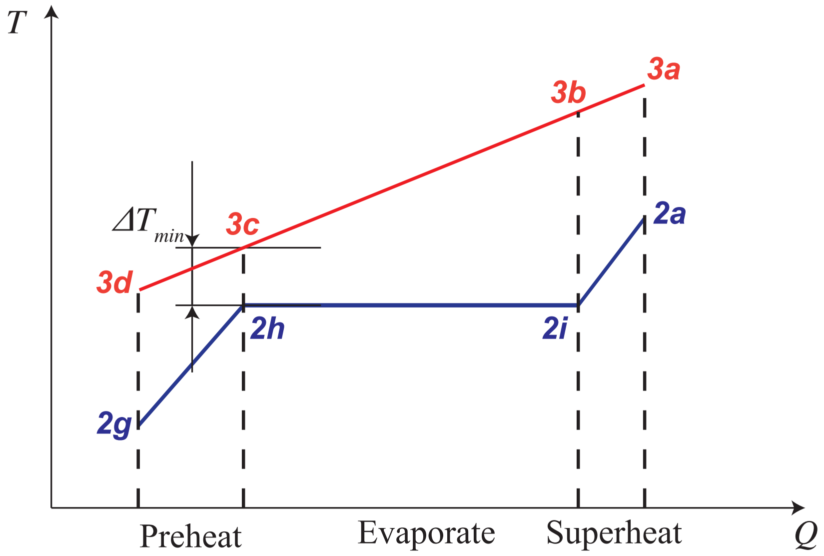

Figure 5-2 The steam generating process in countertlow heat exchangers

The heat-transfer fluid at $3a$ represents the solar field outlet temperature and at $3d$, the field return temperature. The difference between these can be reduced by increasing the flow rate of heat-transfer fluid through the field and thus the parasitic pumping power.

Since the heat exchangers must always stay a positive temperature difference for heat transfer, the temperature of oil must always be higher than the temperature of water. On the other hand, the temperature of oil should not be much higher that that of the water. Higher oil temperature leads more heat losses in the solar field hence lower efficiency, more entropy production generated in the heat exchange process. Besides, higher oil temperature brings greater operational risks for the solar system. Setting the appropriate temperature difference between the oil and water is particularly important. The oil temperature must always higher (but no too much higher) than that of the water.

To find out the inlet and outlet temperatures of oil at the solar field, the lowest temperature difference of oil and water is defined as the pinch temperature ΔT_{min}. The temperatures of state points $2h$ and $2i$ are determined by the main pressure of the steam turbine in Figure 5-1, and T_{3b} is larger than T_{3c}. So state points $3c$ and $2h$, called the pinch point, are set to satisfy the pinch temperature, $T_{3c} - T_{2h} = \Delta T_{min}$. The pinch temperature ΔT_{min} is usually set to be 10~20 K. It has to be mentioned that the temperature differences $T_{3d} - T_{2g}$ and $T_{3a} - T_{2j}$ worth attention to be not larger than ΔT_{min}.

However, even with the chosen pinch temperature ΔT_{min}, the temperature difference during the heat exchange process in SGSS is still large due to the phase change of water. Large temperature differences always exists at the inlet/outlet of the exchangers. As shown in Figure 5-3, it is a tradeoff to choose a mass flow rate of oil ($\dot{m}_3$). $\dot{m}_3$ affects the slope of curve $3a$-$3b$-$3c$-$3d$. A smaller $\dot{m}_3$ leads to a steeper curve, hence a larger $T_{3a} - T_{2j}$. A larger $\dot{m}_3$ leads to a more gentle curve, hence a larger $T_{3d} - T_{2g}$. The heat transfer processes in SGSS always produce large entropy and exergy losses. In this regard, a new steam generating system to reduce exergy loss is put forward.

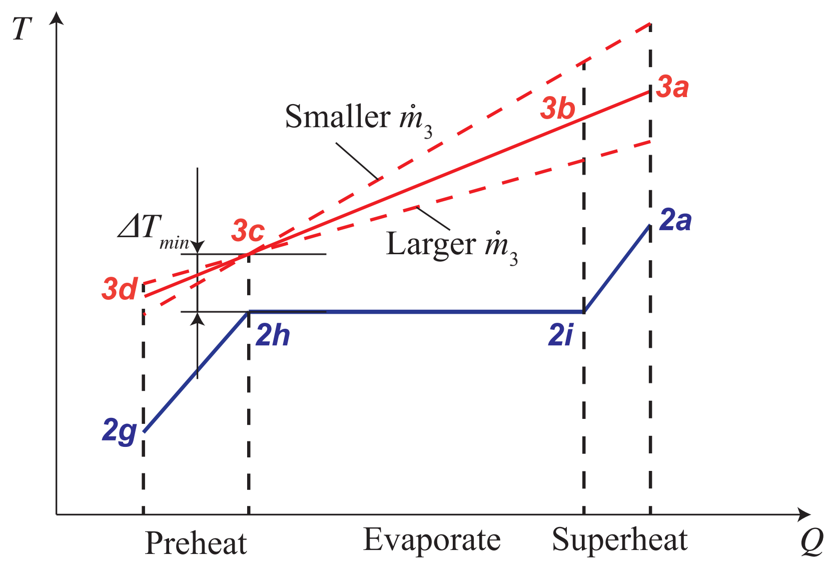

Figure 5-3　The tradeoff to choose $\dot{m}_3$

5.2　Multi-stage exergy loss reduction system

The reason of large temperature differences of the two curves in Figure 5-2 is that, the slope of oil curve changes slightly in different heat exchangers (preheater, evaporator and superheater), while the water curve changes dramatically due to large heat capacity c_p differences.

$$\Delta Q = c_p \dot{m} \Delta T \tag{5.1}$$

The slope of the curves are determined by $c_p\dot{m}$, $\dot{m}$ can be altered to adjust the slope of the curves despite the c_p is unalterable. All the water needs to be heated from supercooled water to superheated steam, which means $\dot{m}_2$ remains the same in the three heat exchangers. The last way is to change $\dot{m}_3$ in the heat exchangers.

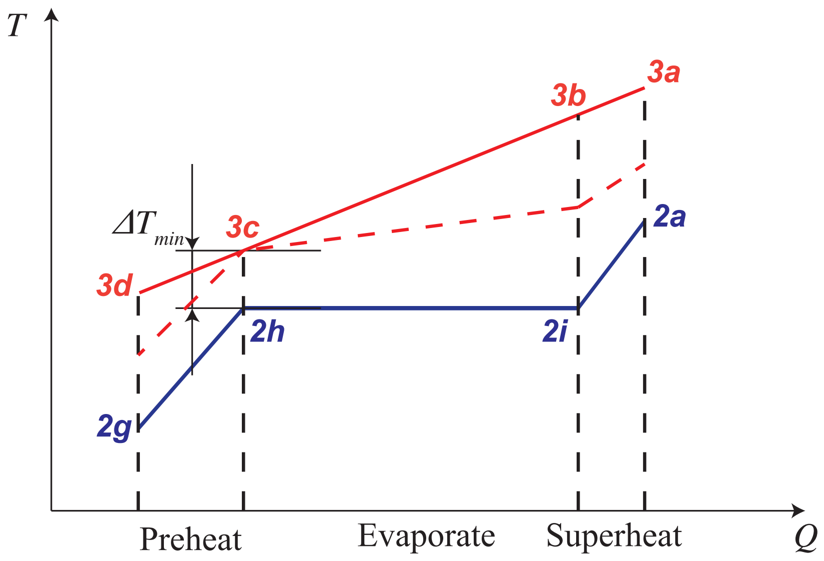

Figure 5-4 Change $\dot{m}_3$ in the heat exchangers to reduce the temperature difference

As shown in Figure 5-4, the oil curve can be changed to the dashed curve. The temperature difference between the water curve and oil curve reduces significantly. Water is heated in three stages and the exergy loss reduces. The corresponding steam generating system is so called Multi-stage exergy loss reduction system (MERS). Figure 5-5 shows the schematic diagram of the MERS for comparison of typical solar parabolic trough system in Figure 5-1. The solar field in Figure 5-1 has been divided into three independent sectors. Each sector becomes the heat source of a range for the steam heating process: the first corresponds to overheating, the second to evaporation, and the third to preheating. It has to be mentioned that the collectors in the schematic diagram are only used for explanation. The arrangement of these collectors can be in series, in parallel or combination of both.

To optimize the MERS, considering the limitation of pinch temperature, temperatures

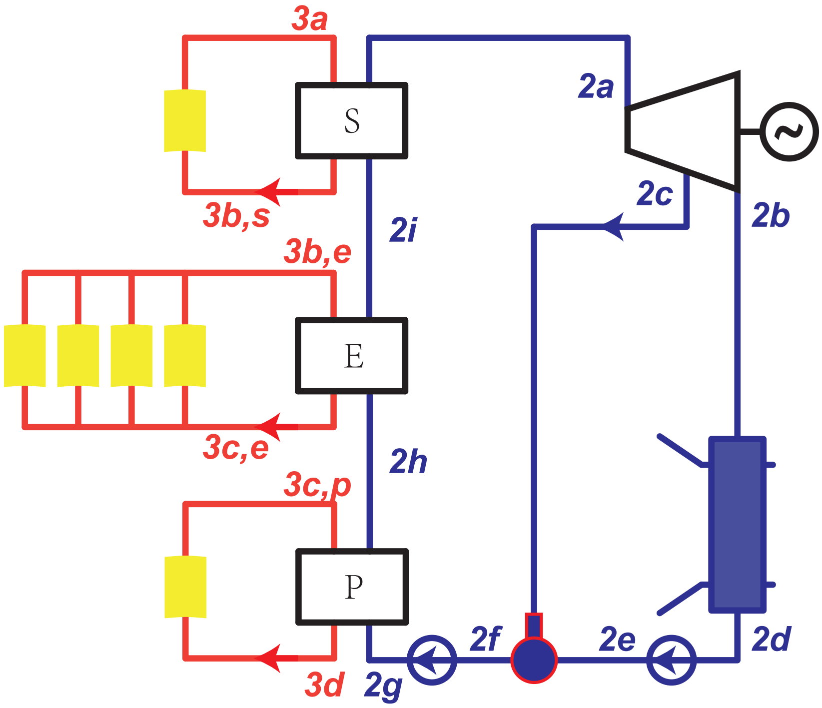

Figure 5-5 The schematic diagram of the MERS

of the oil at the inlet/outlet of the heat exchangers can be set according to following rules:

$$T_{3d} - T_{2g} = \Delta T_{min}$$
$$T_{3c,p} = T_{3c,e} = T_{3c}$$
$$T_{3c} - T_{2h} = \Delta T_{min}$$
$$T_{3b,e} = T_{3b,s} = T_{3b}$$
$$T_{3a} - T_{2a} = \Delta T_{min}$$

A large flow rate of oil in the evaporator $\dot{m}_{3,e}$ can be applied to decrease the temperature T_{3b} hence the temperature differences of the oil and water. However, a large $\dot{m}_{3,e}$ requires more oil usage and more pump power for the oil circuits. Besides, $\dot{m}_{3,e}$ is limited for the limitation of oil velocity in the pipes.

The enthalpy of each state point can be determined by its temperature and pressure.

The optimum oil average temperature in the solar field corresponds to the preheater is

$$T_{3,p} = (T_{2g} + T_{2h})/2 + \Delta T_{min} \tag{5.2}$$

The optimum oil flow rate in the solar field corresponds to the preheater is

$$\dot{m}_{3,p} = \dot{m}_2(h_{2h} - h_{2g})/(h_{3c} - h_{3d}) \tag{5.3}$$

The optimum oil average temperature in the solar field corresponds to the evaporator is

$$T_{3,e} = (T_{3b} + T_{3c})/2 \tag{5.4}$$

The optimum oil flow rate in the solar field corresponds to the evaporator is

$$\dot{m}_{3,e} = \dot{m}_2(h_{2i} - h_{2h})/(h_{3b} - h_{3c}) \tag{5.5}$$

The optimum oil average temperature in the solar field corresponds to the superheater is

$$T_{3,s} = (T_{3b} + T_{2a} + \Delta T_{min})/2 \tag{5.6}$$

The optimum oil flow rate in the solar field corresponds to the superheater is

$$\dot{m}_{3,s} = \dot{m}_2(h_{2a} - h_{2i})/(h_{3a} - h_{3b}) \tag{5.7}$$

5.3 Comparison

To find out the effect of MERS, models of traditional SGSS and proposed MERS are developed based on the models of the components. To clear find out the influence of oil temperature on the performance of the trough collectors, the equation summarized by[111] is used.

$$\eta(T) = 0.69563 + 0.000313T - 0.0000013T^2 \tag{5.8}$$

where T is the average temperature of the tube. Since the Nu number in the tube is large (about 1×10^4), small temperature difference exists between the absorber and oil. So the average oil temperature can be used as the average value of the tube.

The exergy loss caused by a heat exchange process per unit time

$$\dot{I} = T_{amb}(\sum \dot{m}_o s_o - \sum \dot{m}_i s_i) \tag{5.9}$$

The turbine and deaerator are the same for the two systems (SGSS and MERS), so that the corresponding state points of water are the same. The main parameters are listed in Table 5.1.

Table 5.1 Main parameters used for both SGSS and MERS

Parameter	Value	Parameter	Value
I_r	700 W/m^2	T_s	613.15 K
P_{ge}	6×10^6 W	p_s	2.35×10^6 Pa
$\eta_{i,tb}$	0.711	p_c	1.5×10^4 Pa
η_{ge}	0.975	p_{de}	1×10^6 Pa
ΔT_{min}	15 K		

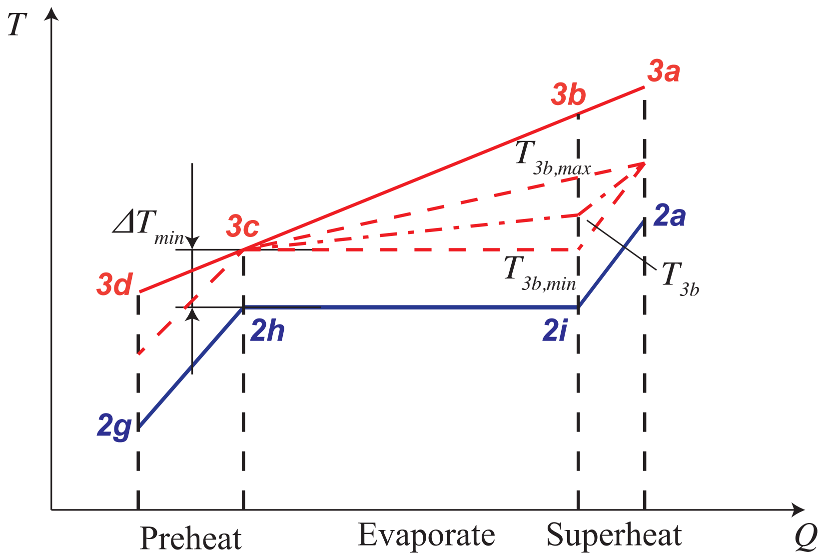

Figure 5-6 T_{3b} in the T-Q diagram of the heat transfer processes

As discussed in Section 5.2, T_{3b} is an undetermined value. Figure 5-6 shows the minimum and maximum value of it. $T_{3b,min}$ means the limit situation of unlimited flow rate of oil in the evaporator, $T_{3b,min} = T_{3c}$. (see Equation 5.5) T_{max} has the traditional effect of temperature differences in the evaporator and superheater, $\dot{m}_{3,e} = \dot{m}_{3,s}$. In our research, T_{3b} is set to be the average value of the two limitations, $T_{3b} = (T_{3b,min} + T_{3n,max})/2$.

$$\frac{T_{b,max} - T_{3c}}{T_{3a} - T_{3c}} = \frac{T'_{3b} - T_{3c}}{T'_{3a} - T_{3c}} \tag{5.10}$$

where T'_{3a} and T'_{3b} are the inlet oil temperature of superheater and evaporator in SGSS respectively. Simulation results of the two system models are listed in Table 5.2. It can be found that the MERS can effectively reduce exergy loss hence improve the system efficiency compared to traditional SGSS.

Table 5.2　Simulation results of SGSS and MERS

	SGSS	MERS		
		$T_{3b,max}$	T_{3b}	$T_{3b,min}$
T_{2a}	613.15 K			
T_{2i}	493.83 K			
T_{2h}	493.83 K			
T_{2g}	453.28 K			
T_{3c}	508.83 K			
T_{3a}	653.15 K	628.15 K	628.15 K	628.15 K
T_{3b}	634.11 K	612.41 K	560.62 K	508.83 K
T_{3d}	495.43 K	468.28 K	468.28 K	468.28 K
$\dot{m}_{3p}$	47.8 kg/s	16.1 kg/s	16.1 kg/s	16.1 kg/s
$\dot{m}_{3e}$	47.8 kg/s	58.6 kg/s	120.8 kg/s	∞
$\dot{m}_{3s}$	47.8 kg/s	59.4 kg/s	14.3 kg/s	8.3 kg/s
$\dot{I}_p$	4.80×10^4 W	2.58×10^4 W	2.58×10^4 W	2.58×10^4 W
$\dot{I}_e$	1.10×10^6 W	9.68×10^5 W	6.24×10^5 W	2.41×10^5 W
$\dot{I}_s$	1.81×10^5 W	1.42×10^5 W	9.19×10^4 W	4.24×10^4 W
$\dot{I}_{total}$	1.33×10^6 W	1.14×10^6 W	7.44×10^5 W	3.10×10^5 W
η_p	0.525	0.538	0.538	0.538
η_e	0.450	0.463	0.491	0.518
η_s	0.359	0.390	0.422	0.453
η_{total}	0.440	0.456	0.484	0.510

Chapter 6 Cascade system performance evaluation

6.1 System description

In the cascade system, dish collectors are used to provide heat for Stirling engines and air-to-water heat exchanger. Trough collectors are used to provide heat for steam generating processes (preheating, evaporating and superheating) in the Rankine cycle. Figure 6-1 shows the scheme sketch of the cascade system. In this system, hot air is produced by the dish collectors. High temperature (1073 K) air is used to provide heat to Stirling cycle to get higher conversion efficiency, then the air is used to provide heat for air-to-water heat exchanger to use the lower temperature energy in Rankine cycle effectively. Besides, feed water of Rankine cycle is used to cool the Stirling engines to recycle the heat wasted conventionally.

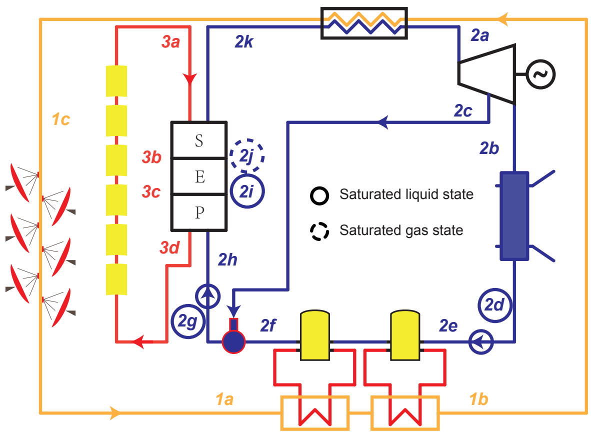

Figure 6-1 Sketch of the cascade system

State points of different fluids are marked on the sketch. The number indicates the type of the fluid, the letter indicates the state point of the fluid. State points with solid circle indicate saturated liquid states ($x = 0$), and with dotted circle indicates saturated gas states ($x = 1$). Figure 6-2a shows the T-s diagram of the water circuit in the cascade system. In this Rankine cycle, the heat provided in process $2e$-$2f$ comes from the Stirling engines, which increases the power of Rankine cycle. Figure 6-2b shows the heat transfer diagram of this process.

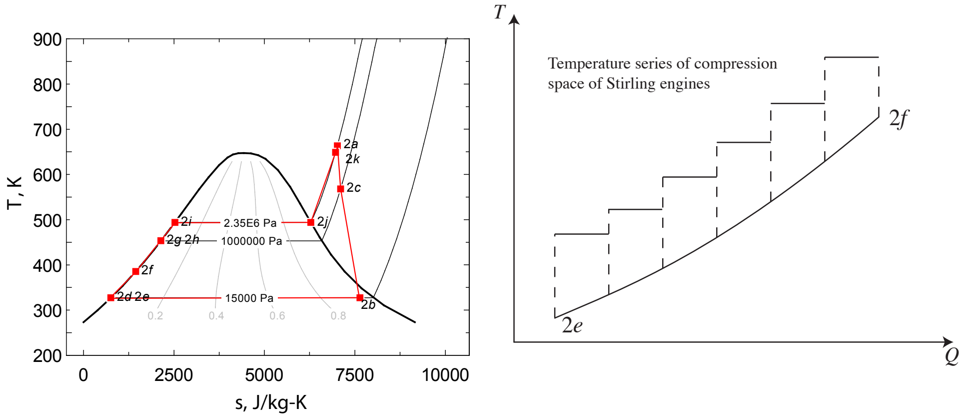

(a) T-s diagram of the water circuit　　(b) Diagram of process $2e$-$2f$

Figure 6-2　Diagrams of water circuit and $2e$-$2f$ process

To build the cascade system model, several simplifying assumptions are made:

- Steady state at nominal load of the system is analysed.
- Pressure drop due to flow is negligible.
- The leak of working fluid in the pipes is neglected.
- Same isentropic efficiency of steam turbine with different loads and in different stages.
- Heat loss that occurs from the tube to the atmosphere is not considered.
- There is no heat loss to the environment for Stirling engines.
- Simple models are used of some processes and equipment.
- A symmetrical regenerator behavior is assumed so that a single effectiveness can be defined as $e = (T_R - T_L)/(T_H - T_L)$.[100,101]
- A linear temperature profile across the regenerator exists, the mean effective temperature $T_R = (T_H - T_L)/\ln(T_H/T_L)$.[108,109]

6.2 Determination of system parameters

6.3 System simulation

6.4 Stand-alone system selection

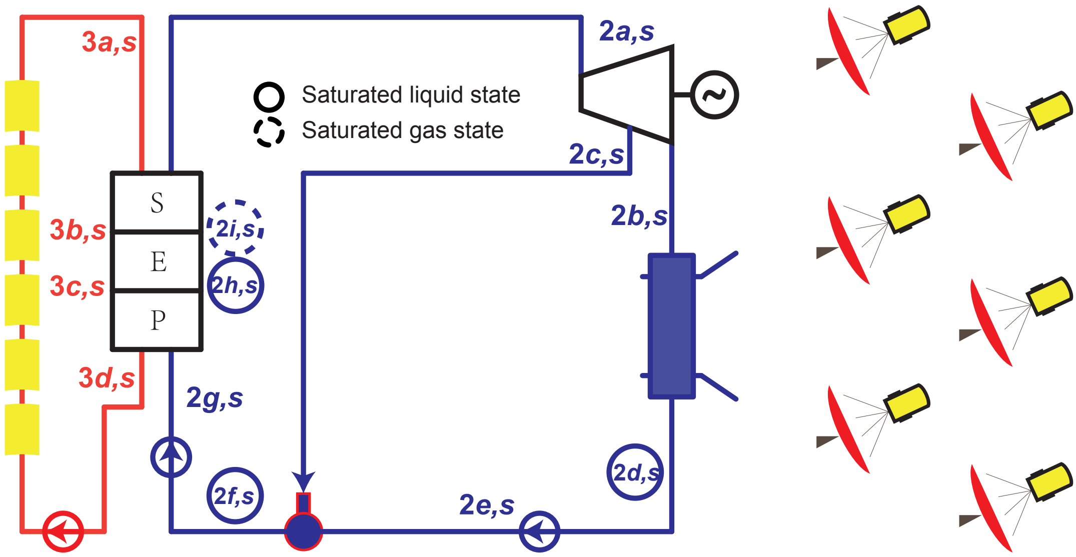

(a) Trough-Rankine system (b) Dish-Stirling system

Figure 6-3 Sketch of the stand-alone systems

Figure 6-3 shows the sketch of the stand-alone systems. These two stand-alone systems were developed for comparison. They use the same dish collectors and trough collectors with the same thermal efficiencies.

6.4.1 Stand-alone trough-Rankine system

Steam turbine has the same main parameters and isentropic efficiency with that of the cascade system. Working pressure of deaerator is the same of the cascade system. So parameters of state $2b,s$ and $2c,s$ in Figure 6-3 of the steam turbine can be obtained by $\eta_{i,tb} = (h_{2a,s} - h_{2b,s})/(h_{2a,s} - h_{i,2b,s}) = (h_{2a,s} - h_{2c,s})/(h_{2a,s} - h_{i,2c,s})$.

The output power of steam turbine $P_{tb,s} = (1 - y_s)\,\dot{m}_{2,s}\,(h_{2a,s} - h_{2b,s}) + y_s \dot{m}_{2,s}\,(h_{2a,s} - h_{2c,s})$.

The output power of generator $P_{ge,s} = P_{tb,s}\eta_{ge}$.

The total power of pumps $P_{pu,s} = (1 - y_s)\,\dot{m}_{2,s}\,(h_{2e,s} - h_{2d,s}) + \dot{m}_{2,s}\,(h_{2g,s} - h_{2f,s})$.

Heat injected in the water circuit $Q_{2,s} = \dot{m}_{2,s}\,(h_{2a,s} - h_{2g,s})$.

The generator efficiency is the same of that in the cascade system, and the efficiency of Rankine cycle can be expressed as $\eta_{rk,s} = (P_{tb,s} - P_{pu,s}/\eta_{ge})/Q_{2,s}$.

6.4.2 Stand-alone dish-Stirling system

In the stand-alone dish-Stirling system, Stirling engines with the same number of dish collectors are directly put on the focuses of the dish collectors. Water is used for cooling the Stirling engines. $T_{H,s}$ is chosen to be equal to outlet temperature of air in dish receiver. $T_{L,s}$ is chosen to be 310 K, the default expansion temperature in Fraser's dissertation[112] for the calculation of 4-95 NKII engine. k and γ are chosen the same value as that of the Stirling engines in the cascade system.

The power of Stirling engines $P_{sea,s} = n_{dc} A_{dc} I_r \eta_{dc} \eta_{sea,s}$.

6.5 Comparison with stand-alone system

6.6 System evaluation

Chapter 7 Conclusion and outlook

7.1 Conclusion

This chapter is needed to conclude the overall goal of our research. Considering the advantages and disadvantages of the existing solar thermal power generation technologies, a novel idea of energy cascade collection and energy cascade utilization for solar thermal power generation is put forward. Different types of collectors and thermodynamic cycles were used in the cascade system. The research of the cascade system is carried out with the selection of the system topology, the construction of the system model, the optimization of the system model and parameters, and the comparison with the independent system. The main works are concluded as follow:

(1) The topological structure of solar thermal cascade power generation system was proposed and analyzed. According to the analysis of thermal characteristics and the working characteristics of each component in the system, rationally arranged topological structures of cascade system were proposed. Specifically, by selecting and analyzing the basic system, the Rankine cycle fluid, the solar chimney, the cascade of the various types of collectors, the direct steam production system, the heat exchanger between the different working fluids, the heat between the different cycles Recovery, etc., to identify the representative of the project for the representative of the solar heat and heat cascade power generation system program. That is, on the basis of the slotted Rankine cycle and the disc-type Stirling cycle, the traditional dish-type Stirling machine is changed to hot air as a closed circulation system for the media, and the hot air heated by the dish collector The Stirling unit is used to heat the Stirling unit and use the condensed water of the Rankine cycle to cool the Stirling machine to utilize the hot air flowing from the Stirling unit to achieve overheating for the steam.

(2) Mechanism models were established for the components of solar thermal power generation system. The mechanism mathematical models were developed according to the operation mechanism of the target object and physical equations. The key components in the system, such as collectors, steam generating system, steam turbine and Stirling engine, were modeled with details. The mathematical model of each component is a

model verified by the classical theory or a large number of experimental data, which is the basic of the model of the cascade solar thermal power generation system. Heat loss models were established for the receivers of trough collector and dish collector. For the Stirling engine, based on the reasonable simplification and hypothesis, the model of the Stirling machine considered various losses and irrevisibilities was developed. The component models were developed in MATLAB by using object-oriented method. It makes full use of inheritance and polymorphism to ensure both the independence and the relevance of the components.

(3) A solar thermal power generation system design software was designed and the solar thermal power generation system models were developed. Based on the selected solar thermal cascade generation systems, solar thermal cascade generation system models were established based on the model of each component in the systems. The object-oriented features of inheritance, combination and polymorphism were used for the model development. The change rules of the main parameters and the performance indexes under the coupling of external and internal factors were studied. The change mechanism was studied and the calculation method of its performance characteristics was established. After setting up the components, setting the parameters and compiling the environment, the thesis completes the system construction of each system scheme, and finally completes the simulation system of solar thermal cascade generation based on MATLAB with the copyright of independent computer software.

(4) Simulation and optimization of cascade solar thermal power generation system model. Based on the study of the performance characteristics of solar thermal cascade generation system, the system is optimized and the structure is reconstructed. In particular, by analyzing the steam generation system of the system, a method of staged heating is proposed to reduce the heat transfer temperature difference in the steam generating system by changing the mass flow rate of the heat conduction oil, effectively reducing the heat generated during the heat exchange process in the steam generating system. Which can improve the efficiency of the whole system. Based on Stirling unit in cascade system, five kinds of basic arrangement forms of Stirling unit are summarized, and the difference of unit efficiency and output power under various arrangement forms is analyzed, and a given cold and heat source fluid Stirling unit under the conditions of the best arrangement.

7.2 Innovation

- Usage of different types of collectors and different thermodynamic cycles is used in this research.
- Multi-stage exerge lose reduction system is applied to reduce the temperature difference between oil and water in the steam generating system.
- Influence of the arrangement of Stirling engine array in the cascade system is analyzed.

7.3 Outlooks

In this research, effective topologies of the proposed cascade system were designed, models of the systems developed based on the detailed component models, simulation of the cascade system and corresponding stand alone systems were carried out and the results were analyzed. However, there are many points valuable for further research.

- Solar power tower technology is gaining more and more attention, which represents the future of CSP technology and needs to be investigated in the future work.
- With the development of solar collectors, combination of different types of collectors will overcome the current drawbacks and deserves more focus.
- Series connection of different collectors, such as flat plate and parabolic trough collectors, needs to be further studied to reduce the cost of solar power system.
- Economical analysis of the cascade system is required for the implement of the technology.

Acknowledge

I offer the sincerest gratitude to my supervisors Prof. Wei Gao, Inmaculada Arauzo and Yanping Zhang. They contributed much more time and effort to my research and reports than I expected. My technical skills have been greatly improved as a result of working and learning with them.

I also owe my gratitude to Prof. Shuhong Huang. It would not have been possible to complete my research on the solar thermal power without his help. Prof. Huang spent a lot of time for the coordination and technology improvement.

Thanks to my research partners, Chongzhe Zou, Xiaohong Huang, and Xiaolin Lei. They provided a good study atmosphere. Owing to their efforts, the cascade solar thermal test system is under construction and experiment investigation thereby will be carried out.

Thanks are given to the support of International S&T Cooperation Program of China, under Grant No. 2014DFA60990.

Bibliography

[1] Babaelahi M, Sayyaadi H. A new thermal model based on polytropic numerical simulation of Stirling engines. Applied Energy, 2015, 141:143 – 159.

[2] MARTINI W R. Stirling engine design manual, 2nd edition. Technical report, Martini Engineering, Richland, WA (USA), 1983.

[3] Renewables 2016 Global Status Report. http://www.ren21.net/wp-content/uploads/2016/10/REN21_GSR2016_FullReport_en_11.pdf. Accessed: 2017-05-04.

[4] International Energy Agency (2014). http://www.iea.org/publications/freepublications/publication/TechnologyRoadmapSolarPhotovoltaicEnergy_2014edition.pdf. Accessed: 2017-05-04.

[5] Price H, Lupfert E, Kearney D, et al. Advances in Parabolic Trough Solar Power Technology. Journal of Solar Energy Engineering, 2002, 124(2):109–125.

[6] Dudley V E, Kolb G J, Mahoney A R, et al. Test results: SEGS LS-2 solar collector. Nasa Sti/recon Technical Report N, 1994, 96(4):2506–2514.

[7] Burkholder F, Kutscher C. Heat Loss Testing of Schott's 2008 PTR70 Parabolic Trough Receiver. May, 2009.

[8] Reddy K, Kumar K R, Ajay C. Experimental investigation of porous disc enhanced receiver for solar parabolic trough collector. Renewable Energy, 2015, 77(Supplement C):308 – 319.

[9] Li M, Xu C, Ji X, et al. A new study on the end loss effect for parabolic trough solar collectors. Energy, 2015, 82(Supplement C):382 – 394.

[10] Wang J, Wang J, Bi X, et al. Performance Simulation Comparison for Parabolic Trough Solar Collectors in China. International Journal of Photoenergy, 2016, 2016(18):1–16.

[11] Zou B, Yang H, Yao Y, et al. A detailed study on the effects of sunshape and incident angle on the optical performance of parabolic trough solar collectors. Applied Thermal Engineering, 2017, 126(Supplement C):81 – 91.

[12] Lüpfert E, Pottler K, Ulmer S, et al. Parabolic Trough Optical Performance Analysis Techniques. Journal of Solar Energy Engineering, 2006, 129(2):147–152.

[13] Xu C, Chen Z, Li M, et al. Research on the compensation of the end loss effect for parabolic trough solar collectors. Applied Energy, 2014, 115:128 – 139.

[14] Huang W, Hu P, Chen Z. Performance simulation of a parabolic trough solar collector. Solar Energy, 2012, 86(2):746 – 755.

[15] Padilla R V, Fontalvo A, Demirkaya G, et al. Exergy analysis of parabolic trough solar receiver. Applied Thermal Engineering, 2014, 67(1-2):579 – 586.

[16] Padilla R V, Demirkaya G, Goswami D Y, et al. Heat transfer analysis of parabolic trough solar receiver. Applied Energy, 2011, 88(12):5097 – 5110.

[17] Al-Sulaiman F A. Exergy analysis of parabolic trough solar collectors integrated with com-

bined steam and organic Rankine cycles. Energy Conversion and Management, 2014, 77:441 – 449.

[18] Guo J, Huai X, Liu Z. Performance investigation of parabolic trough solar receiver. Applied Thermal Engineering, 2016, 95:357 – 364.

[19] Behar O, Khellaf A, Mohammedi K. A novel parabolic trough solar collector model – Validation with experimental data and comparison to Engineering Equation Solver (EES). Energy Conversion and Management, 2015, 106(Supplement C):268 – 281.

[20] Hachicha A, Rodriguez I, Capdevila R, et al. Heat transfer analysis and numerical simulation of a parabolic trough solar collector. Applied Energy, 2013, 111:581 – 592.

[21] Guo J, Huai X. Multi-parameter optimization design of parabolic trough solar receiver. Applied Thermal Engineering, 2016, 98:73 – 79.

[22] Boukelia T, Arslan O, Mecibah M. ANN-based optimization of a parabolic trough solar thermal power plant. Applied Thermal Engineering, 2016, 107:1210 – 1218.

[23] Liu Q, Yang M, Lei J, et al. Modeling and optimizing parabolic trough solar collector systems using the least squares support vector machine method. Solar Energy, 2012, 86(7):1973 – 1980.

[24] Lobon D H, Valenzuela L, Baglietto E. Modeling the dynamics of the multiphase fluid in the parabolic-trough solar steam generating systems. Energy Conversion and Management, 2014, 78:393 – 404.

[25] Mohamad A, Orfi J, Alansary H. Heat losses from parabolic trough solar collectors. International Journal of Energy Research, 2014, 38(1):20–28.

[26] Guo S, Liu D, Chu Y, et al. Real-time dynamic analysis for complete loop of direct steam generation solar trough collector. Energy Conversion and Management, 2016, 126:573 – 580.

[27] Ashouri M, Vandani A M K, Mehrpooya M, et al. Techno-economic assessment of a Kalina cycle driven by a parabolic Trough solar collector. Energy Conversion and Management, 2015, 105:1328 – 1339.

[28] Bader R, Pedretti A, Barbato M, et al. An air-based corrugated cavity-receiver for solar parabolic trough concentrators. Applied Energy, 2015, 138:337 – 345.

[29] Good P, Ambrosetti G, Pedretti A, et al. An array of coiled absorber tubes for solar trough concentrators operating with air at 600°C and above. Solar Energy, 2015, 111:378 – 395.

[30] Kaloudis E, Papanicolaou E, Belessiotis V. Numerical simulations of a parabolic trough solar collector with nanofluid using a two-phase model. Renewable Energy, 2016, 97:218 – 229.

[31] Tan L, Ji X, Li M, et al. The experimental study of a two-stage photovoltaic thermal system based on solar trough concentration. Energy Conversion and Management, 2014, 86:410 – 417.

[32] Al-Sulaiman F A, Hamdullahpur F, Dincer I. Performance assessment of a novel system using parabolic trough solar collectors for combined cooling, heating, and power production. Renewable Energy, 2012, 48:161 – 172.

[33] Tan Y, Zhao L, Bao J, et al. Experimental investigation on heat loss of semi-spherical cavity receiver. Energy Conversion and Management, 2014, 87(Supplement C):576 – 583.

[34] Chaudhary A, Kumar A, Yadav A. Experimental investigation of a solar cooker based on parabolic dish collector with phase change thermal storage unit in Indian climatic conditions. Journal of Renewable and Sustainable Energy, 2013, 5(2):023107.

[35] Mawire A, Taole S H. Experimental energy and exergy performance of a solar receiver for a domestic parabolic dish concentrator for teaching purposes. Energy for Sustainable Development, 2014, 19:162 – 169.

[36] Zhu J, Wang K, Wu H, et al. Experimental investigation on the energy and exergy performance of a coiled tube solar receiver. Applied Energy, 2015, 156:519 – 527.

[37] Skouri S, Bouadila S, Salah M B, et al. Comparative study of different means of concentrated solar flux measurement of solar parabolic dish. Energy Conversion and Management, 2013, 76:1043 – 1052.

[38] Thirunavukkarasu V, Sornanathan M, Cheralathan M. An experimental study on energy and exergy performance of a cavity receiver for solar parabolic dish concentrator. International Journal of Exergy, 2017, 23(2):129.

[39] Pavlovic S, Bellos E, Roux W G L, et al. Experimental investigation and parametric analysis of a solar thermal dish collector with spiral absorber. Applied Thermal Engineering, 2017, 121(Supplement C):126 – 135.

[40] Lovegrove K, Burgess G, Pye J. A new 500m2 paraboloidal dish solar concentrator. Solar Energy, 2011, 85(4):620 – 626. SolarPACES 2009.

[41] Berumen C R, Benítez R R, Mendoza J L, et al. Design and Construction of a Parabolic Dish in Mexico. in: Proceedings of ASME 2004 International Solar Energy Conference, 2004, 653-657.

[42] PAVLOVIĆ S R, STEFANOVIĆ V P, SULJKOVIĆ S H. OPTICAL MODELING OF A SOLAR DISH THERMAL CONCENTRATOR BASED ON SQUARE FLAT FACETS. Thermal Science, 2014, 18(3):989 – 998.

[43] Hijazi H, Mokhiamar O, Elsamni O. Mechanical design of a low cost parabolic solar dish concentrator. Alexandria Engineering Journal, 2016, 55(1):1 – 11.

[44] Ma H, Jin G, Xing Z, et al. Optical Design of a Solar Dish Concentrator Based on Triangular Membrane Facets. International Journal of Photoenergy, 2012, 2012(2012):3109–3109.

[45] Schertz P T, Brown D C, Konnerth I. Facet development for a faceted stretched-membrane dish by Solar Kinetics, Inc. Parabolic Dish Collectors, 1991, 91.

[46] Shuai Y, Xia X, Tan H. Numerical simulation and experiment research of radiation performance in a dish solar collector system. Frontiers of Energy & Power Engineering in China, 2010, 4(4):488–495.

[47] Qianjun M, Ming X, Yong S, et al. Study on solar photo-thermal conversion efficiency of a solar parabolic dish system. Environmental Progress & Sustainable Energy, 2014, 33(4):1438–1444.

[48] Li Z, Tang D, Du J, et al. Study on the radiation flux and temperature distributions of the concentrator–receiver system in a solar dish/Stirling power facility. Applied Thermal Engineering, 2011, 31(10):1780 – 1789.

[49] Wang W, Laumert B. Effect of cavity surface material on the concentrated solar flux distribution for an impinging receiver. Solar Energy Materials and Solar Cells, 2017, 161(Supplement C):177 – 182.

[50] Blázquez R, Carballo J, Silva M. Optical design and optimization of parabolic dish solar concentrator with a cavity hybrid receiver. AIP Conference Proceedings, 2016, 1734(1).

[51] Reddy K, Vikram T S, Veershetty G. Combined heat loss analysis of solar parabolic dish – modified cavity receiver for superheated steam generation. Solar Energy, 2015, 121:78 – 93. {ISES} Solar World Congress 2013 (SWC2013) Special Issue.

[52] Vikram T S, Reddy K. Investigation of convective and radiative heat losses from modified cavity based solar dish steam generator using {ANN}. International Journal of Thermal Sciences, 2015, 87:19 – 30.

[53] Patil P N, Khandekar M A, Patil S N. Automatic dual-axis solar tracking system for parabolic dish. in: Proceedings of 2016 2nd International Conference on Advances in Electrical, Electronics, Information, Communication and Bio-Informatics (AEEICB), Feb, 2016, 699-703.

[54] Besarati S M, Yogi Goswami D. A computationally efficient method for the design of the heliostat field for solar power tower plant. Renewable Energy, 2014, 69:226–232.

[55] Sassi G. Some notes on shadow and blockage effects. Solar Energy, 1983, 31(3):331 – 333.

[56] El-Haroun A. Investigation of a Novel Combination for Both Solar Chimney and Solar Tower Systems. Journal of Energy Engineering, 2015, page 04015042.

[57] Franchini G, Perdichizzi A, Ravelli S, et al. A comparative study between parabolic trough and solar tower technologies in Solar Rankine Cycle and Integrated Solar Combined Cycle plants. Solar Energy, 2013, 98, Part C:302 – 314.

[58] Kim J, Kim J S, Stein W. Simplified heat loss model for central tower solar receiver. Solar Energy, 2015, 116:314 – 322.

[59] Lara-Cerecedo L O, Moreno-Cruz I, Pitalúa-Diaz N, et al. Modeling of Drift Effects on Solar Tower Concentrated Flux Distributions. International Journal of Photoenergy, 2016, 2016:1–9.

[60] Wei X, Lu Z, Wang Z, et al. A new method for the design of the heliostat field layout for solar tower power plant. Renewable Energy, 2010, 35(9):1970–1975.

[61] Wei X, Lu Z, Yu W, et al. A new code for the design and analysis of the heliostat field layout for power tower system. Solar Energy, 2010, 84(4):685–690.

[62] Xu E, Yu Q, Wang Z, et al. Modeling and simulation of 1 MW DAHAN solar thermal power tower plant. Renewable Energy, 2011, 36(2):848–857.

[63] Xu E, Wang Z, Wei G, et al. Dynamic simulation of thermal energy storage system of Badaling 1 MW solar power tower plant. Renewable Energy, 2012, 39(1):455–462.

[64] Suzuki A. Cascade connection of solar collectors for effective energy gain. Journal of Solar Energy Engineering Transactions of the Asme, 1986, 108(3):172–177.

[65] Kribus A, Doron P, Rubin R, et al. A Multistage Solar Receiver:: The Route To High Temperature. Solar Energy, 1999, 67(1–3):3 – 11.

[66] Gordon J M, Saltiel C. Analysis and Optimization of a Multi-Stage Solar Collector System.

Journal of Solar Energy Engineering, 1986, 108(3):192–198.

[67] Oshida I, Suzuki A. Optical Cascade Heat-Collection for Effective Solar Energy Gain. Journal of Solar Energy Engineering, 1987, 109(4):298–302.

[68] Desai N B, Bandyopadhyay S. Integration of parabolic trough and linear Fresnel collectors for optimum design of concentrating solar thermal power plant. Clean Technologies and Environmental Policy, 2015, 17(7):1945–1961.

[69] Coco-Enríquez L, Muñoz-Antón J, Martínez-Val J. Integration between direct steam generation in linear solar collectors and supercritical carbon dioxide Brayton power cycles. International Journal of Hydrogen Energy, 2015, 40(44):15284 – 15300. The 4th International Conference on Nuclear and Renewable Energy Resources (NURER2014), 26-29 October 2014, Antalya, Turkey.

[70] Li Y, Yang Y. Thermodynamic analysis of a novel integrated solar combined cycle. Applied Energy, 2014, 122:133 – 142.

[71] Behar O, Khellaf A, Mohammedi K, et al. A review of integrated solar combined cycle system (ISCCS) with a parabolic trough technology. Renewable and Sustainable Energy Reviews, 2014, 39(0):223–250.

[72] Gülen S C. Second Law Analysis of Integrated Solar Combined Cycle Power Plants. Journal of Engineering for Gas Turbines and Power, 2015, 137(5):51701.

[73] Shaaban S. Analysis of an integrated solar combined cycle with steam and organic Rankine cycles as bottoming cycles. Energy Conversion and Management, 2016, 126:1003–1012.

[74] Alqahtani B J, Patiño-Echeverri D. Integrated Solar Combined Cycle Power Plants: Paving the way for thermal solar. Applied Energy, 2016, 169:927 – 936.

[75] Manente G. High performance integrated solar combined cycles with minimum modifications to the combined cycle power plant design. Energy Conversion and Management, 2016, 111:186 – 197.

[76] Turchi C S, Ma Z. Co-located gas turbine/solar thermal hybrid designs for power production. Renewable Energy, 2014, 64:172 – 179.

[77] Mukhopadhyay S, Ghosh S. Solar tower combined cycle plant with thermal storage: energy and exergy analyses. Advances in Energy Research, 2016, 4(1):29–45.

[78] Li J, Li P, Pei G, et al. Analysis of a novel solar electricity generation system using cascade Rankine cycle and steam screw expander. Applied Energy, 2016, 165:627–638.

[79] Bahari S S, Sameti M, Ahmadi M H, et al. Optimisation of a combined Stirling cycle–organic Rankine cycle using a genetic algorithm. International Journal of Ambient Energy, 2016, 37(4):398–402.

[80] Abbin J, Leuenberger W. Program CYCLE: a Rankine cycle analysis routine. [For solar–thermal electricity production for Sandia's Solar Community study]. Oct, 1977.

[81] Roschke E J, Wen L, Steele H, et al. A preliminary assessment of small steam Rankine and Brayton point-focusing solar modules. Nasa Sti/recon Technical Report N, 1979, 79.

[82] Dunham M T, Lipiński W. Thermodynamic Analyses of Single Brayton and Combined Brayton–Rankine Cycles for Distributed Solar Thermal Power Generation. Journal of Solar

Energy Engineering, 2013, 135(3):031008–031008–8.

[83] Bahrami M, Hamidi A A, Porkhial S. Investigation of the effect of organic working fluids on thermodynamic performance of combined cycle Stirling-ORC. International Journal of Energy and Environmental Engineering, 2013, 4(1):12.

[84] Thierry D M, Flores-Tlacuahuac A, Grossmann I E. Simultaneous optimal design of multi-stage organic Rankine cycles and working fluid mixtures for low-temperature heat sources. Computers & Chemical Engineering, 2016, 89:106 – 126.

[85] Bao J, Zhao L. A review of working fluid and expander selections for organic Rankine cycle. Renewable and Sustainable Energy Reviews, 2013, 24:325 – 342.

[86] Bilgen E, Rheault J. Solar chimney power plants for high latitudes. Solar Energy, 2005, 79(5):449 – 458.

[87] Fernández-García A, Zarza E, Valenzuela L, et al. Parabolic-trough solar collectors and their applications. Renewable and Sustainable Energy Reviews, 2010, 14(7):1695 – 1721.

[88] Giglio A, Lanzini A, Leone P, et al. Direct steam generation in parabolic-trough collectors: A review about the technology and a thermo-economic analysis of a hybrid system. Renewable and Sustainable Energy Reviews, 2017, 74:453–473.

[89] Khenissi A, Krüger D, Hirsch T, et al. Return of Experience on Transient Behavior at the DSG Solar Thermal Power Plant in Kanchanaburi, Thailand. Energy Procedia, 2015, 69:1603 – 1612. International Conference on Concentrating Solar Power and Chemical Energy Systems, SolarPACES 2014.

[90] Romero-Alvarez M, Zarza E. Concentrating solar thermal power. Efficiency and Renewable Energy, 2007.

[91] Adkins D R. Control strategies and hardware used in solar thermal applications. Nasa Sti/recon Technical Report N, 1987, 88.

[92] Coronel P, Sandeep K. Heat transfer coefficient in helical heat exchangers under turbulent flow conditions. International Journal of Food Engineering, 2008, 4(1).

[93] Serth R W. Process heat transfer principles and applications. Amsterdam; London: Elsevier Academic Press, 2007.

[94] Churchill S W, Bernstein M. A Correlating Equation for Forced Convection From Gases and Liquids to a Circular Cylinder in Crossflow. Journal of Heat Transfer, 1977, 99(2):300–306.

[95] Ma R Y. Wind Effects on Convective Heat Loss From a Cavity Receiver for a Parabolic Concentrating Solar Collector. Sandia National Laboratory, 1993, SAND92-7293(September).

[96] Wu S Y, Xiao L, Cao Y, et al. Convection heat loss from cavity receiver in parabolic dish solar thermal power system: A review. Solar Energy, 2010, 84(8):1342 – 1355.

[97] Leibfried U, Ortjohann J. Convective Heat Loss from Upward and Downward-Facing Cavity Solar Receivers: Measurements and Calculations. Journal of Solar Energy Engineering, 1995, 117(2):75–84.

[98] Koenig A, Marvin M. Convection heat loss sensitivity in open cavity solar receivers. Technical report, Department of Energy, USA, 1981.

[99] Stine W B, Diver R B. A compendium of solar dish/Stirling technology. Technical report, DTIC Document, 1994.

[100] Formosa F, Despesse G. Analytical model for Stirling cycle machine design. Energy Conversion and Management, 2010, 51(10):1855–1863.

[101] Juhasz A. A mass computation model for lightweight brayton cycle regenerator heat exchangers. in: Proceedings of 8th Annual International Energy Conversion Engineering Conference, 2010.

[102] Duan C, Wang X, Shu S, et al. Thermodynamic design of Stirling engine using multi-objective particle swarm optimization algorithm. Energy Conversion & Management, 2014, 84:88–96.

[103] Urieli I, Berchowitz D M. Stirling cycle engine analysis. Bristol: A. Hilger, 1984.

[104] Heywood, JohnB. Internal combustion engine fundamentals. Amsterdam; London: McGraw-Hill, 1988.

[105] Strauss J M, Dobson R T. Evaluation of a second order simulation for Sterling engine design and optimisation. Journal of Energy in Southern Africa, 2010, 21(2):17–29.

[106] Timoumi Y, Tlili I, Nasrallah S B. Design and performance optimization of GPU-3 Stirling engines. Energy, 2008, 33(7):1100 – 1114.

[107] Hosseinzade H, Sayyaadi H, Babaelahi M. A new closed-form analytical thermal model for simulating Stirling engines based on polytropic-finite speed thermodynamics. Energy Conversion and Management, 2015, 90:395 – 408.

[108] Der Minassians A. Stirling Engines for Low-temperature Solar-thermal-electric Power Generation: [PhD Dissertation]. Berkeley: EECS Department, University of California, Berkeley, December 20, 2007.

[109] Cavazzuti M. Optimization Methods: From Theory to Design Scientific and Technological Aspects in Mechanics. Berlin Heidelberg: Springer, 2012.

[110] Hooshang M, Moghadam R A, AlizadehNia S. Dynamic response simulation and experiment for gamma-type Stirling engine. Renewable Energy, 2016, 86:192 – 205.

[111] Rovira A, Montes M J, Valdes M, et al. Energy management in solar thermal power plants with double thermal storage system and subdivided solar field. Applied Energy, 2011, 88(11):4055 – 4066.

[112] Fraser P, Klein P S a. Stirling Dish System Performance Prediction Model. Mechanical Engineering, 2008, Master of:203.

Appendix A Heat transfer under constant temperature

Assuming U, T_c, q_m,c_p to be constant, for given T_i,

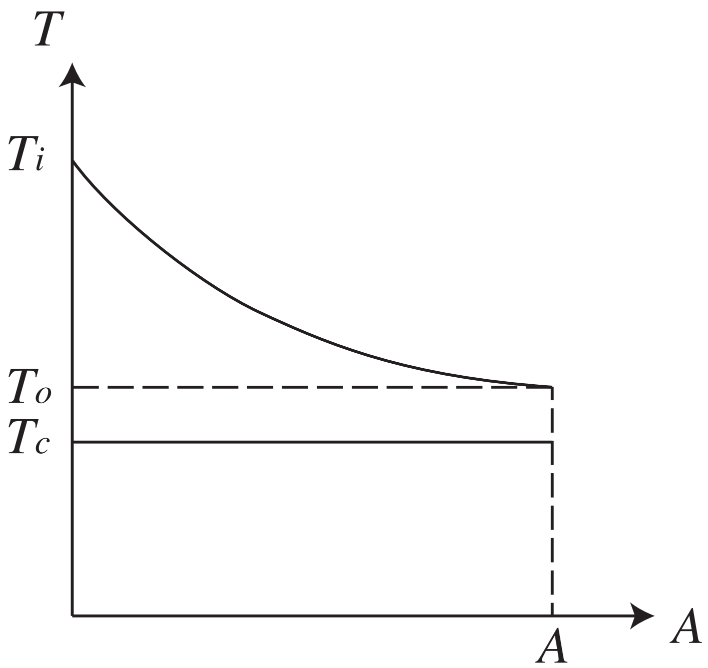

Figure 1-1 Diagram of heat transfer under constant temperature

For $A(x) = Px$, x from 0 to L, while $T(x)$ from T_i to T_o,

$$q_m c_p dT(x) = (T_c - T(x))UPdx \tag{A.1}$$

so

$$\frac{dT(x)}{dx} = -\frac{UP}{q_m c_p}(T(x) - T_c) \tag{A.2}$$

$$T_g(x) = T_p(x) + T_h(x) \tag{A.3}$$

where $T_g(x)$ is the general solution, $T_p(x)$ is the particular solution, $T_h(x)$ is the homogeneous solution.

$$-\frac{UP}{q_m c_p}(T_p(x) - T_c) = 0 \tag{A.4}$$

$$T_p(x) = T_c \tag{A.5}$$

$$\frac{dT_h(x)}{dx} = -\frac{UP}{q_m c_p} T_h(x) \tag{A.6}$$

$$\int_{T_h(x)=T_h(0)}^{T_h(x)=T_h(L)} \frac{dT_h(x)}{T_h(x)} = -\int_{x=0}^{x=L} \frac{UP}{q_m c_p} dx \tag{A.7}$$

$$\frac{T_h(L)}{T_h(0)} = \exp(-\frac{UPL}{q_m c_p}) \tag{A.8}$$

that is

$$\frac{T_g(L) - T_p(L)}{T_g(0) - T_p(0)} = \exp(-\frac{UA}{q_m c_p}) \tag{A.9}$$

$$\frac{T_o - T_c}{T_i - T_c} = \exp(-\frac{UA}{q_m c_p}) \tag{A.10}$$

Appendix B Thermal gradient under constant heat flux

Assuming U, T_c, $\dot{m}$, c_p, q'' to be constant, for given T_i,

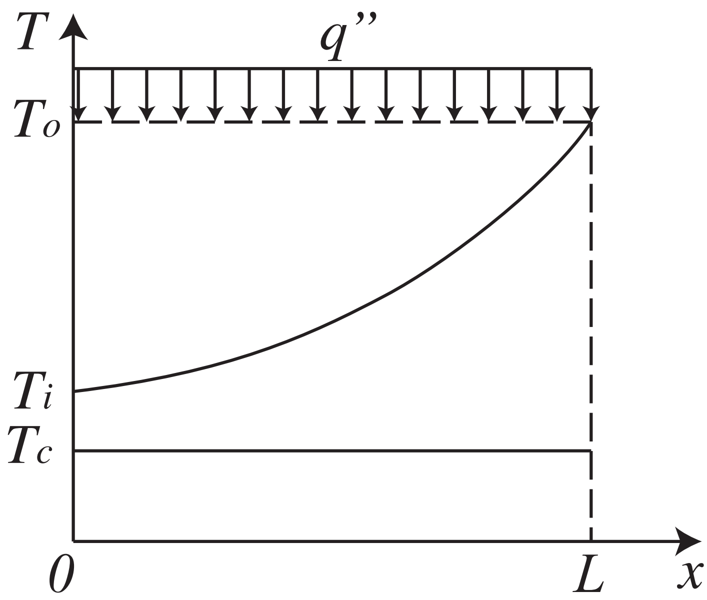

Figure 2-1 Diagram of heat transfer with one constant temperature heat source and constant heat flux

For $A(x) = Px$, x from 0 to L, while $T(x)$ from T_i to T_o,

$$q_m c_p dT(x) = (T_c - T(x))UPdx + q''Pdx \tag{B.1}$$

so

$$\frac{dT(x)}{dx} = -\frac{UP}{q_m c_p}T(x) + \frac{q''P + UPT_c}{q_m c_p} \tag{B.2}$$

$$T_g(x) = T_p(x) + T_h(x) \tag{B.3}$$

where $T_g(x)$ is the general solution, $T_p(x)$ is the particular solution, $T_h(x)$ is the homogeneous solution.

$$-\frac{UP}{q_m c_p} T_p(x) + \frac{q''P + UPT_c}{q_m c_p} = 0 \tag{B.4}$$

$$T_p(x) = T_c + \frac{q''}{U} \tag{B.5}$$

$$\frac{dT_h(x)}{dx} = -\frac{UP}{q_m c_p} T_h(x) \tag{B.6}$$

the same as Equation (A.6), so we have

$$\frac{T_g(L) - T_p(L)}{T_g(0) - T_p(0)} = \exp(-\frac{UA}{q_m c_p}) \tag{B.7}$$

$$\frac{T_o - T_c - \frac{q''}{U}}{T_i - T_c - \frac{q''}{U}} = \exp(-\frac{UA}{q_m c_p}) \tag{B.8}$$

Appendix C Publication

[1] Zhang Cheng, Kun Wang. International Conference on Power Engineering: ICOPE 2013: FEA simulation on the alignment of the shafts of three-fulcrum turbine.

[2] Performance comparison of new and traditional arrangements of a dish-Stirling system

[3] A multi-stage exergy-loss reduction system for solar parabolic trough power plants

[4] Zhang Cheng, Zhang Yanping, Arauzo Inmaculada, Gao Wei, Zou Chongzhe. Cascade system using both trough system and dish system for power generation. Energy Convers Manag 2017;142:494–503. doi:10.1016/j.enconman.2017.03.073.

[5] Thermal Modeling of a Pressurized Air Cavity Receiver for a Solar Dish Stirling System

[6] A solar thermal cascade system, No. 201610806296.5

[7] A flow control method used in a multi-stage heating system, No. 201610805604.2